Dissertation zur Erlangung des Doktorgrades
der Fakultät für Chemie und Pharmazie
der Ludwig-Maximilians-Universität München

Analysis of eukaryotic translation by integrating cryo-EM and ribosome profiling

Vivekanandan Shanmuganathan
aus
Pondicherry, India

2022

Erklärung

Diese Dissertation wurde im Sinne von §7 der Promotionsordnung vom 28. November 2011 von Herrn Prof. Dr. Roland Beckmann betreut.

Eidesstattliche Versicherung

Diese Dissertation wurde eigenständig und ohne unerlaubte Hilfe erarbeitet.

Berlin, 10.11.2022

Vivekanandan Shanmuganathan

Dissertation eingereicht am: 23.11.2022

1. Gutachter: Prof. Dr. Roland Beckmann

2. Gutachter: Prof. Dr. Klaus Förstemann

Mündliche Prüfung am: 03.03.2023

Parts of this thesis have been published in scientific journals:

"Structural and mutational analysis of the ribosome-arresting human XBP1u"

Vivekanandan Shanmuganathan*, Nina Schiller*, Anastasia Magoupoulou, Jingdong Cheng, Katharina Braunger, Florian Cymer, Otto Berninghausen, Brigitta Beatrix, Kenji Kohno, Gunnar von Heijne**, and Roland Beckmann**

Published in eLife 2019 Jun 27;8:e46267.

"Reconstitution of the human SRP system and quantitative and systematic analysis of its ribosome interactions"

Klemens Wild, Kevin D Juaire, Komal Soni, **Vivekanandan Shanmuganathan**, Astrid Hendricks, Bernd Segnitz, Roland Beckmann, and Irmgard Sinning**

Published in Nucleic Acids Research 2019 Apr 8; 47(6): 3184-3196.

"The cryo-EM structure of a ribosome-Ski2-Ski3-Ski8 helicase complex"

Christian Schmidt, Eva kowalinski, **Vivekanandan Shanmuganathan**, Quentin Defenouillere, Katharina Braunger, Andre Heuer, Markus Pech, Abdelkader Namane, Otto Berninghausen, Micheline Fromont-Racine, Alain Jacquier, Elena Conti**, Thomas Becker**, and Roland Beckmann**

Published in Science 354 (6318), 1431-1433. 2016 Dec 16.

"Structure of the hypusinylated eukaryotic translation factor eIF-5A bound to the ribosome"

Christian Schmidt*, Thomas Becker*, Andre Heuer, Katharina Brunager, Vivekanandan Shanmuganathan, Markus Pech, Otto Berninghausen, Daniel N Wilson**, and Roland Beckmann**

Published in Nucleic Acids Research 2016 Feb 29;44(4):19544-51.

* These authors contributed equally to the work

** Corresponding Author

Parts of this thesis have been presented at international conferences:

Poster presented at the Protein Synthesis and Translational Control Meeting, Heidelberg, Germany 2015

“Ribosome profiling of maturing dendritic cells”

Vivekanandan Shanmuganathan, Markus Pech, Basak Eraslan, Frauke Schnorfeil, Julien Gagneur, Marion Subklewe and Roland Beckmann

Poster presented at the Translational Control Meeting, Cold Spring Harbor Laboratory, USA 2018

“Molecular Mechanism of translational pausing by the XBP1u nascent chain in UPR”

Vivekanandan Shanmuganathan, Nina Schiller, Jingdong Cheng, Katharina Braunger, Otto Berninghausen, Birgitta Beatrix, Gunnar von Heijne and Roland Beckmann

Summary

Translational control plays a critical role in maintaining proteome homeostasis, and in influencing cellular differentiation, proliferation, growth and developmental pathways. Protein synthesis is closely linked to cellular metabolism and any aberrations in its regulation lead to diseased states. In this thesis presented here, translational regulation has been investigated in three different biological contexts by integrating two different techniques namely, cryo-electron microscopy and ribosomal profiling.

Translational regulation has been investigated in maturing dendritic cells using ribosome profiling and RNAseq respectively. Dendritic cells (DC) are the professional antigen-presenting cells of the immune system. In the immature state (immature DC), they have the ability to monitor the environment and upon encountering antigens they mature to launch immune responses. Here, a defined cytokine mixture combined with TLR agonist (R848) has been used for *in vitro* DC maturation. Upon induction of maturation, pathways such as the 'TNF signaling pathway', the 'cytokine-cytokine receptor interaction' and the 'IL-17 signaling pathway' were up regulated both at the level of transcriptome and translatome respectively. Transcripts encoding for proteins involved in oxidative phosphorylation pathway were strongly repressed at the later stages of DC maturation (24 h). As observed in previous studies transcripts encoding for ribosomal proteins, antigen processing and presentation were also translationally up-regulated at 4 h while being translationally repressed at the 24 h time point. Transcripts of the glycolytic pathway are also translationally repressed at the 24 h time-point. Further, during the course of DC maturation, globally there was increased ribosome occupancy in the 5' UTR. During the later stages of DC maturation, down regulation of ABCE1 led to accumulation of post-termination ribosomes in the 3' UTR. Moreover, ribosome occupancy in the 3' UTR showed strong correlation to its GC content.

Ski proteins function as accessory factors and are essential for exosome function, which mediates the 3' to 5' mRNA decay pathway. Non-stop transcripts are primarily decayed via the 3' to 5' pathway. It has been shown here that the Ski complex, interacts with the ribosome independent of

Ski7. Ribosomal profiling of 80S-Ski-complexes revealed a fraction of longer footprints, and contained more poly-A containing footprints. Further, RNAseq analysis of the purified 80S-Ski-complexes revealed strong asymmetric distribution of reads, where more reads mapped towards the 5’ end of the transcripts. Also, transcripts with shorter half-life (< 5 min) and with more non-optimal codon content showed enrichment for Ski-80S footprints. This hinted at the possibility that Ski complex might interact with ribosomes for turnover of canonical transcripts via the 3’-5’ decay pathway.

The endoplasmic reticulum (ER) is responsible for properly modifying and folding most of the secretory and membrane proteins. Its functioning capacity is challenged during stressful circumstances such as in hypoxia, calcium imbalance and viral infection. Unfolded protein response (UPR) is the cellular mechanism that is activated to alleviate the ER stress. UPR acts via three main pathways in mammals, and of this IRE1α-XBP1u branch is the most evolutionarily conserved. XBP1u contains a C-terminal ribosomal pausing site and plays a critical role in mediating UPR. Using cryo-EM, XBP1u has been visualized in the ribosomal exit tunnel. Structural characterization revealed that XBP1u forms a turn in the vicinity of the peptidyl transferase center and causes a subtle distortion of the base C4398 to inhibit ribosomal activity. This explains the temporary nature of the ribosomal arrest mediated by XBP1u. During ribosomal pausing, HR2 of XBP1u is being recognized by SRP, but it fails to successfully engage with the Sec61 translocon. XBP1u has evolved with an intermediate ribosomal pausing strength, but this allows it to be efficiently targeted by SRP onto the Sec61 translocon, albeit without gating it.

Table of Contents

List of Figures

List of Tables

1 Introduction

Proteins contribute to more than half the dry weight of the cell, and play a critical role in executing various cellular functions. Proteins are synthesized by the ribosomes, which are comprised of ribosomal RNAs (rRNA) and several ribosomal proteins. Ribosomes are conserved across evolution, and are structurally organized into large (LSU) and small subunit (SSU). The subunits are named according to their ultra-centrifugation sedimentation coefficients expressed in Svedberg units as 60S and 40S respectively for eukaryotic ribosomes. Each subunit has distinct functions; 40S (SSU) is responsible for binding and decoding of mRNAs, while the 60S (LSU) catalyzes peptide bond formation. Another characteristic feature of the 60S is a channel for newly synthesized nascent chain called the ribosomal exit tunnel. Newly synthesized nascent chain traverse through it before exiting on the solvent side, where the nascent chain can be contacted by various factors. Both subunits interact via the inter-subunit bridges, and contain three transfer-RNA (tRNA) binding sites, the amino-acyl- (A-tRNA), peptidyl- (P-tRNA) and exit- (E-tRNA) site respectively.

1.1 Eukaryotic translation cycle

The ribosomal translation involves four distinct steps: initiation elongation, termination, and recycling (Figure 1.1).

1.1.1 Eukaryotic translation initiation

Translation initiation on eukaryotic mRNAs is a complex process mediated by at least 12 eukaryotic initiation factors (eIFs), and it begins on the split SSU from the previous round of translation (Hinnebusch & Lorsch, 2012; Jackson et al., 2010). Eukaryotic mRNAs possess 5’ 7-methylguanosine cap (m7G) and 3’ end post transcriptionally added poly-A tail protecting them against premature degradation. eIFs recognize these features to select intact mRNAs for translation initiation. Eukaryotic mRNAs typically possess a 5’ UTR of length 50 – 200 nucleotides lacking Shine-Dalgarno sequence (Lynch et al., 2005; Mignone et al., 2002; Pesole et al., 2001), which is often used to

position ribosomes over the start codon in prokaryotes by base-pairing with 3'-end of 16S rRNA. Start codon selection and mRNA affinity in eukaryotes depends on the sequence context around the start codon, secondary structure and overall start codon accessibility. Moreover, 43S pre-initiation complex containing amongst other initiation factors and also the initiator tRNA does not bind directly in the vicinity of the start codon but scans the mRNA from the 5' end for start codon selection. This process is termed as ribosomal scanning and is a characteristic feature of eukaryotic translation initiation.

eIF2 delivers the initiator tRNA (Met-tRNA$_i$) to the SSU in the form of a ternary complex: eIF2-GTP-Met-tRNA$_i$. Further, eIF2-GTP-Met-tRNA$_i$ associates with eIF5, 1, 1A and 3, which all assemble on the 40S to form the 43S pre-initiation complex (43S-PIC). 43S-PIC now binds to mRNA thereby leading to the formation of the 48S complex. mRNA binding to 43S-PIC is promoted by contacts between eIF3 and eIF4F complex, which is pre-assembled on the mRNAs. eIF4F complex is composed of eIF4A, B, E and G. eIF4E subunit recognizes the 5'-cap (m7G) of the mRNAs, while eIF4G binds to poly-A binding protein-1 (Pab1) at the poly-A tail, leading to the circularization of mRNAs. 48S complex now scans the mRNA in 5' – 3' direction to identify the start codon. Scanning is processive, and this is further facilitated by the ATPase activity of eIF4A helicase. Upon start codon recognition, eIF5 and eIF5B promote the hydrolysis of eIF2-bound GTP. Following hydrolysis, initiation factors get dissociated from 40S and 60S joins to form the 80S. At this stage, tRNA$_i$ is in the P-site contacting the start codon, with an empty A-site.

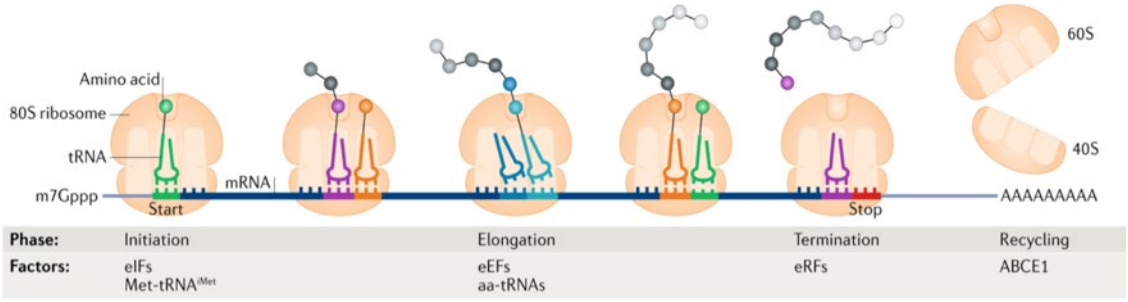

Figure 1.1 Overview of eukaryotic translation cycle.

Ribosomal subunits, initiator methionyl-tRNA (Met-tRNA^{iMet}) and multitude of eukaryotic initiation factors (eIFs) come together at the AUG start codon for translational initiation. Peptide chain is synthesized during the elongation phase, and it is mediated by eukaryotic elongation factors (eEFs). Elongation continues until the ribosome reaches a stop codon for termination. During termination, peptide chain is released through the actions of eRF1 and eRF3. After peptide release, ATPase binding cassette subfamily E member 1 (ABCE1) splits the 80S thereby, the ribosomal subunits can engage in next rounds of translation. Figure adapted from (Schuller and Green, 2018).

1.1.2 Eukaryotic translation elongation

Translation elongation proceeds with the delivery of aminoacyl-tRNA (aa-tRNA) to the ribosomal A-site. tRNA delivery is mediated by the GTP bound eEF1A (eukaryotic elongation factor 1 alpha) ternary complex (Thomas E Dever & Green, 2012), and it is recruited to the ribosome via interactions with the P1/P2 stalk. eEF1A positions aa-tRNA in the 40S A-site. Upon cognate codon-anticodon interaction, conformational changes cause eEF1A to hydrolyze the bound GTP, leading to its dissociation from the tRNA. This allows tRNA to be properly accommodated into the A-site, ensuing peptide bond formation. After peptide bond formation, a deacylated t-RNA is bound to the P-site, while the nascent chain is attached to the A-site tRNA. This is a highly dynamic state, where the tRNA acceptor ends are repositioned in the LSU, leading to a so-called rotated state with hybrid tRNA states: A/P- and P/E-tRNA (first and second letter denotes position in SSU and LSU respectively). Rotated state formation is coupled to the rotation of ribosomal subunits with respect to each other (Frank & Agrawal, 2000). At this stage, ribosomal translocation shifts the deacylated tRNA into the E-site and

peptidyl-tRNA into the P-site. Coupled to this translocation, is also the movement of mRNA by single codon. Translocation is catalyzed by the GTPase eEF2 (Thomas E Dever & Green, 2012), which binds preferentially to rotated state ribosomes with hybrid tRNAs. Elongation cycle is repeated until a stop codon appears in the A-site.

1.1.3 Translation termination and ribosome recycling

Protein synthesis is terminated when a stop codon reaches the ribosomal A-site (A. Brown et al., 2015b; Thomas E Dever & Green, 2012; Matheisl et al., 2015; Preis et al., 2014). In eukaryotes all three stop codons are recognized by the eukaryotic release factor-1 (eRF1), in contrast to two release factors (RF1 and RF2) in prokaryotes. Prokaryotic and eukaryotic release factors share less sequence similarity; however, they employ the conserved GGQ motif to terminate protein synthesis. eRF1 associates with the GTPase eRF3 to form the eRF1-eRF3-GTP ternary complex. This allows eRF3 to access the ribosomal GTPase binding site, while N-domain of eRF1 can probe into the 40S A-site. eRF1 contacts the stop codon via three motifs (NIKS, GTS and YxCxxxF) and the glutamate residue 55 (Glu55) located in the N-domain. Recently, it has been shown that, eRF1 recognizes the quadruplet stop codon (Matheisl et al., 2015). All four bases contribute to the formation of UNR-type U-turn geometry, which is recognized by eRF1 N-domain (Matheisl et al., 2015). eRF1 fixes stop codon in a defined position, and its recognition causes a change in ribosomal conformation to activate eRF3 GTPase function. Hydrolysis of GTP by eRF3, leads to its release. This allows eRF1 to accommodate its M-domain with GGQ motif into the PTC to hydrolyze the ester bond connecting the nascent chain and P-tRNA (Song et al., 2000).

Binding of ribosomal splitting factor ABCE1 (ATPase binding cassette subfamily E member 1) stimulates the hydrolysis activity of eRF1, leading to translational termination and nascent chain release. eRF1 serves as a binding platform for ABCE1 and also enhances its intrinsic ATPase activity (Becker et al., 2012; Franckenberg et al., 2012; Pisarev et al., 2007). ATP hydrolysis by ABCE1 causes a conformational change in its conserved rRNA binding iron-sulfur (Fe-S) cluster domain. This is thought to split the 80S into 40S and 60S ribosomal subunits, concomitantly releasing eRF1 and ABCE1. In eukaryotes,

translation termination is coupled to ribosome recycling. This coupling is facilitated by the directionality provided by the delivery of eRF1 by the eRF1-eRF3 complex and followed by ABCE1 binding to eRF1. Furthermore, several initiation factors like eIF2, 2D, 3, 1 and 5 show interactions with ABCE1 linking recycling to translation initiation as well (Pisarev et al., 2007).

1.2 Principles of eukaryotic translational control

Protein synthesis is a complex and energy consuming process involving a multitude of factors (Rolfe & Brown, 1997). Therefore, eukaryotic cellular systems have evolved with various strategies to control and regulate translation. Furthermore, regulation of protein synthesis has been shown to play a central role during cellular development and differentiation, response to infection, stress and many other external stimuli as well. Apart from transcriptional control and mRNA stability, translational control is the most determining factor for final protein levels (Hershey et al., 2012).

Translational control of gene expression provides multiple advantages. First, the response at the level of translation circumvents the need for mRNA synthesis, processing and its export to the cytosol. The majority of eukaryotic mRNAs have a half-life of longer than 2 h (Raghavan et al., 2002), therefore regulating translational efficiency and protein degradation rates can rapidly alter cellular proteome homeostasis. Second, a majority of the translational control pathways are rapidly reversible; this is a significant advantage to mount quick responses. Third, localized translation provides spatial control within the cells, such as synthesis of membrane proteins, secretory proteins etc. Notably, spatial control of translation is shown to be important for synaptic development and memory formation. Finally, translational control mechanisms exist, that can affect several transcripts globally or can be specific for an individual transcript (Gebauer & Hentze, 2004).

1.2.1 Translational regulation by eIF2α kinases

Global pathways rapidly alter the translational status of several transcripts and are mediated via modification of translation initiation factors. Especially during limiting conditions, this enables the cell to conserve energy and divert resources for selective translation to alleviate stress. One of the well-studied

mechanisms to down regulate global translation is mediated by eIF2α kinases, which inhibit the formation of active ternary complex (eIF2-GTP-Met-tRNAi) required for initiator tRNA delivery. During stress, the α-subunit of eIF2 gets phosphorylated at Ser51; phosphorylated eIF2α inhibits the activity of eIF2B to exchange GDP with GTP (Wek, 2018). eIF2α phosphorylation reduces cap dependent translation by limiting the delivery of initiator tRNA for translational initiation. There are four eIF2α kinases in vertebrates (Wek, 2018), namely heme-regulated inhibitor (HRI), protein kinase R (PKR), protein kinase R-like endoplasmic reticulum kinase (PERK) and general control nonderepressible 2 (GCN2). These kinases can sense various cellular perturbations to down regulate global translation by eIF2α phosphorylation.

1.2.2 Regulation of cap dependent protein synthesis by the mTOR kinase

mTOR (mechanistic target of rapamycin) is a phosphatidylinositol 3-kinase-related kinase (PIKK) conserved from yeast to mammals. In mammals, mTOR exists as two functional complexes: mTORC1 and mTORC2 (Loewith et al., 2002). Rapamycin sensitive mTORC1 affects translation by regulating the activity of various factors associated with translation initiation and additionally the function of eEF2 as well. Direct substrates of mTORC1 affecting translation include eIF4E-BP1, S6Ks (S6 kinases -1 and -2), eIF4G and eEF2K. Activated mTORC1 enhances cap-dependent protein synthesis, and this complex is at the nexus of various cellular pathways (PI3K-Akt, Ras-ERK, TNFα, Wnt). The mTORC1 complex is also sensitive to intracellular energy and nutrient levels, therefore integrating both intra- and extracellular metabolic signals to regulate global protein synthesis (Ma & Blenis, 2009).

1.2.2.1 Translational regulation during the maturation of dendritic cells

Dendritic cells (DCs) are the professional antigen presenting cells of the immune system, and are uniquely equipped to stimulate naïve T-cells (Hubo et al., 2013; Segura & Amigorena, 2013). DCs are ubiquitously present in the peripheral tissues as immature state. In this state they constantly sample the environment and process intra- or extracellular antigens, and further present the processed peptides either on MHC-I or II complexes.

DCs sense the invading pathogens with the pattern recognition receptors (PRR) such as toll-like receptors (TLR), nucleotide binding oligomerization domain (NOD)-like receptors, retinoic acid inducible gene I (RIG-I)-like receptors (RLR) or C-type lectins (Walsh & Mills, 2013). Upon encountering an antigen through one of the PRRs, immature DCs are differentiated into mature DCs, and induce T-cell mediated immunity. Given that DCs can be used to elicit tumor specific T-cell mediated, for more than past two decades they have been used for cancer immunotherapy (F. J. Hsu et al., 1996).

During the maturation process, DCs undergo a dramatic change in their morphology developing cellular projections. Mature DCs thereby have increased surface area and ability to stimulate T-cells (Hubo et al., 2013). Further, major maturation events are marked by increased surface expression of co-stimulatory and MHC molecules, secretion of cytokines (such as IL12), and up-regulation of the homing receptor CCR7 resulting in enhanced migratory capacity of mature DCs (Figure 1.2). This enables mature DCs to enter T-cell resident areas such as secondary lymphoid organs (Dieu et al., 1998; Sallusto & Lanzavecchia, 2000). Another property of mature DCs is to cease antigen uptake and processing, thereby the antigens presented to T-cells represent the current state of the inflammation site. These processes finally transform immature DCs to mature DCs with potent ability to induce and differentiate T-cells, profoundly impacting their homeostasis.

Maturation of DCs also alters their metabolic patterns and biosynthetic requirements (Pearce & Everts, 2015). Such drastic phenotypic changes during maturation need to be accompanied by remodeling of their proteome. At the same time, DCs need to sense the available nutrients in the environment and adapt accordingly to support the rapid synthesis of cytokines, co-stimulatory and MHC molecules after stimulation. A cellular regulator that can integrate extracellular signals and also affect translation is mTOR (Laplante & Sabatini, 2012; Weichhart et al., 2015). One of the activators of mTOR includes TLR ligands, and accordingly mTOR plays a central role in reprogramming translation and metabolism during DC maturation (Jovanovic et al., 2015).

LPS (lipopolysaccharide) stimulated DCs show tight temporal regulation of protein translation. The DC maturation process can be classified into two phases namely early (up to 4 h) and late stages of maturation (24 or 48 h). The early phase is marked by rapid increase in cap-dependent protein synthesis and peaks at about 4 h. This increase in translation is mainly mediated via the PI3K-Akt-mTORC1 pathway (Lelouard et al., 2007). Polysome profiling analysis of LPS stimulated DCs further revealed the translational regulation of mRNAs encoding for ribosomal proteins and transcripts associated with antigen processing and presentation. Specifically, these transcripts were engaged by polysomes at the early phase of maturation, and disengaged during the later stage of maturation (Ceppi et al., 2009).

Later stages of maturation are marked by increased cap independent protein synthesis facilitated by eIF2α phosphorylation. Further during this stage there is increased production and degradation of eIF4GI and eIF4GI-like factor DAP5, correlating with the inhibition of cap-dependent translation. It has also been shown that the switch to cap-independent translation during the later stages is critical for synthesis of anti-apoptotic factors (Lelouard et al., 2007). Taken together, translational regulation plays an essential role during the maturation process and also necessary for the survival of mature DCs.

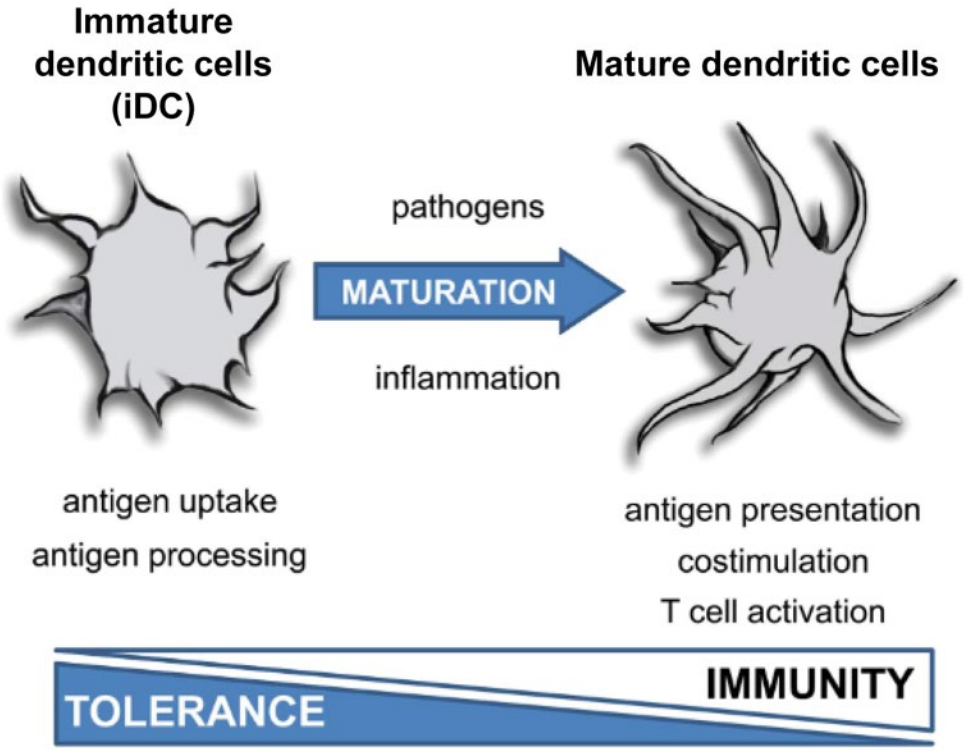

Figure 1.2 Maturation state determines the function of dendritic cells.

Foreign pathogens and inflammatory signals stimulate the differentiation of immature dendritic cells (iDC) to terminal mature dendritic cells. This results in dramatic change in cellular morphology; thereby leading to mature DCs with increased capacity to present processed antigens. Importantly, mature DCs further engage with T-cells to elicit T-cell specific responses. Figure adapted from (Hubo et al., 2013) .

1.2.3 Translational regulation by the 5' untranslated region

Canonical translational initiation in eukaryotes involves cap recognition and formation of scanning-competent 48S PIC. Stable elements such as RNA G-quadruplex (Halder et al., 2009; Kumari et al., 2008) and cap-proximal hairpin structures in 5' UTR are detrimental for mRNA translation, since they would impede the scanning of small subunit during initiation (Figure 1.3). Certain structural elements can be unwound by DEAD-box adenosine triphosphate (ATP) dependent RNA helicases. Ded1 (DDX3 in mammals) and eIF4A are the two RNA helicases in yeast, and their activity seems to be specialized to certain types or locations of the structural elements in the 5'UTR (Sen et al., 2015). Some structural elements can recruit proteins under certain conditions to form a stable ribonucleoprotein complex, which can also impede the

scanning process. A well-studied example is the iron response element (IRE) (W. et al., 1987) present in the 5' UTR recruiting iron regulatory protein (IRP) under low-iron conditions to inhibit translational initiation.

In contrastingly, highly structured RNA elements in the 5' UTR called internal ribosome entry sites (IRES) can directly recruit 40S ribosomes internally onto 5'UTR for translation initiation (Figure 1.3). IRESs do not require a 5' cap or a free 5' end, and are pretty diverse in their structure and composition. Depending on the type, IRESs may need a range of eIFs and IRES trans-activating factors (ITAFs). ITAFs are RNA chaperones that bind to IRESs to enhance or repress their activity. The simplest known IRES is the *Discitroviridae* intergenic region (IGR) IRES, requiring neither eIFs nor ITAFs for translational initiation. IRESs were initially discovered in viruses and later in cellular mRNAs as well. During stress, when cap dependent initiation is inhibited, these limiting conditions are reversed by translation of cellular mRNA containing IRESs (Jackson, 2013).

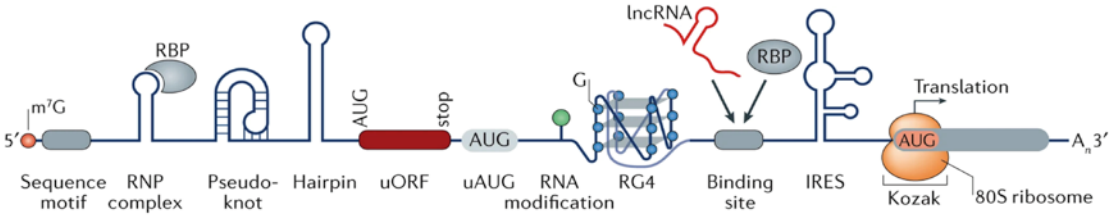

Figure 1.3 RNA sequence and structural elements in eukaryotic 5' UTR regulating mRNA translation.

Eukaryotic mRNA contains the 7-methylguanosine (m^7G) 5' cap structure and the poly-A tail (A_n) at the 3' end of the mRNA. These elements stabilize the mRNA and stimulate translation. 5' UTR also contains structural and sequence elements that can affect translation. Upstream open reading frames (uORF) and upstream start codons (uAUG) mainly inhibit translation. While the context of Kozak sequence around the start codon can significantly influence translation initiation. Secondary structures such as pseudo-knot, hairpin and RNA G-quadraplexes impede ribosomal scanning thereby inhibiting translation initiation. Structures such as internal ribosome entry sites (IRES) can recruit ribosomes independently of the cap structure for initiation of translation. Figure adapted from (Leppek et al., 2018).

Genome wide sequencing has revealed the presence of upstream ORFs (uORFs) in approximately 50% of mammalian mRNAs. Moreover, ribosome-profiling studies have revealed increased ribosome occupancy over

these uORFs indicating pervasive translation. A majority of uORFs functions to down regulate main ORF translation in a couple of ways. First, translation of an uORF can preclude re-initiation at the main ORF or translation termination at the uORF can destabilize mRNAs by pathways that degrade mRNAs with a premature termination codon. Second, certain uORFs function as ligand dependent ribosome stallers, as in the case of arginine-responsive yeast *CPA1* (Gaba et al., 2005) or spermidine-responsive *ADM1* (Raney, Law, et al., 2002). Ribosomal stalling creates a roadblock for downstream re-initiation at the main ORF; therefore, uORFs provide translational control based on intracellular conditions. A process called leaky scanning overcomes the inhibitory effects of uORFs. Leaky scanning is supported by uORFs containing start codons in a suboptimal context, and this process is prevalent during stress induced eIF2α phosphorylation. Interestingly, some of the stress alleviating genes are preferentially translated under limiting conditions using this mechanism (S. K. Young et al., 2015).

Certain sequences in 5’ UTR can also serve as regulatory elements such as TOP (terminal oligopyrimidine) mRNAs. TOP mRNAs contain oligopyrimidine sequence motifs at their very 5’ end. TOP mRNAs encode for most of the ribosomal proteins and are preferentially translated during mTORC1 activation (Gandin et al., 2016). Another important sequence element in the 5’ UTR is the Kozak sequence motif (Kozak, 1986). It helps in improved recognition of the start codon and is present in most of the highly translated mRNAs.

1.2.4 Translational regulation by 3’ untranslated region

3’ UTRs are much longer than 5’ UTRs in eukaryotes, and primarily affect mRNA stability, localization and translation through RNA binding proteins (RBP) and microRNAs (miRNAs) (Mayr, 2019). Presence of AU-rich elements in the 3’ UTR highlights the complexity of 3’ UTR mediated regulation of gene expression. Initially it was thought to destabilize mRNA, thereby drastically reducing protein output levels (C. Y. Chen et al., 2001; Lykke-Andersen & Wagner, 2005). However, later studies show that AU-rich elements can sometimes serve as a temporal switch to regulate translation (Kontoyiannis et al., 1999), and have also been shown to interact with at least 10 RNA-binding

proteins (RBPs) (Barreau et al., 2005; Brennan & Steitz, 2001; C. Y. Chen et al., 2001; Lebedeva et al., 2011). Binding of tristetraprolin (TTP) to AU-rich elements results in recruitment of the exosome, a complex that degrades mRNA (Figure 1.4). In contrast, binding of HuR stabilizes AU-rich elements containing mRNAs (C. Y. Chen et al., 2001). Moreover, RBPs bound to the 3' UTR can serve as adapters for recruitment of effector proteins, leading to some of the 3' UTR mediated observed effects (Figure 1.4).

Different alternate 3'UTR isoforms have varying capacity to interact with RBPs. It is interesting to note that the function encoded in the sequence of the 3' UTR can be transferred to the protein. 3' UTRs have expanded vastly in higher organisms, and may well contribute to the higher organismal complexity by influencing post-translational protein modification, localization, PPI and protein complex formation (Mayr, 2019).

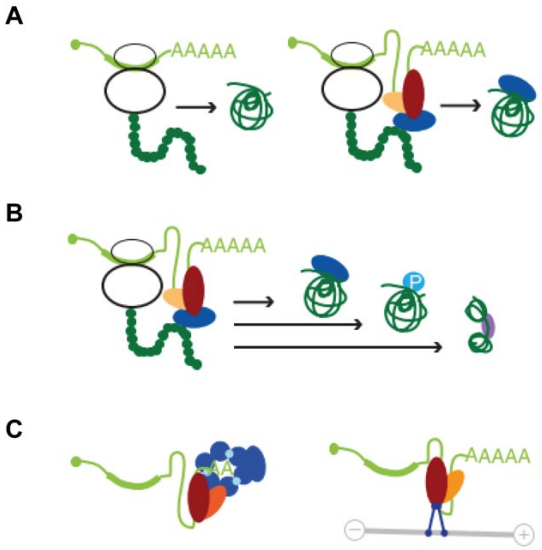

Figure 1.4 Functional roles of the 3' untranslated region.

A. 3' UTR (light green) contains sequences that are recognized by various RNA binding proteins (RBPs shown in red, orange and blue), which then interact with the translated protein. Alternative 3' UTRs affect this protein-protein interaction (PPI) although the CDS encodes for the same protein. In the example depicted here only the longer 3' UTR isoform (right) can mediate PPI while the shorter isoform cannot (left). B. 3' UTR dependent PPI affects diverse protein features. Proteins recruited by the 3' UTR can be involved in complex formation, post-translational modification (P) of the protein and also stimulate protein folding. C. At the mRNA level 3' UTR affects stability as well as localization by recruiting various effector proteins such as exosome (blue, left) or motor proteins (right). Figure adapted from (Mayr, 2019).

1.2.5 Nascent chain mediated control of translation

During translation elongation, the rate of peptide bond formation between amino acids is not uniform (Wohlgemuth et al., 2008), but depends on the chemistry and geometry of the incoming amino acid or combination of amino acids in the peptidyl transferase center (PTC). An unfavorable combination of amino acids can reduce the speed of elongation, and in certain cases can cause translational arrest (Ito & Chiba, 2013). Proline with its unique chemistry is both a poor acceptor (Johansson et al., 2011; Pavlov et al., 2009) and donor of electrons (K. et al., 2013; Muto & Ito, 2008; Wohlgemuth et al., 2008) during peptide bond formation. Consecutive proline residues are problematic for ribosomes to synthesize, and cause translational stalling during elongation and termination (Tanner et al., 2009; Woolstenhulme et al., 2013) (Figure 1.5B). Therefore, there exists a specialized factor both in prokaryotes and eukaryotes to alleviate such stalls, namely elongation factor P (EF-P) in bacteria (K. et al., 2013; Susanne et al., 2013) and eukaryotic initiation factor 5A (eIF5A) in eukaryotes (Gutierrez et al., 2013). These factors aid through translation of poly-Pro regions on mRNA by decreasing the activation energy needed for the formation of subsequent peptide bonds through favorable entropy change (Doerfel et al., 2015). Ribosome profiling of EF-P-lacking bacteria showed significant stalling events on poly-Pro stretches (Woolstenhulme et al., 2015). A cryo-EM structure of EF-P bound to a stalled ribosome revealed that EF-P stabilizes the conformation of the nascent chain and tRNAs, for efficient translation (Huter et al., 2017). EF-P cellular levels and in combination with poly-Pro stretches affects the expression levels of corresponding proteins (Elgamal et al., 2014). A mouse ribosome profiling study identified several proline-containing motifs that cause ribosomal stalling (Ingolia et al., 2011). Also, a stretch of basic amino acids such as lysine or arginine was also shown to cause elongation stalling in eukaryotes (Brandman et al., 2012; Dimitrova et al., 2009; Koutmou et al., 2015; J. Lu & Deutsch, 2008). Proline is shown to be present in several prokaryotic leader peptides, which typically regulate the expression of a downstream gene by programmed ribosomal stalling (Wilson et al., 2016).

1.2.6 Nascent chain mediated translational arrest

Nascent chains containing a ribosomal arrest peptide (AP) can stall or temporarily pause ongoing ribosomal translation to regulate the expression of a downstream gene. Proline-rich antimicrobial peptides typically act *in trans* by binding within the ribosomal exit tunnel to modulate translation (Roy et al., 2015; Seefeldt et al., 2015), while, APs act *in cis* to regulate expression during their own translation (Figure 1.5A). Typically, APs are approximately 20 amino acids in length, and several have been identified in prokaryotes (secretion monitor [SecM], vibrio export monitoring peptide [VemP] (Ishii et al., 2015), MifM and, TnaC (Gong et al., 2001)) and in eukaryotes (human cytomegalovirus upstream open reading frame 2 [hCMV uORF2], arginine attenuator peptide [AAP], S-adenosine methionine decarboxylase uORF [SAM-DC uORF], and AMD1 (Yordanova et al., 2018)) as well. Depending on the type they can either inhibit translation elongation (Figure 1.5A) (SecM, VemP) (Ishii et al., 2015; Su et al., 2017; Tsai et al., 2014) or termination (TnaC, CMV *gp48* uORF2 and SAM-DC uORF) (Gong et al., 2001; Janzen et al., 2002; Raney, Lynn Law, et al., 2002) or both in certain cases (MifM, ErmCL and AAP) (Chiba & Ito, 2012; Fang et al., 2000). APs inhibiting the elongation step can arrest ribosomes at a specific position (VemP and ErmCL) or at multiple sites (SecM, MifM) (Ito & Chiba, 2013).

Certain APs have the intrinsic property to arrest translation (SecM, VemP, CMV uORF2), while others need an additional co-factor such as tryptophan for TnaC (Gong & Yanofsky, 2002), arginine for AAP (Z. Wang & Sachs, 1997) and polyamines for SAM-DC uORF (Law et al., 2001) to exert their function. Considering that ribosomes are conserved, it is predictable that APs can induce ribosome stalling in other species as well. AAP from the fungus *Neurospora crassa* or the arrest peptide from *Arabidopsis thaliana* CGS1 have been both shown *in vitro* to stall yeast, rabbit reticulocyte and wheat germ ribosomes (Fang et al., 2004; Spevak et al., 2010). Likewise, the product of hCMV *gp48* uORF2 (“CMV stalling” peptide) arrests not only human ribosomes (Matheisl et al., 2015), but also ribosomes in wheat germ, rabbit reticulocyte, *Drosophila melanogaster* and yeast translation systems (Bhushan et al., 2010). Yet, other APs such as MifM and SecM are strictly species specific. For example, ribosomes of the Gram-positive bacterium

Bacillus subtilis are sensitive to MifM-mediated translational stalling, while Gram-negative *Escherichia coli* ribosomes are not inhibited. Similarly, an opposite effect is observed with the SecM arrest peptide (Chiba et al., 2011). Also, some of the APs are force-sensitive. meaning the arrested state of the ribosome can be rescued by application of force (VemP, SecM and MifM) (Butkus et al., 2003; Chiba et al., 2009; Ishii et al., 2015; Ismail et al., 2012), while, some APs are dead-end ribosome stallers (TnaC) and are being targeted by decay pathways.

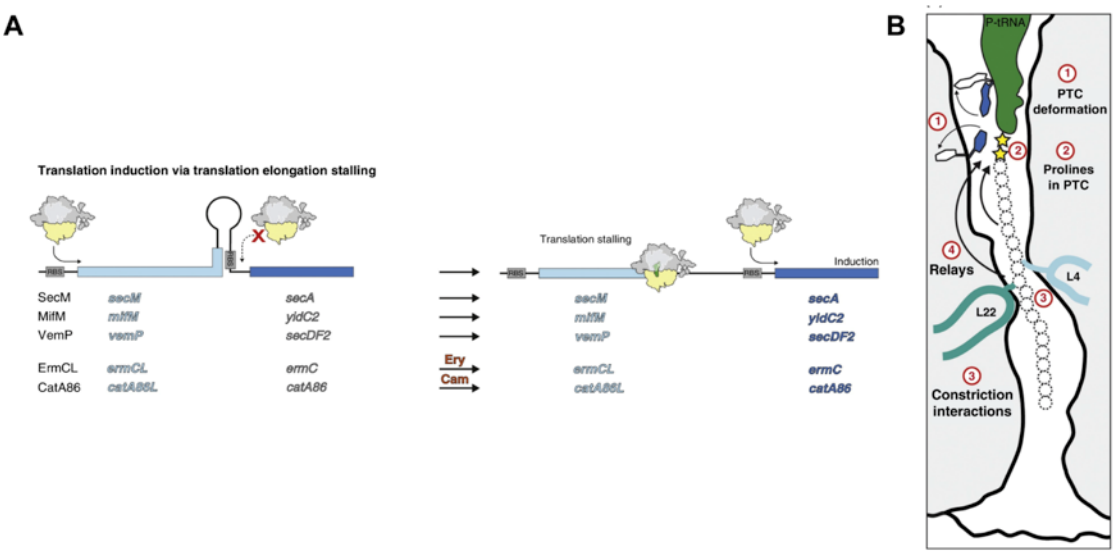

Figure 1.5 Mode of action by ribosomal arrest peptides (APs).

A. Translational elongation stalling mediated by leader peptides of SecM, MifM, VemP, ErmCL and CatA86 prevent stem-loop formation. This results in the exposure of ribosome binding site (RBS) and thereby translation of downstream genes. B. Common modes by which ribosomal APs inhibit translation. Severe deformation of peptidyl transferase center (PTC) (1), consecutive proline residues of the nascent chain at the PTC (2), strong interactions between the nascent chain and the ribosomal exit tunnel (3), and information relays through the ribosome and/or nascent chain to the PTC (4), resulting in its deformation. Figure adapted from (Wilson et al., 2016).

Cryo-electron microscopy (cryo-EM) has enabled to visualize various bacterial APs (Arenz, Meydan, et al., 2014; Arenz, Ramu, et al., 2014; Bhushan et al., 2011; Sohmen et al., 2015; Su et al., 2017) in the ribosomal exit tunnel, and provided unprecedented insights into their mode of function. These structures revealed the extensive contacts made by APs with the exit tunnel of the LSU and shed light on the conformations adopted by each AP to

inhibit ribosome function. It is interesting to note that there is no general consensus in the conformation of AP in the tunnel, as they can be in an extended conformation or form a secondary structure such as α-helix within the tunnel (Matheisl et al., 2015; Su et al., 2017). The tunnel wall interaction occurs primarily between the PTC and the constriction site of the exit tunnel. These interactions with the AP restrict or reposition some of the critical bases (A2602, U2585 and U2506 in bacteria) constituting the PTC, thereby inhibiting ribosomal function (Wilson et al., 2016) (Figure 1.5B).

Bacterial ribosome stallers positively regulate the expression of downstream gene(s) in two ways. First, in the case of TnaC, via anti-termination of transcription, ribosomal stalling occludes the Rho binding site for transcription termination (Ito & Chiba, 2013; Wilson & Beckmann, 2011). TnaC is part of the tnaCAB operon where *tnaA* and *tnaB* encodes for tryptophanase (TnaA) and tryptophan-specific permease (TnaB). TnaC is a co-factor-dependent ribosome staller and its stalling is dependent on the presence of the small molecule, the amino acid L-tryptophan (L-Trp). C-terminal part of TnaC encodes for an AP that arrests ribosome during translation termination. A spacer between *tnaC* and *tnaA* contains the Rho binding site, and ribosomal stalling shields this region resulting in anti-termination of transcription, and induction of downstream genes *tnaA* and *tnaB* during high intracellular levels of free L-Trp.

Second, ribosomal stalling can induce mRNA conformational changes to expose the Shine-Dalgarno sequence, which leads to ribosomal binding and subsequent translation of the downstream gene (for example in SecM, MifM, ErmCL, Cat86L) (Figure 1.5A) (Wilson & Beckmann, 2011). In contrast, eukaryotic uORF ribosome stallers repress the expression of main ORF as in the case of “CMV-stalling”, AAP and Sam-DC. CMV uORF2 inhibits ribosomal scanning and initiation at the downstream gp48/UL4 gene (Degnin et al., 1993; Geballe et al., 1986). Mammalian ribosome profiling studies have identified several ribosomal stalling sites within the coding region of the genome (Arpat et al., 2020; Ingolia et al., 2011). Further studies are required to understand the biological role of these newly identified ribosomal stalling sites. One of the best-characterized mammalian ribosome stallers with a known function is the arrest peptide of X-box binding protein-1 unspliced

(XBP1u-AP). Ribosome arresting activity of XBP1u-AP plays a critical role in mediating the mammalian unfolded protein response (UPR).

1.2.7 UPR

Approximately one third of the proteome that is destined for extracellular secretion, the plasma membrane, lysosomes, and Golgi apparatus traverse through the endoplasmic reticulum (ER). The ER is also the major site for production of lipids (Jacquemyn et al., 2017) such as cholesterol, glycerophospholipids, and ceramide, and plays a critical role in the regulation of calcium storage. The ER harbors specialized enzymes and chaperones, and provides an environment for post-translational protein modification and folding (Schwarz & Blower, 2016). Intracellular perturbations such as glucose deprivation, aberrant calcium regulation, oxidative stress, and viral infection lead to accumulation of unfolded or misfolded proteins causing ER stress. During ER stress folding capacity of the organelle is challenged, and this leads to activation of UPR pathways to restore folding capacity and to maintain proper protein homeostasis (Walter & Ron, 2011).

In mammals, there are three distinct branches of UPR and its activation leads to production of bZIP transcription factors that work alone or in unison to activate the UPR target genes (Figure 1.6). The three ER membrane-resident sensors are activating transcription factor 6 (ATF6), double stranded RNA-activated protein kinase like ER-kinase (PERK) and inositol-requiring enzyme 1 alpha (IRE1α). During unstressed conditions the lumenal domain of all three sensors is bound by the ER-resident chaperone binding immunoglobulin protein (BiP or Grp78), thus keeping them inactive. The presence of misfolded proteins during ER stress titrates BiP away from the sensors (Anne Bertolotti et al., 2000; Okamura et al., 2000), thereby promoting dimerization and autophosphorylation to activate IRE1α and PERK, while ATF6 is activated by a regulated membrane proteolysis.

One of the adaptive responses to ER stress is to transiently shutoff global translation to reduce the flux of newly synthesized proteins translocating into the ER. During ER stress, PERK serves this purpose by phosphorylating eIF2α to globally reduce translation initiation (Kaufman, 2002; Ron & Walter, 2007) (Figure 1.6), although under these limiting conditions,

selective mRNAs that contain one or multiple uORFs within the 5' UTR are still translated (T E Dever et al., 1992; P. D. Lu et al., 2004; Vattem & Wek, 2004; Yaman et al., 2003). One such mRNA is *ATF4* mRNA, encoding a stress-responsive transcription factor that can activate genes involved in protein synthesis, amino acid metabolism, redox homeostasis, apoptosis and autophagy. ATF4 restores protein synthesis by being part of the pathway to dephosphorylate eIF2α (J. Han et al., 2013; H P Harding et al., 1999; Heather P Harding et al., 2003).

During ER stress ATF6 transits from ER to the Golgi apparatus, where site-1- and site-2-protease (S1P and S2P) process ATF6 to release a fragment termed as ATF6p50, which is an active transcription factor (Figure 1.6). Of the three, the IRE1α branch is the most evolutionarily conserved pathway (Mori, 2009), and also being the only sensor present in lower eukaryotes. In mammals IRE1α acts via the *XBP1u* mRNA, to splice *XBP1u* (unspliced) mRNA to *XBP1s* (spliced) mRNA, coding for the transcription factor XBP1s (Figure 1.6). XBP1s together with ATF6/p50 activates genes coding for ER resident chaperones and enzymes to increase ER protein translocation, folding, maturation and secretion capacity. Also, both these transcription factors promote biogenesis of ER and Golgi apparatus, thereby increasing the overall secretory capacity of the cell during ER stress.

.

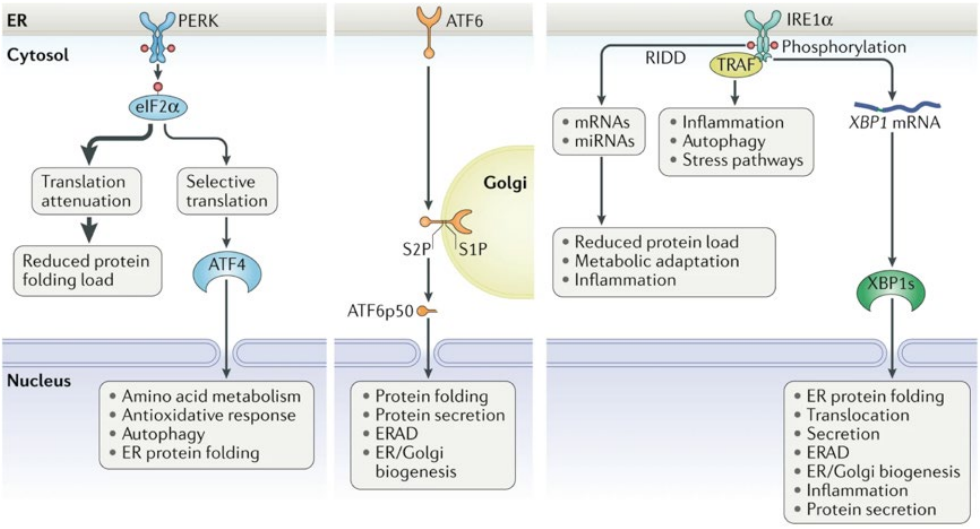

Figure 1.6 UPR pathways.

(1) During endoplasmic reticulum (ER) stress, PERK phosphorylates eIF2α leading to global reduction in translation initiation. Although under these conditions some mRNAs are preferentially translated, such as *ATF4* mRNA. ATF4 is a transcription factor, and it activates UPR target genes involved in amino acid biosynthesis, the antioxidative response, autophagy and apoptosis. (2) From the ER ATF6 transits to the Golgi apparatus, where it is processed by the S1P (site-1-protease) and S2P (site-2-protease) proteases giving rise to an active cytosolic fragment ATF6p50. This active fragment can migrate to the nucleus to initiate transcription of UPR target genes involved in the ER secretion and protein folding homeostasis. Further, it can also activate genes to initiate ER and Golgi biogenesis. (3) Activated IRE1α splices *XBP1u* mRNA to *XBP1s* mRNA, which encodes for the transcription factor XBP1s. XBP1s activates genes to increase protein folding and secretion capacity of the ER and the Golgi apparatus. IRE1α cleaves the ER associated mRNAs or functional non-coding RNAs through regulated IRE1α dependent decay (RIDD). This result in the influx reduction of newly synthesized proteins into the ER, thereby modulating its protein folding capacity. Under non-canonical ER stress conditions, cytosolic domain of the IRE1α can act as a scaffold to recruit adaptor proteins, such as tumor necrosis factor receptor-associated factor (TRAF) family members, resulting in the activation of inflammatory responses. Figure adapted from (Hetz et al., 2020).

1.2.8 The IRE1α - XBP1 pathway in UPR

IRE1 has two paralogs in mammals; IRE1α and IRE1β. IRE1α is ubiquitously expressed in all tissues while IRE1β is restricted to intestinal epithelia (A Bertolotti et al., 2001). IRE1α is a bifunctional transmembrane signal transducer with kinase and endo-ribonuclease (RNase) activities. Once activated, the RNAse domain of IRE1α cytoplasmically cleaves the *XBP1-unspliced* (*XBP1u*) mRNA at specific sites on the ER membrane to excise a

26 base unconventional intron (Calfon et al., 2002; Yoshida et al., 2001). The cleaved *XBP1u* mRNA is re-ligated by the ligase RtcB to generate *XBP1-spliced* mRNA (XBP1s). Translation of *XBP1s* mRNA generates the active transcription factor XBP1s, which can translocate into nucleus to transcriptionally upregulate UPR genes responsible for increasing ER abundance, lipid biosynthesis, and chaperones (Shaffer et al., 2004; Sriburi et al., 2004).

In order to be spliced by IRE1α during ER stress, the cytoplasmic *XBP1u* mRNA is targeted to the ER membrane by an ingenious mechanism. XBP1u contains two hydrophobic regions, HR1 and HR2, and also a very C-terminal ribosome AP which transiently pauses translation (Yanagitani et al., 2009, 2011). During this pause the HR2 domain is exposed outside of the ribosomal tunnel and is used to encounter components of the co-translational protein translocation pathway, such as the signal recognition particle (SRP) or the Sec61 complex (Figure 1.7) (Kanda et al., 2016). Once being bound to the ER-membrane via the Sec61 complex, *XBP1u* mRNA can be spliced by IRE1α (Kanda et al., 2016; Plumb et al., 2015), an unconventional splicing event on the ER membrane. Given the moderate hydrophobicity of HR2 domain, translational pausing mediated by the XBP1u AP is obligatory for SRP recruitment by HR2 domain. Therefore, the localization of *XBP1u* mRNA on the ER membrane is dependent on translational pausing mediated by its C-terminal ribosomal AP. Truncation analysis showed that C-terminal 26 residues (position 236 – 261, full length numbering) of XBP1u contribute to translational pausing. This region is evolutionarily conserved, and alanine-scanning mutagenesis revealed 14 out of 26 residues that are critical for translational pausing. It is interesting to note that XBP1u AP with a S255A mutation elongates the duration of the pause (Yanagitani et al., 2011).

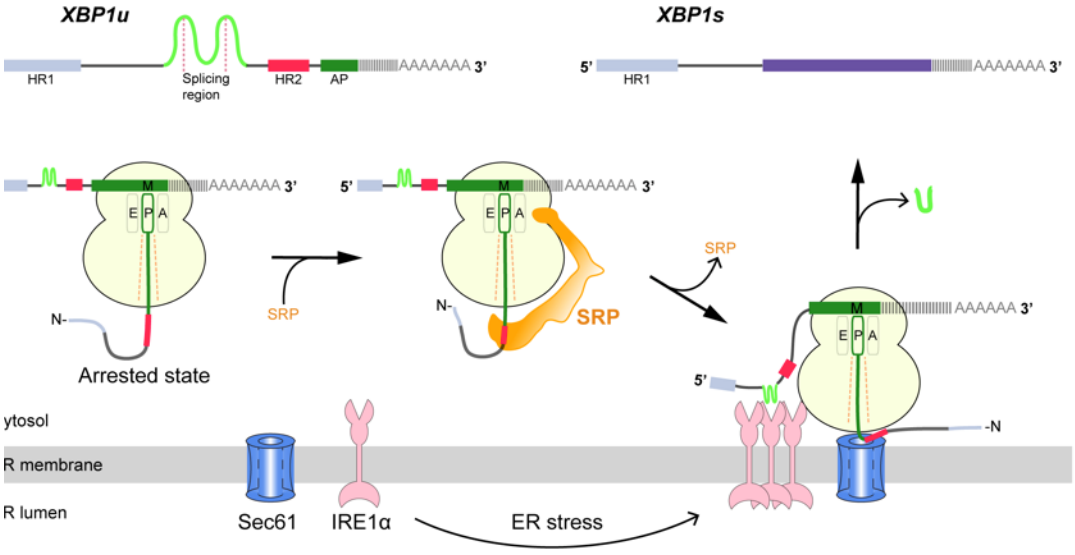

Figure 1.7 Overview of the IRE1α-XBP1u pathway in mediating UPR.

Interaction of the XBP1u nascent peptide with the ribosomal exit tunnel leads to translational pausing with the HR2 domain exposed outside. Paused state of this ribosome-nascent chain complex (RNC) enables successful recruitment of SRP and subsequent transfer to the Sec61 complex located in the ER membrane. During ER stress IRE1α is localized near Sec61, therefore can splice *XBP1u* mRNA to *XBP1s* mRNA, which then encodes for the active transcription factor XBP1s.

1.3 Ribosomal profiling, a genome-wide technique to investigate translation

Genetic information is decoded in two steps, namely transcription and translation. Techniques like microarray and RNAseq have enabled steady-state measurement of mRNA abundance for hundreds and thousands of genes, and its analysis revealed the critical role of transcriptional control in gene expression. Although transcriptional levels correlate strongly with protein abundance, translational control also plays a definitive role in determining final protein levels. Therefore, studying translational regulation would provide rich insights into the final stage of gene expression.

One of the techniques that can be used for investigating the *in vivo* translational landscape is ribosome profiling. Nicholas Ingolia developed this

technique, while in the lab of Jonathan Weissman. Since its introduction (Ingolia et al., 2009), it has been widely used to study translation in bacteria (Li et al., 2012; Oh et al., 2011), fungi (Kasari et al., 2019; Wallace et al., 2020), plants (Merchante et al., 2015; Zoschke et al., 2013), mouse embryonic stem cells (Ingolia et al., 2011), viruses (Irigoyen et al., 2018; Stern-Ginossar et al., 2012) and human cells (Fields et al., 2015; Guo et al., 2011). Ribosome profiling has enabled to monitor all aspects of protein synthesis in a global manner. Steady-state estimation of ribosome density over individual mRNAs correlates better with protein amounts in comparison to transcriptome levels.

Ribosomes translating an mRNA template typically protect a fragment of approximately ≈ 28 - 30 nts of mRNA upon nuclease treatment (Steitz, 1969). Ribosome profiling involves sequencing of these ribosome-protected mRNA fragments (RPFs or ribosomal footprints) using the next-generation-sequencing (NGS) technology. Each sequenced RPF reveals the mRNA that is being translated, and also the position of the ribosome on the transcript.

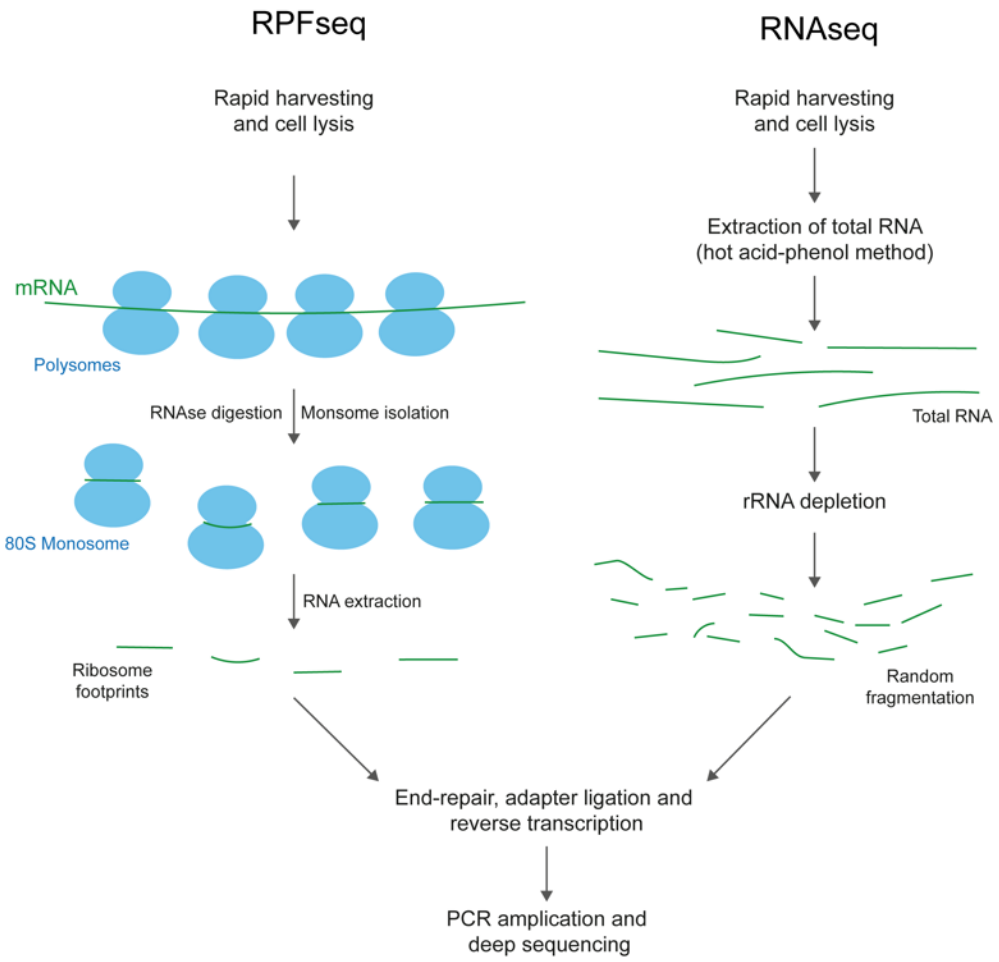

Figure 1.8 Schematic overview of ribosome profiling.

Cells are harvested and lysed, and ribosomes remain bound to mRNA thereby forming polysomes. RNAse I treatment digests the exposed mRNA but the bound ribosome physically protects a small fragment of this mRNA which is termed as the ribosome protected fragment (RPF) or ribosomal footprint. Generated monosomes are isolated by sucrose gradient centrifugation, and ribosomal footprints are extracted by size selection. In parallel, for RNAseq, total RNA is extracted, followed by removal of rRNA fragments and heat fragmentation in alkaline conditions. Further, both ribosomal footprints and fragmented total RNA are converted into DNA libraries for deep sequencing.

The technique involves isolation of ribosomes in a physiological context for inferring useful biological insight. In order to arrest translating ribosomes on mRNAs, prior to lysate preparation samples are treated either with translation elongation inhibitors such as cycloheximide (CLX) or chloramphenicol, or rapidly frozen to prevent ribosomal run-off. After cell lysis, the lysate is treated with a nuclease in order to collapse polysomes into

monosomes (Figure 1.8, left). Nuclease treated lysate is centrifuged through sucrose gradient solution using ultracentrifugation for monosome isolation. Footprints from these monosomes are extracted by size selection and further converted into a DNA library for deep sequencing. With the exact same biological lysate, RNAseq libraries are also prepared in parallel to account for transcriptome levels (Figure 1.8, right). The density of ribosomal footprints on the mRNA template represents the protein synthesis rate, while normalizing for mRNA levels provides translational efficiency for each mRNA. With the advent of improved sequencing technology, comprehensive sampling of RPFs has been made possible, providing a global snapshot of the translational landscape. Ribosome profiling data is quantitative in nature, and often with sub-codon resolution.

1.3.1 Monitoring cotranslational processes by selective ribosomal profiling

Ribosome profiling has also provided insights into co-translational processes during protein synthesis. There are several cellular factors that interact with ribosomes cotranslationally, which are often dependent on the synthesized nascent chain. Previously, there has been lack of techniques to systematically investigate these cotranslational interactions at a genome wide scale. Ribosome profiling of ribosomes co-purified with a factor of interest is performed, in addition to ribosome profiling of all cytosolic ribosomes. This method is broadly termed as selective ribosome profiling (SeRP) (Figure 1.9). Analysis of SeRP data reveals several properties of the cotranslational factor of interest, such as its substrate specificity, its point of cotranslational engagement, and how often does it interact with its substrates. SeRP has been performed with various ribosome interacting factors such as SRP (Chartron et al., 2016; Schibich et al., 2016) (Figure 1.9), trigger factor (TF) (Oh et al., 2011) and Hsp70 chaperone Ssb (Döring et al., 2017). These studies expanded the pool of substrates engaged by these factors and deciphered the determinants for cotranslational recruitment.

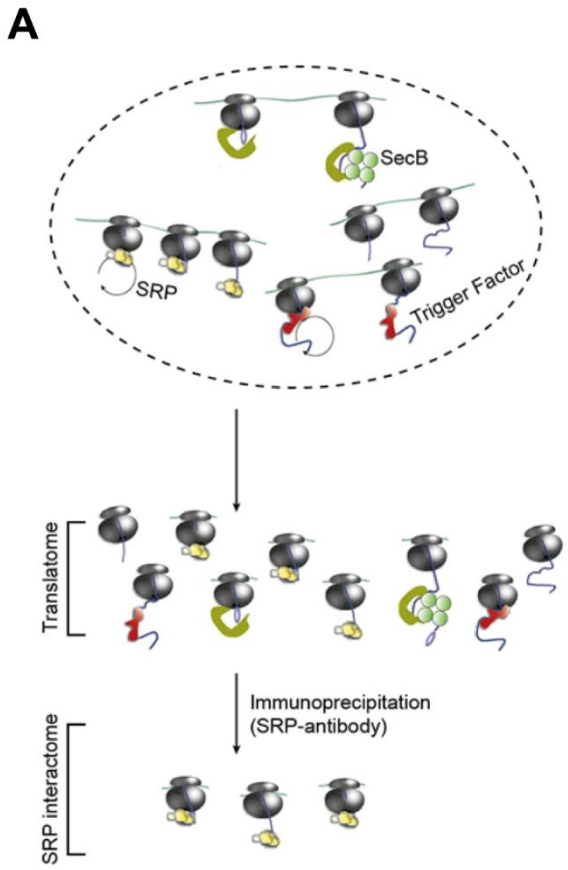

Figure 1.9 Selective ribosome profiling (SeRP).

SeRP involves ribosome profiling of ribosomes co-purified with a factor of interest (SRP, as shown in figure). Analysis of this enriched fraction provides insight into substrate specificity and temporal nature of cotranslational interaction of the factor with the ribosome. Figure adapted from (Schibich et al., 2016).

1.3.2 Ribosome profiling strengths

Advanced next generation sequencing machines and improved library preparation methods have enabled comprehensive sampling of footprints across the genome, providing enough depth. This increased the sensitivity of the technique and facilitated the capture of even rare translational events (G. a Brar & Weissman, 2015). Previously, polysome profiling has been used to study translational regulation *in vivo*. Although it provided rich qualitative data, the positional information of ribosomes on the mRNA template cannot be inferred. Also, in polysome profiling, resolving higher polysome fractions is difficult and experimentally challenging.

Ribosome profiling circumvents this problem and provides precise positional information of the ribosome. The characteristic length of RPFs enables reliable identification of P-site and A-site codon position within the RPFs. Typically, for yeast RPFs of 28 nts length, the P-site is located 12 or 13 nts downstream of the 5' ribosomal footprint end (Ingolia et al., 2009). Moreover, the RPFs display three-nucleotide periodicity, representing the movement of ribosome across the ORF. Such analysis has allowed investigating aspects of translation such as ribosomal pausing, stop-codon read-through, translation initiation at non-AUG codons and uORF (upstream ORF) translation (G. A. Brar et al., 2012; Ingolia et al., 2014; Li et al., 2012; Woolstenhulme et al., 2015). Finally, a notable advantage of ribosome profiling is that it allows instantaneous sampling of *in vivo* translational landscape (Andreev et al., 2015). RNA-seq and mass spectrometry based approaches has shed light on regulation at the level of transcriptome and the proteome. But the information may not reflect the rapid cellular decision-making that occurs at the level of translation.

1.3.3 Caveats of ribosome profiling

In ribosome profiling, translation needs to be rapidly halted in order to capture the actual *in vivo* ribosomal position on mRNAs. Given that elongation is faster, slower inhibition of translational elongation would result in blurring of the ribosomal footprint signal. Therefore, cells are usually pre-treated with higher amounts of elongation inhibitors (*e.g* CHX) to arrest translation. Although such treatments never affected the global measurement of ribosome density, it did cause accumulation of ribosomes especially near the start codon (Ingolia et al., 2009, 2011). In addition, recent studies have pointed out that elongation inhibitors can shift the position of ribosome density downstream in comparison to untreated samples. To overcome this caveat, rapid freezing of samples without any pre-treatment with inhibitors has been shown to reliably capture ribosomal positions *in vivo* (Ingolia et al., 2012).

Contaminating RNA fragments can confound the analysis of ribosomal profiling data. For example, one of the sources could be a large ribonucleoprotein complex, which can co-migrate with the ribosomal fraction during sucrose density gradient centrifugation. There are computational

methods based on footprint length, which can differentiate between fragments derived from translating ribosome or contaminating ones (Ingolia et al., 2014).

During the isolation of ribosomal footprints, rRNA fragments from the ribosome itself can cause severe contamination. Therefore, inclusion of a step to remove rRNA contaminants is highly effective and recommended. Lastly, in contrast to RNAseq, amounts of biological sample required to prepare libraries can be a limitation. This can be either due to the extra step involved in the isolation of ribosomal footprints, or a too small portion of any given mRNA molecule undergoing translation at a given time. Therefore, the number of recoverable ribosomal footprints is reduced.

1.4 Translation and mRNA turnover

Transcript amounts and protein products ultimately determine the functionality of a gene. These quantities are in turn kinetically maintained by balancing their synthesis and degradation rates. The process of canonical mRNA turnover is critical for the maintenance of transcriptome homeostasis, and serves as a major control point in gene expression. Apart from canonical mRNA turnover mechanisms, faulty and error prone messages need to be degraded to prevent generation of proteins with deleterious effects. Accordingly, multiple specialized pathways have been discovered to recognize and decay such mRNAs.

1.4.1 Canonical mRNA turnover

Yeast mRNAs are degraded in the cytoplasm by two major pathways (Parker, 2012). The pathways are termed as 5’-to-3’ or 3’-to-5’ degradation pathway, referring to the direction mRNAs are degraded (Figure 1.10). The 5’-to-3’ pathway is mediated by the exonuclease Xrn1 (C. L. Hsu & Stevens, 1993; Muhlrad & Parker, 1994), while the 3’-to-5’ pathway is executed by the cytosolic exosome (Anderson & Parker, 1998). 5’-to-3’ is the major turnover pathway in yeast (Parker, 2012), and both pathways are initiated by shortening of the 3’ poly-A tail, a process referred to as deadenylation.

1.4.2 Deadenylation and decapping

In yeast, Pan2/Pan3 and Ccr4-NOT complexes deadenylate mRNA molecules, and they act in a coordinated temporal manner. mRNAs are initially engaged by the Pan2/Pan3 complex, which reduces the poly-A tail length to approximately 65 residues. After initial deadenylation, the Ccr4-NOT complex (Ccr4/Pop2/Not) continues to deadenylate until the poly-A tail reaches a length of approximately 10 residues (Tucker et al., 2001). mRNAs with such short poly-A tails are targeted for decapping, and the bound Pab1 is exchanged with Pat-1/Lsm-7 complex. Binding of Pat1-1/Lsm1-7 promotes mRNA decapping after deadenylation.

Dcp1 and Dcp2 proteins of the Nudix family of pyrophosphatases carry out mRNA decapping in yeast (Tharun & Parker, 2001). Decapping leaves mRNA with 5’ monophosphate, and Xrn1 prefers such mRNA substrates. Therefore, they are subsequently degraded in 5’-to-3’ direction by the Xrn1 nuclease (Figure 1.10).

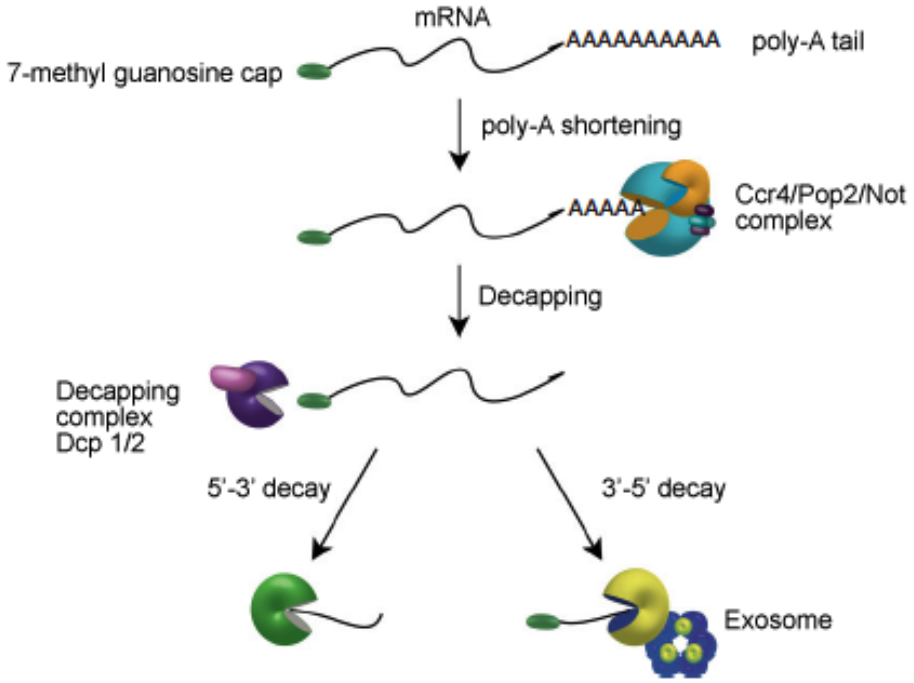

Figure 1.10 Messenger RNA degradation in yeast.

Transcript ends are modified with 7-methyl guanosine cap and 3' end poly-A tail of approximately 60 nts in length. These elements then regulate the decay process. Decay is initiated by deadenylation primarily mediated by Pan2/3 and then by the Ccr4/Pop2/Not deadenylase complex. Once the poly-A tails are trimmed short enough, Pab1p is dislodged from the poly-A tail, and the mRNA can be degraded in 3'-5' direction mediated by the exosome. On the other hand, decapping by the Dcp1 and 2 is required before transcripts can be decayed via the 5'-3' direction by the Xrn1p exonuclease. Figure adapted from (Huch & Nissan, 2014).

1.4.3 5' to 3' mRNA decay

5'-to-3' decay is the major decay pathway in yeast (Parker, 2012). It was initially thought that decapping and 5'-to3' decay happens in localized foci within the cells called P-bodies. Hence, it was assumed that mRNA undergoing active translation and associated with polysomes are not segregated into P-bodies, while non-translated mRNAs are targeted to P-bodies for degradation (Sheth & Parker, 2003). Thus, the mRNA fate was directly coupled to their translational status. This hypothesis was recently challenged, when it was shown for few yeast mRNAs, that they are decapped while being still associated with polysomes (Hu et al., 2009). Later on, sequencing of 5' monophosphate containing mRNAs in yeast, has shown

evidence strongly arguing for genome-wide co-translational mRNA decay in 5'-to-3' direction (Pelechano et al., 2015). Therefore, Xrn1 mediated degradation of mRNA happens not exclusively in P-bodies, but also co-translationally as well.

1.4.4 3' to 5' mRNA decay

In contrast to 5'-to-3' decay, deadenylation and 3'-to-5' mRNA degradation happens exclusively in the cytoplasm. 3'-to-5' decay is mediated by the cytosolic exosome (Anderson & Parker, 1998) (Figure 1.10). It is a conserved multi-protein complex with ten subunits. Nine out of ten subunits form the core (Exo-9) of the complex (Liu et al., 2006; Makino et al., 2013), but they lack catalytic activity. Exo-9 core associates with Rrp44 to form the active exosome complex (Exo-10) (Dziembowski et al., 2007). Exosome forms a pore like channel, where it threads single stranded RNA into the processive exoribonuclease Rrp44 for degradation (Makino et al., 2013).

1.4.5 Ski proteins

Accessory proteins have been identified that can bind and regulate exosome activity (Anderson & Parker, 1998; Araki et al., 2001; van Hoof et al., 2000). These proteins are called Superkiller (Ski) proteins, and in particular four (Ski2, Ski3, Ski7 and Ski8) of them have been shown to be essential for exosome function during 3'-to-5' mRNA decay. Of these, Ski2, Ski3 and Ski8 form a complex called the Ski complex, while the interaction between the Ski complex and exosome is mediated by Ski7.

Ski7 is a multidomain protein, and is required for exosome mediated 3'-to-5' mRNA decay in yeast. Ski7 is part of the eEF1α family, and it is structurally similar to other translational GTPases such as eEF1α, eRF3 and Hbs1 (Benard et al., 1999). The N-terminal domain of Ski7 mediates interaction with Ski complex and the exosome (Araki et al., 2001). The C-terminal part of Ski7 harbors the GTPase domain, and is shown to be required specifically in the NSD (non-stop decay) pathway (Van Hoof et al., 2002). Due to its similarity to other translational GTPases and given its requirement in NSD it was speculated that Ski7 interacted with ribosomes. However, experimental proof for this is so far lacking.

1.4.6 The Ski complex

The evolutionarily conserved Ski complex takes part in the cytoplasmic exosome mediated RNA turnover mechanism, including 3'-to-5' mRNA pathway, non-stop and RNA interference mediated decay (Halbach et al., 2013). Ski complex interaction with exosome is mediated by Ski7. It's a tetrameric complex with two copies of Ski8, organized in stoichiometric ratios of 1:1:2 (J. T. Brown et al., 2000; Synowsky & Heck, 2008). Ski2 harbors the only ATP-dependent helicase activity of the complex. Interestingly, ATPase activity of Ski2 is decreased and its RNA binding ability is stabilized upon Ski complex formation (Halbach et al., 2012, 2013).

Structural analysis revealed that Ski3 acts a platform for the Ski complex. The C-terminal arm of Ski3 as well as the two Ski8 proteins position the Ski2 helicase core in the center of the complex. Ski2 also contains a highly flexible insertion domain. Removal of this insertion domain increased both its ATPase and helicase activity in context of the Ski complex. Since the N-terminal arm of Ski3 and the Ski2 insertion domain are juxtaposed structurally, it was proposed that both elements act as a regulatory lid modulating the Ski2 helicase activity (Halbach et al., 2013). Finally, RNAse protection assays showed that the Ski complex shields RNA fragments of length of 9 – 10 nts, while the Ski complex together with Ski7 and exosome protected RNA fragments of length of 41 – 44 nts (Halbach et al., 2013). This suggested that the Ski complex and the exosome together form a continuous RNA channel, thereby coupling the helicase and the exoribonuclease activity during RNA degradation.

1.4.7 ORF codon composition determines mRNA stability

All mRNAs are eventually degraded via canonical turnover pathways, but half-lives between mRNAs vary dramatically. mRNA half-lives in yeast have a range of < 1 min to > 60 min or greater (Coller & Parker, 2004). The question is what features of the mRNA determine their half-life? Sequence and structural features of mRNAs in the 5' and 3' UTR were initially proposed to influence mRNA fate (Geisberg et al., 2014; Lee et al., 2015; Muhlrad & Parker, 1994). Such features could regulate the half-life of specific transcripts

or for sub-populations of the transcriptome, but could not account for the varied degradation rates observed across the transcriptome.

One common feature that was suggested to influence mRNA decay rate was the codon usage. Substitution of synonymous codons in reporter constructs with rare codons rapidly decreased their half-lives. This rapid decay was initiated via decapping and deadenylation of the transcript, but the effect was independent of mRNA surveillance pathways such as NMD, NGD, and NSD.

Rare codons were classified as non-optimal codons (dos Reis et al., 2004; Pechmann et al., 2014). Codon optimality basically reflects the amount of charged tRNAs in the cytoplasm and the demand for these tRNAs by the translating ribosome. It has been proposed that optimal codons are decoded faster and more accurately by the ribosomes than non-optimal codons (Akashi, 1994; Drummond & Wilke, 2008). Initially, codon optimality was shown to influence gene expression, protein folding kinetics and translation elongation. Recent work from the group of Jeff Coller group (Presnyak et al., 2015) has suggested that codon optimality is a major determinant of mRNA half-life. It has been shown that mRNAs containing more non-optimal codons were more slowly decoded by the ribosomes. A later study showed that these slow movements of ribosomes on mRNAs with more non-optimal codons are sensed by Dhh1 to repress translation and promote mRNA decay (Radhakrishnan et al., 2016). Therefore, apart from clearance of aberrant mRNAs, ribosomal translation also plays a major role in determining the fate of normal mRNAs.

1.4.8 Decay of aberrant mRNA

Defective mRNAs with errors need to be eliminated effectively. Otherwise, continued translation of these mRNAs can produce aberrant protein products, which can be detrimental to the cell. To reduce such errors, there exist mechanisms broadly referred to as “mRNA surveillance” pathways.

There are three identified pathways in eukaryotes, and each pathway selectively degrades a particular type of defective mRNAs. The three pathways are named as nonsense-mediated decay (NMD), no-go decay (NGD) and non-stop decay (NSD). mRNAs with a premature stop codon are

degraded via NMD, while transcripts with stall-inducing sequence or secondary structure are taken care by NGD. Sometimes, mRNAs lack a stop codon and the NSD pathway eliminates such templates. Most importantly, all these surveillance mechanisms are initiated co-translationally, implicating translation in the decay of defective mRNAs (Shoemaker & Green, 2012).

1.4.9 NMD

In higher eukaryotes, the recognition of premature stop codons is aided by the presence of exon-junction complexes (EJCs). EJCs are deposited near exon junctions, during mRNA splicing in the nucleus, while the stop codon is typically located in the 3' end of the spliced exon. The presence of EJCs defines the mRNA status, since EJCs are displaced by the ribosome during the first round ("pioneer") of translation (Maquat et al., 2010). Therefore, in the presence of premature stop codon, downstream EJCs signal to initiate NMD pathway (Le Hir et al., 2000). However, it must be noted that, even in higher eukaryotes NMD is not strictly dependent on the presence of EJC. NMD is still robust in lower eukaryotes such as in budding yeast, where splicing is not that common. In such cases it has been proposed that the presence of an extended 3' UTR (faux 3' UTR) helps in the recognition of premature stop codons (Amrani et al., 2004; Hogg & Goff, 2010).

Upstream frame-shifting (Upf1, Upf2 and Upf3) proteins are the key factors involved in NMD. Upf proteins together with Smg1 form the SURF complex (Kashima et al., 2006). Upf1 is a helicase with ATPase activity, and both these activities are necessary during NMD. In higher eukaryotes during NMD, the defective mRNA is degraded mostly via the 5'-to-3' pathway (Muhlrad & Parker, 1994). While in lower eukaryotes, the mRNA seems to be eliminated via both the 5'-to-3' and 3'-to-5' pathways.

1.4.10 NGD and NSD

mRNAs with sequences which can form secondary structures such as stable stem-loops, pseudoknots and GC-rich sequences are very effective in inducing strong stalling of ribosomes to initiate NGD (Doma & Parker, 2006). As mentioned before nascent chains functioning as ribosomal arrest peptide can also stall translating ribosomes, and mRNAs coding for these ribosomal arrest peptides can also be targeted by NGD. Dom34 (Pelota in human)

together with Hbs1 forms a heterodimer akin to eRF1-eRF3, and this complex was proposed to recognize the stalled ribosomes (Becker et al., 2011; HH et al., 2007). It was shown that Dom34 could reach into ribosomal decoding center to recognize stalled ribosomes. Moreover, Dom34-Hbs1 are also involved in rescuing ribosomes stalled during quality control. ABCE1 mediates canonical recycling of ribosomes with eRF1 on stop codon. During quality control, ABCE1 partners with Dom34 instead of eRF1 to split stuck ribosomes (Becker et al., 2012; Doma & Parker, 2006; Franckenberg et al., 2012; Saito et al., 2013). Dom34-Hbs1 mediated rescue of stalled ribosomes is very efficient when there is no mRNA in the A-site. Recently, it has been shown that ribosomes stalled internally in the middle of an ORF are recognized and rescued via the ubiquitin-proteasome pathway and mRNA control systems.

Here, first the stalled ribosomes are recognized and ubiquitinated at one or multiple specific residues. In yeast, ubiquitination of stalled ribosomes is performed by the E3 ubiquitin ligase Hel2 (Matsuo et al., 2017). Hel2 ubiquitylates SSU protein us10 at K6/8, and plays a crucial role in inducing subunit dissociation. Further, it has been shown that Hel2 preferentially ubiquitylates stalled disomes *in vitro* than monosomes (Ikeuchi et al., 2019). Second, these stalled and ubiquitinated ribosomes are recognized by RQC-trigger complex (RQT), which also induces subunit dissociation. This allows binding of nuclear export mediator factor (NEMF) to the 60S, which then subsequently recruits the E3 ubiquitin ligase Listerin. Finally, nascent chain is ubiquitinated by Listerin, thereby targeting them for proteasomal degradation.

NSD is involved in eliminating transcripts that lack a stop codon (Frischmeyer et al., 2002; Van Hoof et al., 2002). There can be two types of scenarios when there is a transcript without an in-frame stop codon. First, truncated mRNA without an in-frame stop codon, where ribosomes would translate through and are stuck at the very 3’ end of the transcript. Second, mRNAs lacking an in-frame stop codon but instead contain a poly-A tail. Later type of mRNAs might be generated due to premature poly-adenylation. Human and yeast studies has shown that at least 1% of the transcriptome is prematurely polyadenylated (Ozsolak et al., 2010), highlighting the importance of this mechanism.

With prematurely polyadenylated mRNAs, it was initially assumed that ribosomes would translate through and get stuck at the 3’ end of the transcript. If that would have been the case, NGD substrates can be distinguished from NSD substrates based on where the ribosomes are stalled on the mRNA. Mid-message stalled ribosomes can be targeted by NGD, while ribosomes stalled at the 3’ end will initiate NSD. But recent evidence shows that the distinction between these two pathways is not clear. Translation of the poly-A tail produces a nascent chain with poly-lysine residues, and nascent chain with as less as six consecutive lysine residues can induce ribosomal translation arrest (Inada & Aiba, 2005; Ito-Harashima et al., 2007; Kuroha et al., 2010). It was proposed that the stall might be caused by the interaction of poly-lysine with the negatively charged tunnel. But, recent cryo-EM structure of a poly-A stalled ribosome nascent chain complex revealed that poly-A mRNA contributes more to stalling than the translated stretch of lysine residues in the exit tunnel. Here, they observed that the poly-A mRNA adopts a decoding incompetent π-stack arrays in the A-site (Tesina et al., 2020), thereby hindering proper accommodation of A-site tRNA and leading to translation inhibition.

Moreover, the poly-A tail lengths in human and yeast are much longer than 20 nucleotides, and it is very unlikely ribosomes can translate through them reaching the 3’ end. Therefore, NSD and NGD share more commonalities, and the actual cause of the stall might be important in initiating either of these mRNA quality control pathways.

A unifying theme after initiation of NSD or NGD, is the occurrence of endonucleolytic cleavage events in the aberrant mRNA (Doma & Parker, 2006; Eberle et al., 2009; Gatfield & Izaurralde, 2004). Current understanding is that initial endonucleolytic cleavage happens upstream of the primary stalled ribosome. After this cleavage event, in NGD, the 5’ secondary target will be degraded by the cytosolic exosome via the 3’-to-5’ direction, while the primary target is degraded by Xrn1 in 5’-to3’ direction (Doma & Parker, 2006). Non-stop transcripts seem to be degraded primarily via the 3’-to-5’ decay pathway by the cytosolic exosome (Maquat, 2002; Van Hoof et al., 2002). Especially Ski7 is specifically implicated in the process of NSD. Here, as mentioned before, Ski proteins are essential for the cytosolic activity of the

exosome. Therefore, it was assumed that Ski7 recognizes such non-stop stalled ribosomes and recruit the Ski complex and exosome to decay the aberrant mRNA via 3'-to-5' pathway (Frischmeyer et al., 2002; Van Hoof et al., 2002).

1.5 Aims of this thesis

The thesis presented here comprises three main aims, two of which were tackled with the ribosome profiling technique, that was established in the Beckmann lab by the author of this thesis with the help of Dr. Markus Pech.

Ribosome profiling was first established in the context of dendritic cell (DC) maturation, since it was already known that translational regulation plays a critical part in the DC maturation process. Previous studies used polysome profiling to investigate translational regulation during DC maturation. Although previous work provided much insight, polysome profiling lacks the resolution to study translational regulation at a genome-wide scale. Thus, the first aim was to establish mammalian ribosome profiling and apply it to study translational regulation in maturing dendritic cells. Monocytes isolated from human PBMCs were used as the source for generating immature dendritic cells (iDCs). IDCs were further matured *in vitro* using a cytokine cocktail mixture that is known to generate mature DCs appropriate for immune-therapeutic purposes. During the course of maturation DC samples were collected at three time points: 0 h (iDCs), 4 h and 24 h after induction of maturation. Ribosome profiling and RNAseq NGS (next generation sequencing) libraries were generated and sequenced from these collected samples. Further elaborate bioinformatic analysis of the generated data has been performed. This provided insights about translationally regulated genes during DC maturation, and their roles in the maturation process.

The second application of the ribosomal profiling technique was in context of a project in the Beckmann lab dealing with mRNA decay by the Ski-exosome complex. Here, the first goal was to explore the connection between translation and mRNA turnover especially during NSD. Initially it has been proposed that Ski7 might be involved in recognizing ribosomes stalled in the NSD, and further recruit the Ski complex for mRNA turnover. However, this proposed model lacked biochemical evidence. Therefore. the aim was to

investigate the interaction of Ski7 as well as the Ski complex with the ribosome. Apart from traditional methods like pull-downs, ribosome-Ski interactions were validated, characterized and explored mainly by means of selective ribosome profiling. Such genome-wide data was sought to shed light on the physiological context of ribosome binding by these factors, e.g. to elucidate their role in NSD or general mRNA decay. Moreover, this work complemented a structural study of ribosome-Ski complex performed in the Beckmann lab.

The third project aimed to apply cryo-EM to determine the structure of ribosomes stalled by the XBP1u arrest peptide (XBP1u-RNC). The goal was to visualize for the first time a mammalian ribosome staller in the ribosome exit tunnel, to understand its stalling mechanism and compare it to its well-understood bacterial counterparts. Moreover, the structure should shed light on how SRP is recruited to the XBP1u-RNC, and how this influence targeting to the Sec61, so that *XBP1u* mRNA can be efficiently spliced by IRE1α on the ER membrane. Due to the translational arrest caused by the XBP1u-AP, HR2 domain of XBP1u gains sufficient affinity to be recognized by SRP. In order to study this special mode of SRP recruitment, and also to structurally investigate the state of the XBP1u-AP during targeting, cryo-EM structures of the paused XBP1u-RNC *in vitro* reconstituted with the mammalian SRP or Sec61 were generated. Further, these structures might shed light on the possibility of XBP1u-AP being a force sensitive ribosomal staller.

2 Materials and methods

2.1 Dendritic cell generation

The monocyte-enriched fractions from elutriation were thawed and washed twice with VLE-RPMI medium at 200 g for 15 min. Cells were resuspended and seeded at 4.5 x 10^7 per 80 cm^2 Nunclon flask in 15 ml DC medium. To induce DC differentiation of monocytes, the DC medium was supplemented with 800 IU/ml GM-CSF (Bayer, Germany) and 580 IU/ml rhIL-4 (R&D Systems, Germany), and cells were incubated at 37 °C and 5% CO_2 in a humidified atmosphere. Immature DCs (iDC) were harvested after 48 h. To mature DCs, the DC medium was supplemented after 48 h with a cocktail consisting of 1100 IU/ml TNFα, 2000 IU/ml IL-1β (R&D Systems, Germany), 5000 IU/ml IFNγ (Boehringer Ingelheim, Germany), 250 ng/ml PGE2 (Sigma-Aldrich, Germany), 1 µg/ml R848 (InvivoGen, USA), 800 IU/ml GM-CSF and 580 IU/ml rhIL-4 for 4 or 24 h.

2.2 Lysis of dendritic cells

Lysis was performed at 4 °C on ice. In order to preserve ribosomal footprints, ice-cold PBS (Pan Biotech, Germany) supplemented with cycloheximide (CHX) (Sigma-Aldrich, Germany) was used. Dendritic cells were quickly cooled down by pouring them into a 50 ml Falcon tube containing equal volume of PBS with 200 µg/ml of CHX. To collect remaining cells, flasks were washed with 100 µg/ml CHX-PBS, adherent iDC and 4 h DC were additionally scraped off, and cells were pooled with non-adherent fraction. Cells were washed twice with 100 µg/ml CHX-PBS at 500 g for 6 min. Cells were resuspended in 400 µl lysis buffer/10^7 cells and dispersed by pipetting 8 times. Lysis buffer contained 1X polysome buffer (Illumina, USA), 1% Triton X-100, 1 mM DTT, 10 U/ml Turbo DNase I, 100 µg/ml CHX and RNase free water. Lysate was collected in a nuclease free 1.5 ml Eppendorf tube (Eppendorf, Germany), incubated for 10 min on ice and centrifuged at 1300 g for 10 min. Lysate supernatant was collected and split into several tubes of 200 µl each. These were snap-frozen in liquid nitrogen and stored at -80 °C until further use.

2.3 Immune phenotyping of dendritic cells

After incubation with FcR blocking reagent (Miltenyi, Germany) for 10 min at 4 °C to block non-specific antibody binding, cells were labelled with the following fluorochrome-conjugated mAbs for 15 min at 4 °C. CD14 (FITC, 61D3), CD40 (PE, 5C3) (eBiosciences, USA), CD80 (PE, L307.4), CD83 (APC, HB15), CD274 (FITC, MIH1) (BD Biosciences, Germany), CD86 (Pacific Blue, IT2.2), HLA-DR (Pacific Blue, LN3) (BioLegend, USA) and CCR7 (APC or PE, FR11-11E8, Miltenyi). Corresponding isotype-matched control mAbs were used: IgG1 (FITC, PE and APC, P3628, eBiosciences) and IgG2b (Pacific Blue, BioLegend). Dead cells were excluded by staining with LIVE/DEAD Fixable Aqua Dead Cell Stain Kit (Molecular Probes, Eugene, OR, USA). After washing, cells were analyzed by flow cytometry using a LSR II instrument (BD Biosciences) and post-acquisition analysis was performed using FlowJo software (Tree Star, USA). Median fluorescence intensity (MFI) ratios were calculated by dividing the MFI value of cells stained with a specific mAb by the MFI value of the same cells stained with isotype-matched control mAb. For intracellular staining of CCR7, cells were fixed and permeabilized using the Fixation/Permeabilization Solution Kit (BD Biosciences, USA) according to the manufacturer´s instructions after surface staining with CCR7 mAb and washing. In the presence of FcR Blocking Reagent, cells were incubated with CCR7 mAb or an isotype-matched control mAb for 30 min at 4 °C. After washing, cells were analyzed by flow cytometry as described above.

2.4 Dendritic cell migration assay

DCs were harvested and analyzed in a transwell migration assay. The lower chamber of a 96-transwell plate (Costar, USA) was filled with 235 µl DC medium with or without 100 ng/ml CCL19 (R&D Systems, Germany). 5 x 10^4 DCs in 80 µl DC medium were seeded in the upper chamber and incubated for 2 h at 37 °C and 5% CO_2. Cell numbers in the upper and lower chambers were determined using the CellTiter-Glo Luminescent Cell Viability Assay (Promega, Germany) according to the manufacturer´s instruction. Luminescence was measured with the Orion II luminometer (Berthold Detection Systems, Germany). The percentage of migrated DCs was

calculated by dividing the number of cells in the lower chamber by the total number of cells counted in the upper and lower chamber.

2.5 Cytokine secretion assay

DCs were co-cultured with CD40L-expressing LL8 fibroblast cells to mimic interactions with activated T cells. Briefly, 5 x 10^4/well LL8 cells were seeded into 96-well plates and allowed to adhere for 1 h before coincubation with 2 x 10^4/well DCs. After 24 h plates were centrifuged at 550 g for 5 min and supernatants of three replicate wells were pooled for analysis of IL-12p70 and IL-10 concentrations. Supernatants of DCs and LL8 cultured alone served as controls. Cytokine concentrations were analyzed using the CBA multiplexed bead-based immunoassay (BD Biosciences, USA). In brief, IL-12p70 and IL-10 antibody coated beads were incubated with 25 µl of supernatant for 1 h. Detection antibodies were added and after 2 h beads were washed and samples immediately acquired on a LSR II instrument (BD Biosciences). FCAP software (BD Biosciences, USA) was used to plot standard curves and calculate sample concentrations.

2.6 Generation and isolation of ribosomal footprints

Ribo-seq and RNAseq libraries were prepared using the ARTseq™ ribosome profiling kit commercially bought from Epicentre Technologies (Illumina, USA). Dendritic cell lysates containing atleast 5 A_{260} units of total RNA were used for generation and extraction of ribosomal footprints. Concentrations of lysates were measured using Nanodrop at 1:100 dilutions in nuclease free water. Lysis buffer was used as a blank. RNAse I was used to generate the ribosomal footprints, and was added at the concentration of 40 units per A260 of the lysate. Digestion was carried out at 25 °C for 45 min with shaking at 450 rpm. RNAse I activity was then inhibited by adding Superase.in (0.5 units per unit of RNAse I). Digested lysates were then loaded onto 10-30% sucrose gradients and centrifuged at 31,000 rpm using a SW40 rotor (Beckman Coulter, USA) for 3.5 h at 4 °C. Gradients were then fractionated using a fractionator (Biocomp Instruments, Canada) and 80S fractions were collected. 80S fractions were then centrifuged at 81,000 rpm for 1.5 h. Supernatant was quickly removed and kept at 4 °C, and to the glassy ribosomal pellet 150 µl of

splitting buffer (20 mM Tris (pH-7.8), 400 mM KCl, 2 mM $MgCl_2$, 1 mM DTT and 1 mM puromycin) was added. While being kept in ice for 60 min, using a pipette ribosomal pellet was carefully dissolved in the splitting buffer. After 60 min, ribosomes were pelleted again by centrifuging at 80,000 rpm for 1.5 h at 4 °C. Supernatant (containing the ribosomal footprints) from this centrifugation step is collected and cleaned up using Zymo Research RNA clean and concentrator kit using a protocol to cleanup as described below.

Two volumes of RNA binding buffer (provided with the kit) were added to the supernatant. Then 1.5X volume of 100% ethanol was added and vortexed. This mixture was then transferred to the Zymo Spin column and centrifuged at 10,000 g for 30 sec at room temperature. Flow through was discarded and 400 µL of RNA prep buffer (provided with the kit) was added, and centrifuged at 10,000 g for 30 sec at room temperature. Flow through was discarded and 700 µL of RNA wash buffer (provided with the kit) was added, and centrifuged at 10,000 g for 30 sec at room temperature. Flow through was discarded and 400 µL of RNA wash buffer was added, and centrifuged at 10,000 g for 60 sec at room temperature. Then Zymo Spin column was placed in a new 1.5 ml centrifuge and 15 µL of nuclease free water was added to the matrix. Then cleaned up RNA samples were eluted by centrifuging at 10,000 g for 30 sec at room temperature.

This elute was mixed with equal amounts of 2x RNA loading buffer, heated for 95 °C for 5 min. Then loaded on to a 15% urea-PAGE, and ran the gel at 200 V. Gel fragments were cut using size selection markers of size 26 and 34 nts respectively. Cut gel fragments were made into a slurry by passing through a small hole in 0.5 ml tube. To the slurry added 400 µl nuclease free water, 40 µl 5 M ammonium acetate and 2 µl 10% SDS, and incubated overnight at 4 °C with rotation. Slurry was centrifuged to collect the supernatant containing the ribosomal footprint fragments. To the supernatant, 700 µl of isopropanol and 1.5 µl of Glycoblue™, and incubated at -20 °C for 2 h. Extracted ribosomal footprints were then pelleted by centrifuging at maximum speed for 40 min at 4 °C. Supernatant was discarded and the pellet was washed with 80% ethanol, and centrifuged at maximum speed for 20 min at 4 °C. Supernatant was discarded and the dried pellet was reconstituted in

20 µl of nuclease free water. Further these extracted ribosomal footprint fragments are end-repaired, and proceeded with library preparation.

2.7 Extraction of total RNA for RNAseq library preparation

Lysate containing 40 – 60 µg of RNA (based on absorption at 260 nm) is used for RNAseq library preparation. RNA was extracted from the lysate using commercially bought miRNAeasy Mini Kit (catalog number: 217004) from Qiagen (Hilden, Germany). 700 µl of QIAzol lysis reagent was added to the lysate and incubated at room temperature for 5 min. To this 140 µl chloroform was added and vortexed for 15 sec, and centrifuged at 12,000 g for 15 min at 4 °C. After centrifugation, top aqueous layer was transferred to a new tube and to it added one volume of 70% ethanol and mixed thoroughly by vortexing. This mixture is then transferred into a RNeasy Mini spin column placed in a 2 ml collection tube, and centrifuged at 11,000 rpm for 15 sec at room temperature. Flow through was discarded and to the column 700 µl of buffer RWT was added, and centrifuged at 11,000 rpm for 15 sec at room temperature. Flow though was discarded and to the column 500 µl of buffer RPE was added, and centrifuged at 11,000 rpm for 15 sec at room temperature. Previous step with buffer RPE was repeated one more time. After discarding the flow through, column (lid open) was placed in a new 2 ml collection tube and centrifuged at maximum speed for 1 min. Following this RNA was eluted by adding 30 µL of RNAse free water onto the column membrane by centrifuging at 11,000 rpm for 1 min at room temperature.

2.8 rRNA depletion of total RNA and heat fragmentation

Ribosomal RNA (rRNA) in the total RNA sample was depleted using the commercially bought Rib-Zero^{TM} Magnetic Kit (Human/Mouse/Rat) (Epicentre, USA). 5 µg of extracted total RNA was used for rRNA depletion. Batch washing procedure was followed for preparing the beads, and rRNA fragments were removed magnetically by following the manufacturer's instructions. While removing rRNA fragments using magnetic beads, 50 °C incubation step was excluded. rRNA depleted total RNA was then cleaned up and concentrated using Zymo RNA Clean and Concentrator kit (Zymo Research, CA, USA). Final sample was eluted in 20 µl of nuclease free water

and was mixed with 7.5 µl of ARTseq PNK buffer. Further rRNA depleted total RNA was heat fragmented by incubating at 94 °C for 25 min. Samples were immediately placed on ice after heat fragmentation. From the end repair step both the RNAseq and Ribo-seq samples are processed in parallel.

2.9 Preparation of NGS libraries from ribosomal footprints and total RNA (rRNA depleted)

From the end repair both the RNA and ribosome footprint samples are processed in parallel. To the heat fragmented RNA and to the extracted ribosomal footprints 44.5 µl of nuclease free water and 3 µl of ARTseq PNK enzyme were added bringing the total volume to 75 µl. End repair reactions were carried out at 37 °C for 2 h, and further cleaned up using Zymo Research RNA Clean and Concentrator kit. 25 µl of nuclease free water was added to each sample bringing the total volume to 100 µl. To this 200 µl of RNA binding buffer and 450 µl of absolute ethanol was added. This mixture was then transferred to Zymo Spin column and centrifuged at 10,000 g for 30 sec at room temperature. Following this, Zymo Spin column was treated with RNA prep buffer and RNA wash buffer as per manufacturer's instructions. End repaired fragments were eluted in 9 µl of nuclease free water.

In order to proceed with adapter ligation, first 8 ul of end repaired fragments and 1 µl of ARTseq 3' adapter was mixed and denatured at 65 °C for 2 min. Following this, samples were immediately placed on ice until ligation master mix is added. Ligation master mix is prepared by mixing 3.5 µl of ARTseq ligation buffer, 1 µl of 100 mM DTT and 1.5 µl of ARTseq ligase. Ligation master mix was then added to the denatured samples and mixed by gentle vortexing. Ligation reaction was carried out at 25 °C for 2 h. To remove excess unused 3' adapter, 2 µl of ARTseq AR enzyme was added to each ligation reaction and incubated for 60 min at 30 °C.

For reverse transcription (RT), RT premix was prepared on ice. Adding 4.5 µl of ARTseq RT reaction mix, 1.5 µl of 100 mM DTT, 6 µl of nuclease free water and 1 µl of EpiScript RT enzyme RT premix is prepared. RT premix was then added to the ligation reactions, and incubated for 30 min at 50 °C. To remove excess RT primer, 1 µl of ARTseq exonuclease was added to each reaction and incubated for 30 min at 37 °C, followed by 15 min at 80 °C. Then

placed the samples on ice. Finally, template RNA was removed by adding 1 µl of ARTseq RNAse mix to each reaction and incubated at 55 °C for 5 min, followed by holding the samples on ice.

To each reaction 18 µL of nuclease free water was added bringing the total volume of each sample to 50 µl. Then reactions were cleaned up using Zymo Research RNA Clean and Concentrator kit using the > 17-nt protocol. cDNA was eluted with 11 µL of nuclease free water. To this added DNA loading buffer and heated the samples at 95 °C for 5 min. Then PAGE purified these fragments using a 10% urea-PAGE, and gel fragments were extracted using size selection markers of length between 70 – 85 nts. Excised gel fragments were made into a slurry by passing it through a hole in a 0.5 ml tube. To the slurry was then added 400 µl of water, 40 µl of 5 M ammonium acetate and 2 µl of 10% SDS solution. Incubated this mixture at 37 °C for 1 h with shaking at 750 rpm. To this added 1.5 µl of Glycoblue™ and 700 µl of isopropanol and incubated at -20 °C for 2 h or longer, and precipitated cDNA by centrifuging at maximum speed for 40 min at 4 °C. Pellet was then washed with 80% ice-cold ethanol and centrifuged at maximum speed for 20 min at 4 °C. Supernatant was carefully removed and dried. Dried pellet was reconstituted in 10 µl of nuclease free water. Circularization was performed as per the instructions in the kit. Circularized cDNA fragments were stored in -80 °C until further use.

Final sequencing libraries by PCR amplification using Illumina index primers. Test PCR is performed with 1 µl of circularized cDNA input with 12, 14, 15, 18, and 20 cycles of amplification. Based on the gel analysis, preparative PCR will be performed. Amplified products were run on a 8% native PAGE, and fragments of size between 140 – 160 bp were excised and extracted as before for cDNA fragments. Reconstituted libraries were sequenced on Illumina HiSeq 2500.

2.10 Analysis of DC RPFseq and RNAseq NGS data

Demultiplexed reads were trimmed of the 3’ adapter. Trimmed sequences were further cleaned by removing reads mapped to non-coding sequencing such as rRNA, tRNA, snRNA and snoRNA. Then, these reads are mapped onto the human genome (grCh37, release June 28th, 2013) using the

splice aware mapper GSNAP (Wu et al., 2016; Wu & Nacu, 2010). Only uniquely mapping reads are used for further downstream bioinformatic analysis. Gene boundaries and features of the gene were provided by Dr. Basak Eraslan (Group of Prof. Dr. Julian Gagneur). Number of reads mapping to the gene features such as 5' UTR, 3' UTR and CDS were counted using HTSeq (Anders et al., 2015).

For stop and start codon metagene plots, per nucleotide coverage of all genes around these codons were calculated. Further, the coverage was then normalized the DESeq estimated sizefactor. Counts between the replicates were summed up. Summed coverage were then normalized by gene expression level, which is the sum of the footprint counts mapping onto the CDS. Footprints from first and last 10 codons of the ORF were excluded for this analysis. Genes only with a minimum of 200 footprint counts between the replicates were included. ORFs shorter than 140 amino acids were not included. Genome wide mean per base is then plotted and only transcripts whose boundaries within the plotted window are included for mean calculation.

Stop codon pause score is the ribosome occupancy on the stop codon normalized by ribosome occupancy on the CDS. Scores were calculated on genes at least longer than 70 amino acids. Gene expression level as mentioned before was used as the ribosome occupancy of the CDS. 5' end shifted footprints falling on the stop and upstream 15 bases of it were collectively considered as stop codon occupancy. In this analysis stop and CDS ribosome occupancy were length and library size normalized. Values between the replicates were summed up.

Differentially expressed genes at the level of RNA, RPF and for RPF/RNA were calculated using DEseq (Love et al., 2014). This was done for both the 4 h and the 24 h time point, and fold changes at all levels were calculated with respect to the iDC sample. Here, iDC sample is considered as time point zero. Genes were further sorted into categories, if they show statistically significant changes at the level of both RNA and RPF, or either only at the RNA or at the level of the RPF. Genes showing significant changes at the level of RNA and RPF are categorized as homo-directional, since most of the genes in this category exhibit changes in the same direction at both the

levels. For genes, within each category Spearman correlation was calculated between RNA and RPF log2FoldChange values.

Gene set enrichment analysis was performed using the online tool WebGestalt (http://www.webgestalt.org/) (J. Wang et al., 2017). In the functional database option ‘pathway’ and ‘KEGG’ were chosen with default parameters. For Figure 3.8, DEseq normalized log2FoldChange of ribo-seq values were used. Only gene exhibiting homo-directional changes were included in this analysis. This was performed for both 4 h and 24 h samples. For Figure 3.10, DEseq normalized log2FoldChange of translational efficiency was used. For this analysis, all genes that were detected in the two time points were used for this analysis.

2.11 Quantitation of ABCE1 expression by qPCR

Total RNA was isolated using RNeasy spin columns (Qiagen, Germany) according to the manufacturer's recommendations. Contaminating DNA was removed by DNAse treatment with either dsDNAse (Thermo Fisher Scientific) or the RNase-Free DNase Set (Qiagen). Total RNA was reverse-transcribed with the First Strand cDNA Synthesis kit (Thermo Fisher Scientific Fermentas) and random hexamer primers. Quantitative real-time PCR was performed on a LightCycler 96 real-time PCR detection system (Roche, Switzerland) using FastStart Essential DNA Probes Master kit (Roche) and the TaqMan gene expression assays for ABCE1 (Hs01003010_g1), HPRT1 (Hs02800695_m1), C1orf43 (Hs00367486_m1) and CHMP2A (Hs00205423_m1; all from Thermo Fisher Scientific Applied Biosystems).

The relative expression of ABCE1 was determined in duplicates and normalized to the expression of HPRT1 or C1orf43 or CHMP2A. The three housekeeping genes were selected based on their stable expression profiles (RNASeq). Similar results were obtained by normalization to either housekeeping gene.

2.12 Relative ABCE1 protein levels

Equal protein amount was loaded for all samples. For detecting ABCE1, antibody generated against ABCE1 C-terminal region was used at the dilution 1:3000. Further, actin levels were used as the loading control, and also for

relative quantitation. Band intensity for relative quantitation was estimated using the ImageJ software.

2.13 TAP-tagged pullouts of native Ski-complex interacting with ribosome

Pullouts experiments was performed by Dr. Christian Schmidt (Group of Prof. Roland Beckmann), and provided the samples for preparing riboseq and RNAseq libraries. Yeast strain expressing C-terminally TAP-tagged Ski3 were used for pullouts using Dynabeads® M-270 Epoxy (Life Technologies). Log phase cultures were harvested and resuspended in lysis buffer (20 mM HEPES pH 7.4, 100 mM KoAc, 10 mM MgCl2, 1mM DTT, 0.5 mM PMSF, 10 µg/ml cycloheximide). Further, resuspended cell pellets were lysed using glass beads and clarified by centrifugation. Lysates were then incubated with IgG-coupled magnetic beads for 12 h at 4 °C with rotation. Elution of bound complexes were performed with AcTEV protease for 3 h at 17 °C. For more details regarding the Ski3-TAP tagged pullouts and cryo-EM reconstruction of ribosomal-Ski complexes, refer to this publication (Schmidt et al., 2016).

2.14 Preparation of RPFseq and RNAseq libraries from Ski3-TAP pullout

Total cell lysate amounting to 10 A_{260} units was used to prepare background RNA and RPF samples. For the background RNA, 5 A_{260} of the total cell lysate were used for RNA extraction using miRNAeasy mini kit (Qiagen). Further, extracted total RNA was depleted of ribosomal RNA using the Ribo-Zero rRNA removal kit for Human/Mouse/Rat (Epicentre). rRNA depleted total RNA was heat fragmented in alkaline conditions as mentioned above in the section 2.8. Fragmented RNA was converted to cDNA libraries using the ARTseq™ Ribosome profiling kit as described before. For Ski pulldown RNA sample, RNA was extracted from purified ribosome-Ski complexes and processed into cDNA libraries as mentioned above.

Ribosomal footprints were generated by treating the cell lysate or purified ribosomal-Ski complexes with 40 units per A_{260} of RNase I (Ambion) at 25 °C for 45 min in a shaker at 500 rpm. RNase I activity was inhibited by adding SUPERase-in (Ambion). RNase I treated lysate was applied to 10-30%

sucrose gradient and centrifuged at 121,000 *g* for 3.5 h to separate 80S monosomes from polysomes. Monosome peak was isolated and ribosomes were pelleted by centrifugation as mentioned before in section 2.6. Sucrose gradient centrifugation step was omitted for ribosome-Ski complexes, as the purified complex showed 80S monosomes only. Instead, ribosomes were pelleted through a sucrose cushion. 80S were split and pelleted as mentioned before. Ribosomal footprint containing supernatant from the previous step was further purified and size selected in a 15% denaturing urea-PAGE. Fragments between 26 - 62 nucleotide markers were extracted, these extracted fragments were processed and converted into cDNA libraries as mentioned before. Sequencing was performed on Illumina HiSeq 1500.

2.15 Bioinformatic analysis of RNA- and RPFseq libraries from the native Ski3-TAP pullout

Demultiplexed reads were 3' adapter trimmed using the software Cutadapt (version 1.2.1, EMB) (Martin, 2011). Trimmed reads were then depleted of ribosomal RNA, tRNA, small nuclear and nucleolar RNA. Remaining reads were mapped to the yeast genome using Tophat (v2.0.8b) (Kim et al., 2013). Only uniquely mapped reads were used for most of the downstream bioinformatic analysis (unless otherwise mentioned).

For plotting the relative position of RNAseq reads (Figure 3.22) in the ORFs, multiple mapping of two positions within the genome has been used. This was performed in order to avoid partial coverage due to overlapping genes or duplicated sequences within the coding regions. First, per nucleotide coverage in the ORFs for all genes was calculated. Then, each gene was divided into ten equal segments. Each segment mean coverage was normalized to its corresponding gene mean. Then, genome wide average was calculated for these ten segments, and plotted with standard deviations as well. This analysis was performed for two replicates of the pulldown RNAseq and a single dataset of the background RNA.

In order to identify poly-A transition reads (Figure 3.21), a previously published strategy was modified (Guydosh & Green, 2014). First, adapter trimmed and unmapped reads were taken for further analysis. These reads were further trimmed of consecutive A's from the 3' end of the read and

mapped to the genome and plotted. For displaying the poly-A trimmed footprints (Figure 3.21A) mapping to ORFs and the 3' UTR, 5' end has been shown. Only in the case of poly-A transition reads, position of 3' end has been shown to better delineate these regions. For plotting the amount of poly-A clipped reads, values for the Ski-pulldown RPFseq and control RPFseq were normalized to per million mapped reads. Analysis of poly-A containing reads were performed for the RNAseq and RPFseq datasets. Length analysis of poly-A stretches in poly-A clipped reads was done by calculating the number of clipped A's for each read. Fractions with respect to the total amount of all reads for each number of clipped A's was plotted.

Codon correlation plot (Figure 3.24) was analysed as described before (Presnyak et al., 2015). Here, Spearman correlation was calculated between the footprint count ratio and codon occurrence (in percentage). Optimal and non-optimal codons were adapted from this publication.

2.16 Cloning of XBP1u

Plasmid containing full-length XBP1u was a gift from Prof. Kenji Kohno (Nara Institute of Science and Technology, Takayama, Japan). The S255A which was described before was then truncated to have only the HR2 domain and the pausing motif with N-terminal (8X-His, 3X-Flag and 3C protease cleavage site) and C-terminal (HA-tag) for purification purposes. Here is the final nucleic acid sequence of the construct used for purification.

ATGGGCCACCATCACCATCACCATCACCATGGCTCCGACTACAAGGACC
ATGAC751GGTGATTATAAGGATCACGACATCGACTACAAGGATGACGAT
GACAAGGACTACGATATCCCCACCACACTGGAGGTGCTCTTCCAGGGCC
CTGGCGGCTCCATCTCCCCATGGATTCTGGCGGTATTGACTCTTCAGATT
CAGAGTCTGATATCCTGTTGGGCATTCTGGACAACTTGGACCCAGTCAT
GTTCTTCAAATGCCCTTCCCCAGAGCCTGCCAGCCTGGAGGAGCTCCCA
GAGGTCTACCCAGAAGGACCCAGTTCCTTACCAGCCTCCCTTTCTCTGT
CAGTGGGGACGTCATCAGCCAGCTTGGAAGCCATTAATGAACTACCCAT
ACGATGTTCCAGATTACGCTGGATCTTAA

Here is the final amino acid sequence of the construct

MGHHHHHHHHGSDYKDHDGDYKDHDIDYKDDDDKDYDIPTTLEVLFQGPG
GSISPWILAVLTLQIQSLISCWAFWTTWTQSCSSNALPQSLPAWRSSQRSTQ
KDPVPYQPPFLCQWGRHQPAWKPLMNYPYDVPDYAGS*

2.17 Preparation of linear template for *in vitro* transcription

Linearized plasmid was used as template for capped mRNA generation, and was generated by digesting with NotI-HF enzyme. The linearization reaction is set up as described in the table below.

Table 2-1 Composition for linear template generation

Component	Volume (µl)
Plasmid DNA	100 (20 µg)
10X CutSmart® buffer	20
NotI-HF	3
Nuclease free water	77
Total	200

The mixture is then incubated at 37 °C for 120 min for digestion, and deactivated by incubation at 65 °C for 20 min. 200 µl of phenol:chloroform:isoamyl alcohol mixture (Sigma Aldrich) was added and vortexed vigorously for 5 sec, followed by centrifuging the mixture for 1 min using table-top centrifuge at maximum speed. After centrifugation, top aqueous layer is collected for extraction of template DNA. To this added 10% (vol /vol) of 5 M ammonium acetate solution (Invitrogen) and twice the volume of 100% ethanol. This was then incubated for 1 h at -80 °C, DNA is then pelleted by centrifuging at 14,000 rpm for 20 min at 4 °C. Supernatant is discarded and the pellet is washed once with 1 ml of 70% ethanol, and centrifuged for 20 min at 14,000 rpm at room temperature. After this centrifugation step, supernatant is carefully removed and the pellet is air-dried and reconstituted in nuclease free water. Concentration of the linear template is measured using Nanodrop™ spectrophotometer and the quality of the preparation is assessed by agarose-gel electrophoresis.

2.18 Generation of capped mRNA for *in vitro* translation reaction

Capped mRNA for *in vitro* translation reactions were prepared using the T7 mMessage mMachine® kit (Life Technologies). The *in vitro* transcription

reaction is setup as described in the table below, and components are added in the given order. Reaction is setup at room temperature.

Table 2-2 Composition for *in vitro* transcription reaction

Component	Volume (µl)
Nuclease free water	3
Nucleotides/CAP	10
Linear template DNA	3 (~1 µg)
10X reaction buffer	2
Enzyme mix	2
Total	20

This mixture is then incubated at 37 °C for 2 h. For reactions more than 100 µl in total volume, 40 µl aliquots were made and then incubated. After *in vitro* transcription, 1 µl of DNAse is added in order to digest away the linear template and incubated for another 30 min at 37 °C. The digestion reaction is stopped by adding 30 µl $LiCl_2$ and 30 µl of nuclease free water and incubated for 1 h at -20 °C for precipitating the mRNA. mRNA is then pelleted by centrifuging at 14,000 rpm for 15 min at 4 °C. Supernatant is sucked away carefully, and the pellet is washed with 1 ml of 70% ethanol at room temperature. This was then again pelleted at 14,000 rpm for 15 min at 4 °C, and air-dried for removal of residual ethanol. The pellet is finally reconstituted with RNAse-free water and the mRNA concentration was measured using Nanodrop™ spectrophotometer. The mRNA quality was then assessed by Urea-PAGE analysis.

2.19 His-tag purification of XBP1u ribosome nascent chain complex (XBP1u-RNC)

For the purification of XBP1u- paused complex, 80 ng of mRNA was used for per µl of final translation reaction mix. mRNA reconstituted in nuclease free water was denatured by heating at 65 °C for 3 min, and then rapidly cooled by placing on ice. 800 µl translation reaction was set up, and to this was added the linearized mRNA and mixed well. 200 µl aliquots of the final reaction mix were then incubated at 37 °C for 10 min, and the translation reaction was

stopped by immediately placing it on ice. The reaction was then diluted with ice-cold buffer-1 (50 mM HEPES/KOH pH 7.5, 200 mM KOAc, 15 mM $Mg(OAc)_2$, 1 mM DTT, 0.1% Nikkol and 0.02 units per µl of RNAse inhibitor) to a final volume of 2.4 ml. Diluted reaction volume is then incubated with 800 µl of equilibrated Talon beads for 120 min at 4 °C with rotation. Beads were equilibrated by washing initially with 1.6 ml of buffer-1 for two times, followed by 1.6 ml of buffer-1 (supplemented with 1:1000 yeast tRNA, volume/volume) for two times. After initial incubation, flow through is collected by gravity and beads were washed with 1.6 ml of buffer 1 for three times, which are labeled as W1 - W3. Beads were further washed with 1.6 ml of buffer-1 (supplemented with 10 mM imidazole, W4 – W5) for two times, and finally six times with 1.6 ml of buffer 1 (W6 – W11). Paused XBP1u- ribosome nascent chain complex was eluted by incubating the beads in buffer-1 with 3C protease overnight at 4 °C with rotation. Paused ribosome nascent chain complex in the elution fraction were concentrated by sucrose cushion pelleting. Composition of sucrose cushion buffer is buffer-1 with 500 mM sucrose, PMSF and protease inhibitor cocktails. Pelleting was done using TLA 100.3 rotor (Beckman Coulter, USA), and further centrifuged at 90,000 rpm for 90 min at 4 °C. For 1.6 ml of elution fraction, 0.8 ml of sucrose cushion buffer was used for pelleting. Final pellet was re-suspended in buffer-1, slowly on ice. The preparation yielded 4.2 pmol of XBP1u-paused ribosome nascent chain complex, which was then used for structural analysis using cryo-electron microscopy.

2.20 *In vitro* reconstitution of purified XBP1u-RNC with SRP and Sec61

Canine rough microsomes were used as the source of SRP. SRP was purified from a high salt extract of canine rough microsomes by gel filtration (Sephadex G-150), followed by ion-exchange chromatography (DEAE-Sepharose) as described before (B.Martoglio, S.Hauser, 1998). Further it was purified by sucrose centrifugation as described before (Walter & Blobel, 1983). XBP1u-RNC-SRP was prepared as follows: 1.2X molar excess of purified dog SRP was added to purified XBP1u-RNC in the presence of 2 mM GMP-PNP and 0.1% GDN (glycol-diosgenin), and incubated at 25 °C for 15 min. Further,

4.5X excess of purified SRP receptor (α and β) and six-fold excess of Sec61 was added and incubated at 25 °C for 15 min before being applied onto the grids for cryo-EM analysis.

Canine puromycin/high-salt treated rough membranes (PKRM) were prepared as described before (Gogala et al., 2014). PKRM were pre-treated with RNAsin, and were incubated with purified XBP1u-RNC for 15 min at 25 °C. Membranes were then solubilized with 1.5% digitonin in buffer-1 for 90 min in ice. Solubilized ribosome-translocon complexes were pelleted through sucrose cushion (with 500 mM sucrose, 0.3% digitonin, PMSF and protease inhibitor in buffer-1). Pelleted complexes were resuspended in buffer 1 with 0.1% GDN and used for cryo-EM sample preparation.

2.21 Cryo-electron microscopy and single particle reconstruction

Purified XBP1u-RNC of concentration 5.2 OD_{260} per mL was applied to 2 nm pre-coated Quantfoil R3/3 grids. Cryo-EM data was collected semi-automatically using EM-TOOLS acquisition software (TVIPS, Germay) a Titan Krios. Defocus range was between 0.5 and 3 µm. Pixel size on the object scale was 1.084 Å. All data were recorded on a Falcon II detector (FEI). For XBP1u-RNC, a total of 6080 micrographs were collected with a total exposure of ~28 electrons/$Å^2$ fractionated into 10 frames. Micrographs were manually inspected for ice and aggregation. Particles were picked automatically using Gautomatch (https://www.mrc-lmb.cam.ac.uj/kzhang/). Relion-2.1 (Kimanius et al., 2016) was used for all classification and refinement purposes. After 2D classification, total of 531,952 ribosomal particles were subjected to 3D classification with a prior round of 3D refinement. Two ribosomal states were obtained from the intial 3D classification. These states correspond to post and rotated states with tRNA's, respectively. Further enrichment of the post state XBP1u-RNC was obtained by performing a 3D classification with a mask for P-tRNA and the large subunit. This resulted in a subclass of 223,773 particles, which were refined further with a 60S mask leading to final overall resolution of 3 Å. Rotated state XBP1u-RNC from the initial 3D classification was also refined with a 60S mask to 3.1 Å overall resolution.

2.22 Modeling and refinement of XBP1u-RNC models

For the post state XBP1u-RNC PDB 5LZV (Shao et al., 2016) was used as the initial rabbit ribosome 80S model, and was docked into the sharpened density. Initial fit was done in UCSF Chimera and the model was further adjusted in Coot (Emsley & Cowtan, 2004). The model was refined in Phenix (Adams et al., 2010) using the command phenix.real_space_refine with secondary structure restraints obtained with the command: phenix.secondary_structure_restraints. All manual adjustments were done to fit the local resolution filtered map generated with Relion 2.1 (Kimanius et al., 2016). P-tRNA, E-tRNA, XBP1u nascent chain and mRNA were manually inspected and adjusted to fit into the final map. Some 28S rRNA bases such as C2794, C4398, U4531, U4532, A3908, G3904 and A4388 were individually inspected as well.

Since a proper rotated state model was not available, in two steps the post state model was fitted into the rotated state density. First the large ribosomal subunit 60S was fitted. Then the split small ribosomal subunit 40S was fitted and joined in Coot. tRNAs from PDB 3JBV (J. Zhang et al., 2015) and 3J77 (Svidritskiy et al., 2014) served as initial models for rotated state A/P- and P/E- tRNA respectively.

For the post state XBP1u-RNC with SRP and Sec61, PDB 3JAJ (Voorhees & Hegde, 2015) and 6FTI (Braunger et al., 2018) were used as initial models for SRP and Sec61 respectively. These models were rigid body docked and fitted in Coot. Further refinement with Phenix was performed as mentioned above. Final statistics (Table 6-3) of all the refined models were calculated using Molprobity (V. B. Chen et al., 2010).

2.23 Figure preparation

Figures showing results for ribosomal profiling data is plotted in R using the package ggplot2 (Wickham, 2009). Figures showing molecular models and electron densities were prepared either with UCSF Chimera (Pettersen et al., 2004), UCSF ChimeraX (Goddard et al., 2018) or Pymol Molecular Graphics System (Version 1.8.2 Schrödinger, LLC). Most of the final compositions were generated using Adobe Illustrator.

2.24 Work contribution

Dr. Frauke Schnorfeil (Group of Prof. Marion Subklewe) provided the dendritic cell (DC) lysates for ribosomal profiling analysis Dr. Frauke Schnorfeil also performed the immune phenotyping, cytokine secretion and cell migration assays. Dr. Markus Pech and the author of this thesis did the preliminary analysis of the DC ribosome profiling data. We established the ribosomal profiling technique, and prepared the RPFseq and RNAseq libraries for next generation sequencing (NGS). Dr. Basak Eraslan (Group of Prof. Julien Gagneur) observed the correlation between GC content in 3' UTR and its ribosome density at the 24 h time point. Dr. Basak Eraslan also determined the transcript boundaries using RNAseq data.

Dr. Christian Schmidt (Group of Prof. Roland Beckmann) did the preliminary biochemical experiments and purified the *in vivo* yeast Ski 80S complex for ribosome profiling analysis. Also provided the lysate control for library preparation. I prepared the yeast RPFseq and RNAseq libraries (Pull-out and control) for NGS. I analyzed all the NGS data and generated the figures.

3 Results

3.1 Ribosome profiling of maturing dendritic cells

Translational regulation plays a critical role during the maturation of dendritic cells (DC) (Ceppi et al., 2009; Lelouard et al., 2007). In order to study this regulation, changes at the level of translatome and transcriptome during DC maturation were analyzed using ribo-seq and RNA-seq, respectively.

3.1.1 Dendritic cell maturation and phenotypic characterization

Monocytes from a healthy donor were used as source for generating immature dendritic cells (iDCs). iDCs were matured for 4 or 24 h (4h-DC or 24h-DC) using cytokine cocktail mixture consisting of IFNγ, TNFα, IL-1β, PGE_2 and the TLR7/8 agonist R848 (Figure 3.5A). Previously, this mixture of cytokines has been shown to produce mature DCs that secrete high amounts of IL-12p70 and reduced amounts of IL-10, therefore appropriately inducing Th1 immune responses during immunotherapy (Lichtenegger et al., 2012). During DC maturation process, phenotypic surface markers were monitored using flow cytometry (Figure 3.1A). Differentiation of monocytes into iDC (immature DC), and maturation of DCs were performed by Dr. Frauke Schnorfeil (Group of Prof. Dr. Marion Subklewe). Time points 4 h and 24 h for sample collection were decided based on previous studies (Ceppi et al., 2009; Lelouard et al., 2007). Prior studies investigating DC maturation have shown that protein synthesis peaks at 4 h after stimulation of maturation, and decreases during later stages (16 h and above) of maturation.

CD83, a surface molecule associated with DC maturation, and HLA-DR, a class-II major histocompatibility complex responsible for presenting processed antigen to T-cells is increasingly expressed during the course of maturation. Co-stimulatory molecules that interact with T-cells such as CD40, CD80 and CD86, as well as the co-inhibitory factor CD274 are up regulated during maturation (Figure 3.1A). CCR7 is a key chemokine receptor that governs DC migration to the lymph nodes *in vivo*. Compared to monocytes, iDC show strong increase in expression of CCR7, while during maturation, 4 h and 24 h DCs showed only slight increase in the surface expression of CCR7. It has been shown before that CCR7 is being constantly ubiquitylated and

thereby it is mainly detected intracellularly (Schaeuble et al., 2012). Additionally, the matured DC was functionally characterized by analyzing cytokine secretion upon CD40L stimulation mimicking T-cell interaction. Cytokine secretion analysis reveals that mature DCs significantly secrete more of IL-12p70 upon stimulation, while the levels of IL-10 don't show much change during maturation (Figure 3.1B). Importantly, mature DCs especially at the later time-point show increased capacity for migration (Figure 3.1C).

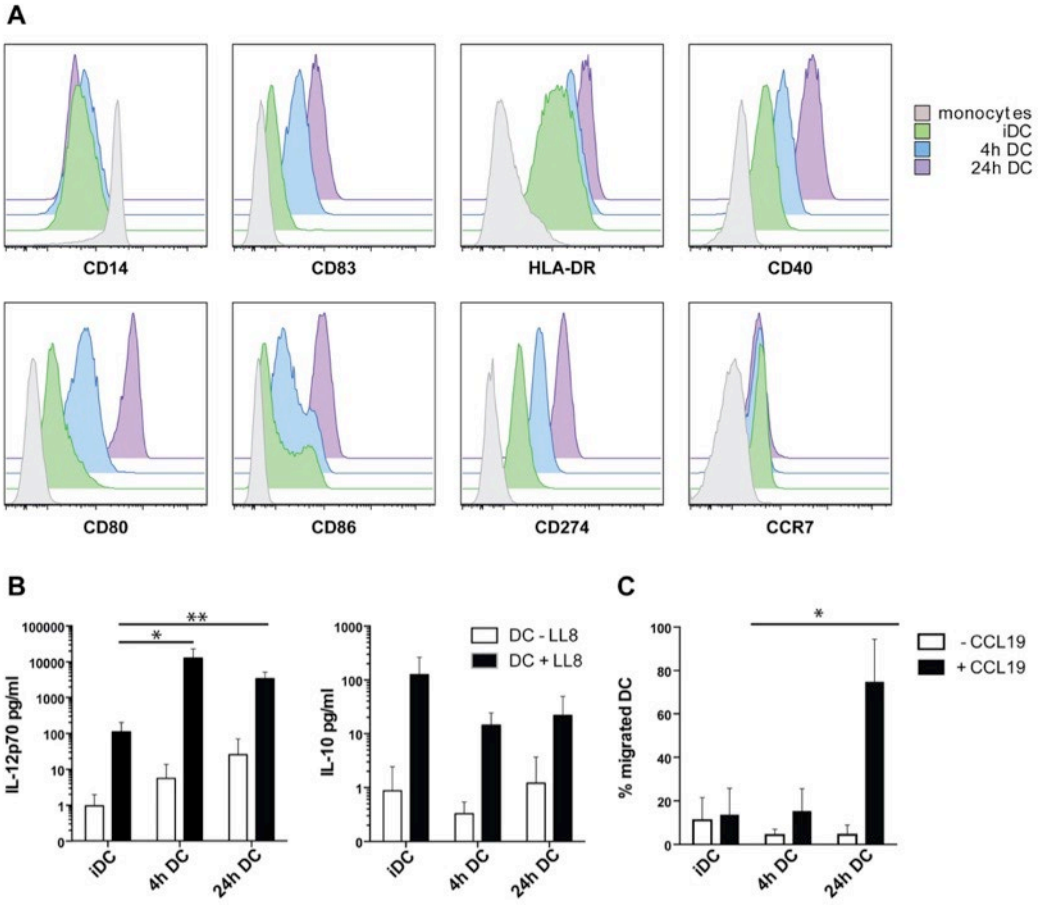

Figure 3.1 Phenotypic characteristics of mature DCs.

(A) Surface markers during DC maturation were monitored using flow cytometry. Surface expression of monocyte marker, CD14 is down regulated upon maturation while surface expression of typical DC maturation markers such as CD80, CD86, and CD274 show increase in expression as maturation progresses. HLA-DR, a MHC class-II complex involved in the processing and presentation of antigens also show increased surface expression. CCR7, a key chemokine receptor governing DC migration to the lymph nodes also shows increased surface expression. (B) Cytokine secretion analysis of iDC, 4h and 24h DC. Upon maturation, 4h and 24h DCs secrete higher amounts of IL-12p70, while IL-10 secretion is reduced. (C) 24h DCs gains significant migratory potential upon maturation.

3.1.2 Ribosome profiling of maturing dendritic cells

Ribosome profiling is a technique to sequence the mRNA fragments that are shielded by ribosomes upon nuclease digestion. These mRNA fragments are termed as ribosome protected mRNA fragments (RPFs) or ribosomal footprints (RPFs). Briefly, the protocol involves treatment of lysate material with RNAse-I, resulting in conversion of polysomes into 80S a monosomal

fraction containing RPFs. Then, the nuclease treated lysate is subjected to sucrose gradient centrifugation resulting in the separation of free RNAs, small and large ribosomal subunits, 80S monosomes and nuclease resistant higher polysome fractions. 80S monosomes isolated from this step are used as the source of RPFs. A traditional method involves acid-phenol-chloroform extraction of this fraction for RPF isolation. Since this did not result in good yields of ribosomal footprints, footprints were extracted by splitting the 80S monosomes using high-salt buffer containing puromycin (see materials and methods for details). Footprints isolated from this step were end-repaired before adapter ligation, and further converted to cDNA molecules. Circularized cDNA molecules were PCR amplified using indexed primers for library generation (RPFseq) and subjected to next generation sequencing. For every biological sample, matched RNAseq was also generated in parallel to estimate transcript levels (see materials and methods).

Sequenced RPF- and RNAseq libraries were first clipped off the 3'-end adapter and then further cleaned by removing the reads that map to non-coding RNAs (rRNA, tRNA, snRNA and snoRNA). Unmapped reads from this step were then mapped to the human genome, and gene specific ribosome occupancy and RNA levels were calculated by counting the reads that map to corresponding gene coordinates within the genome. Numbers of uniquely mapping reads are summarized here (Table 6-1). With the exception of one biological replicate from the 4 h time-point, libraries prepared from all other samples yielded at least 10 million uniquely mapping ribosomal footprints. Similarly, all RNAseq libraries contained at least 20 million uniquely mapping reads.

Length distribution of generated RPFseq range between 26 – 34 nts while the expected length of RPFs is around 28 – 30 nts. It is known that RNAse-I digestion is not completely precise and the length of the ribosomal footprint also depends on the ribosomal state itself. Since there was variation in the length distribution of ribosome protected fragments (Figure 3.2), only fragments between the length of 25 and 32 nts were used for further downstream analysis. 75% of ribosome protected fragments were within this range. Finally, both RNA- and RPFseq datasets showed strong correlation

between the biological replicates (Spearman correlation 0.90 – 0.98) (Figure 3.3).

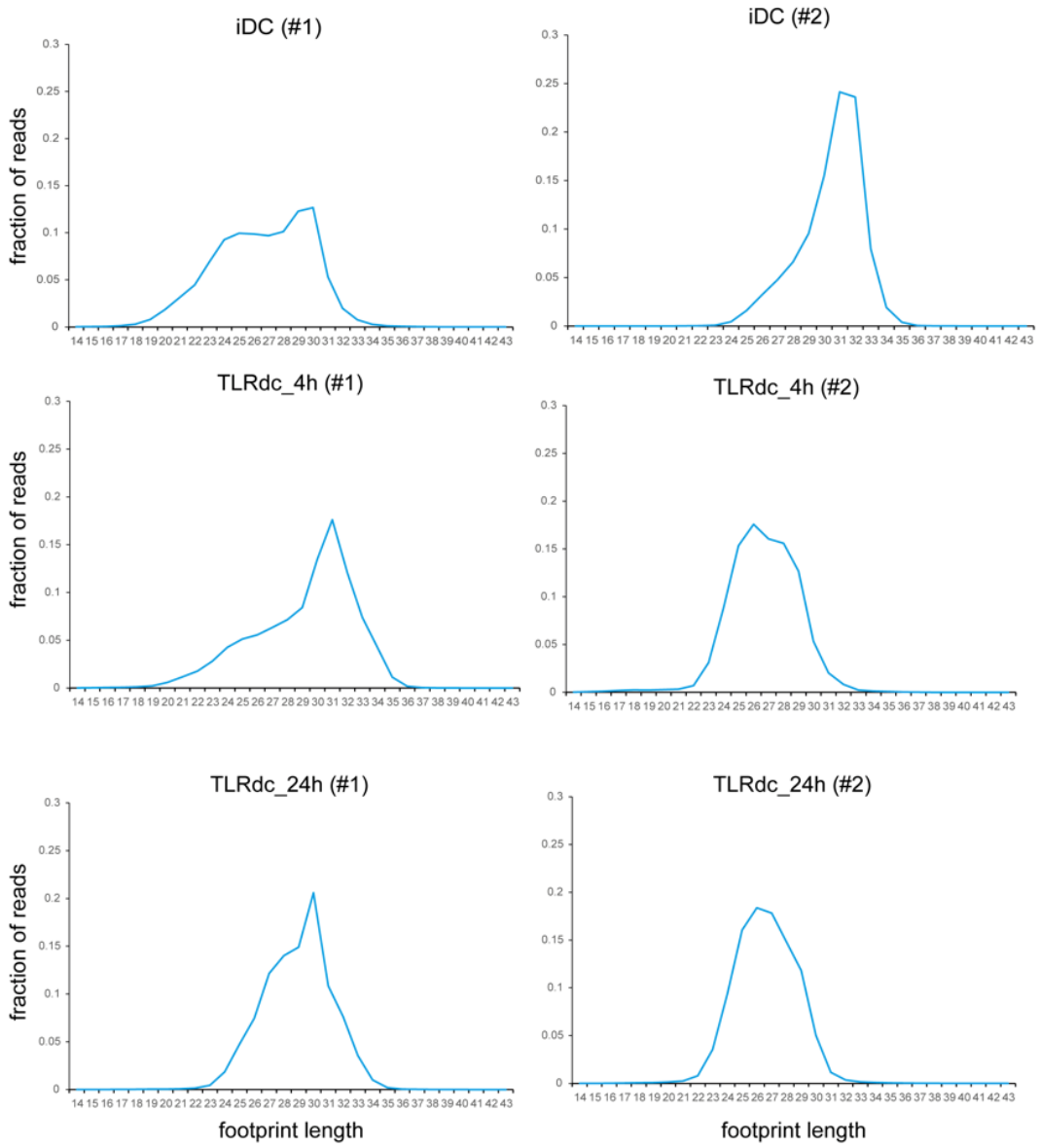

Figure 3.2 Length distribution of ribosomal footprints during the course of DC maturation.

Length distribution of uniquely mapping ribosomal footprints of iDC, TLRdc_4h and TLRdc_24h samples (biological replicates) are plotted. Although there is variation in the length distribution within the same time-point, more than 75% of the footprints are between 25 and 32 nts in length. For further analysis, only footprints between the above-mentioned lengths were used.

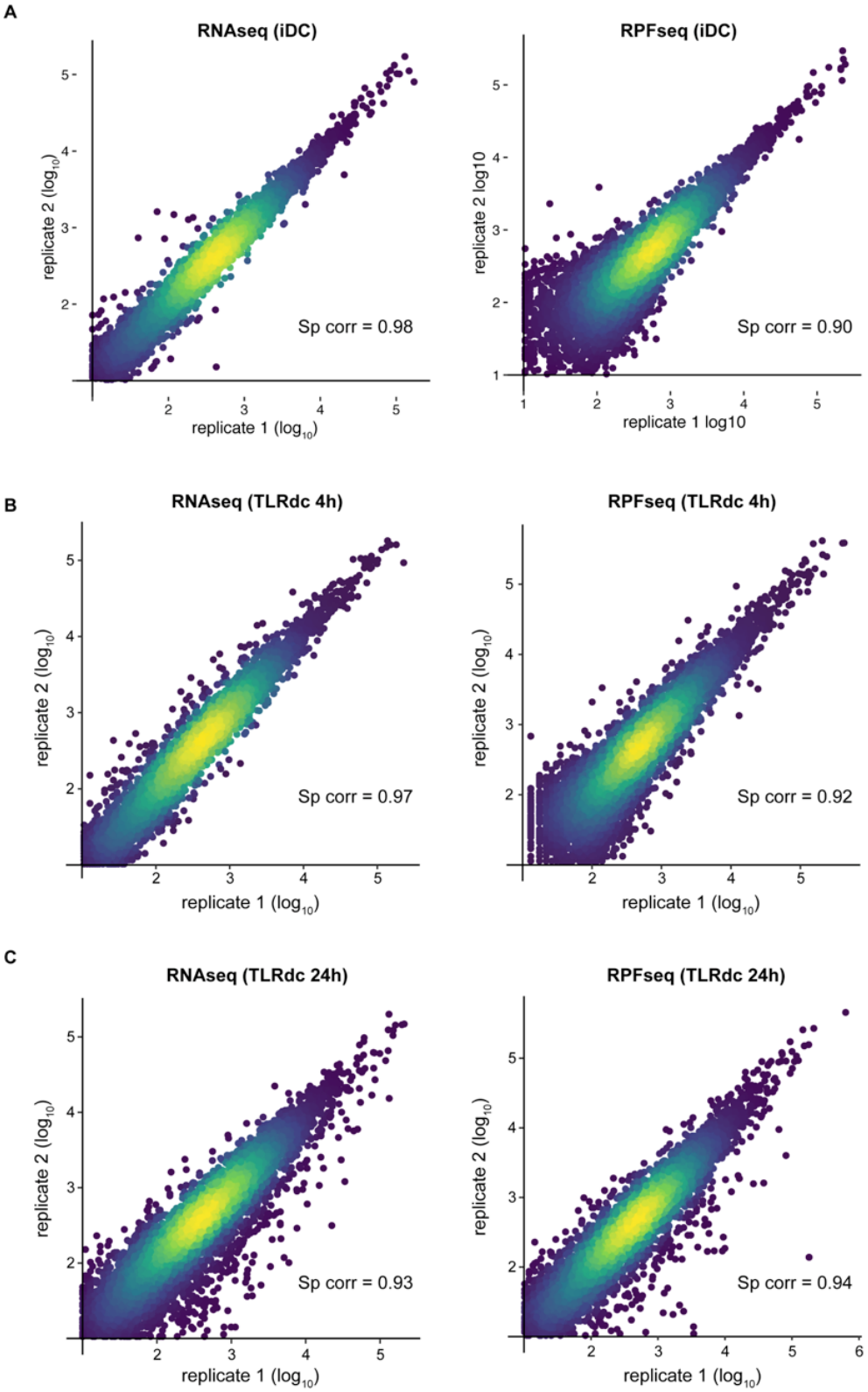

Figure 3.3 Correlation of RPF- and RNAseq replicate datasets.

Both RNAseq and RPFseq reads show strong correlation between biological replicates across all three time-points.

Moreover, more than 75% of sequenced ribosomal footprints map to coding regions of the genome (Table 6-2). This is also reflected quite well in the metagene plot. Metagene plots are used to display the ribosome density around a region of interest. When plotting ribosome density around the stop codon, it can be clearly seen that ribosome density decreases dramatically past the stop codon. Another feature that is striking is the three-nucleotide periodicity exhibited by ribosomal footprints over the CDS (Figure 3.4). This 3-nt periodicity depicts the transition of ribosomes during active translation. Expectedly, the 3-nt periodicity of ribosomal footprints is lost over the UTRs. Overall, considering the correlation between replicates (Figure 3.3), parameters of footprint length (Figure 3.2), percentage of reads mapping to CDS (Table 6-2), 3-nt periodicity and reliability to identify the active site (Figure 3.4) within the footprint, it can be inferred that the generated RPFseq libraries are of high quality.

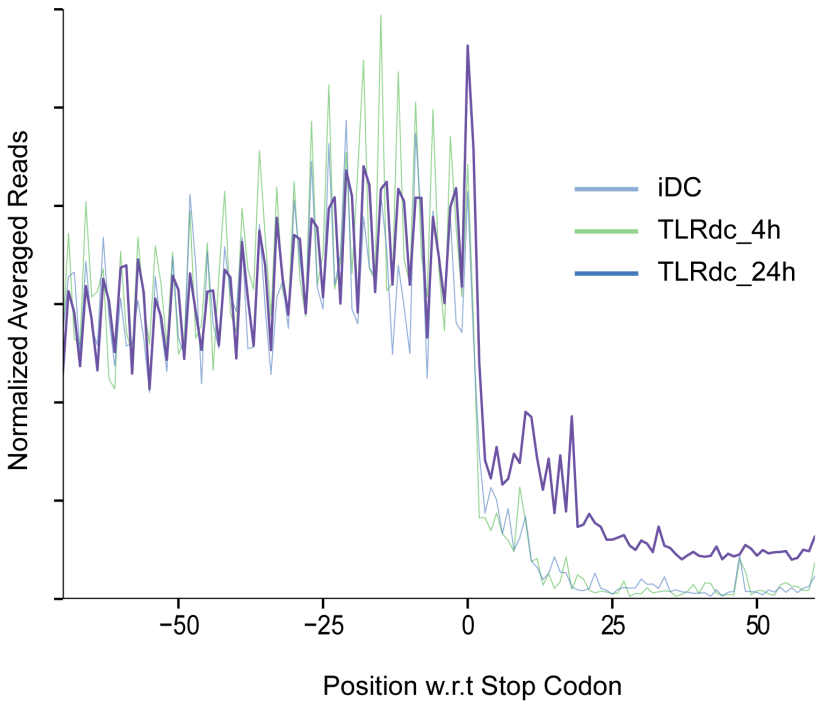

Figure 3.4 Stop codon metagene plot.

Metagene analysis around the stop codon reveals three-nucleotide periodicity of ribosomal footprints. Further, the ribosome density is sharply reduced past the stop codon as expected. The TLRdc_24h time-point shows a increased number of reads in the 3' UTR. This is due to a biological phenomenon discussed in later sections.

3.1.3 Comparison of ribosome profiling data to phenotypic markers

Next, gene expression levels of phenotypic markers involved in DC maturation were determined and those were further examined to assess, whether the results qualitatively reflected the trends from flow cytometry experiments. In order to do this, mean fold change in expression levels (RNA-FC and RPF-FC) were calculated with respect to iDC sample (4h/iDC & 24h/iDC). CD14, a marker for monocytes showed strong down-regulation at both the RNA and RPF levels (Figure 3.5B). Co-stimulatory molecules such as CD40, CD80, CD83, CD86 and CD274 exhibited maximum fold change at 4 h at both RNA and RPF levels, although without further increase at 24 h time-point (Figure 3.5B). This deviates from the phenotypic data (Figure 3.1) as MFI showed further increase at 24 h for co-stimulatory molecules. Most likely this slight deviation could be explained by the time delay involved in protein synthesis and subsequent surface exposure. The strongest difference was observed for the chemokine receptor CCR7. Despite the strong increase observed in RNA and RPF at 4h, there is no apparent change of CCR7 on the surface and only a slight increase at 24h. However, as reported before CCR7 is constitutively ubiquitylated, serving as a signal for recycling by endocytosis (Schaeuble et al., 2012), and can be therefore detected mainly intracellularly as described above (Figure 3.5C). In summary, these data obtained by ribosome profiling are in perfect agreement with the phenotypic characterization of immature and matured DCs.

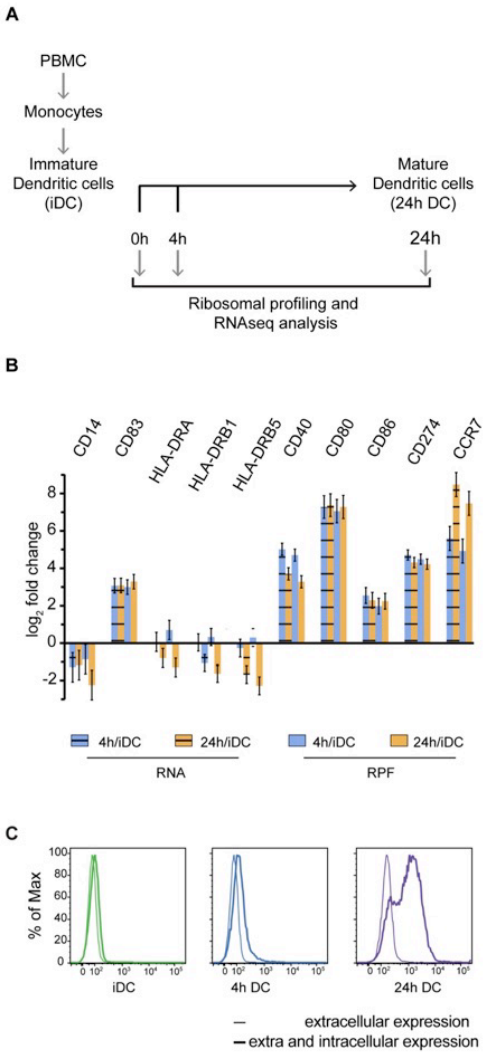

Figure 3.5 DC maturation markers.

(A) PBMCs isolated from a healthy human donor were used as the source for monocytes. Monocytes were further differentiated into immature dendritic cells (iDCs). Using a defined cytokine mixture, iDCs were then induced for maturation. Samples were collected at 4 h and 24 h post-induction for RNAseq and Ribo-seq analysis. (B) DC maturation markers such as CD80, CD86, CCR7 show up-regulation in expression at the level of transcriptome and translatome respectively, while CD14, a monocyte marker is down regulated upon induction of DC maturation. Maturation markers at the level of RNA and RPF reflect phenotypic characteristics of mature DC (TLRdc_24h) analyzed by flow-cytometry (Figure 3.1A).

3.1.4 General changes during DC maturation

In order to find differentially expressed genes (DEG) during the course of DC maturation, time-points 4 h and 24 h were compared to the iDC sample.

Further, DEseq was used to find DEG at the level of transcriptome (RNAseq) and translatome (RPFseq), respectively. Translational efficiency (ribosome density) was also calculated for genes by normalizing RPF reads (ribosome occupancy) with RNA levels: RPF/RNA. Genes that showed significant changes in translational efficiency were also detected for both time points.

A

Number of Differentially Expressed Genes (DEG) over CDS

Analysis	RPF	RNA	RPF&RNA	RPF/RNA
4h vs iDC	2001	1057	2137	157
24h vs iDC	1612	647	3391	11

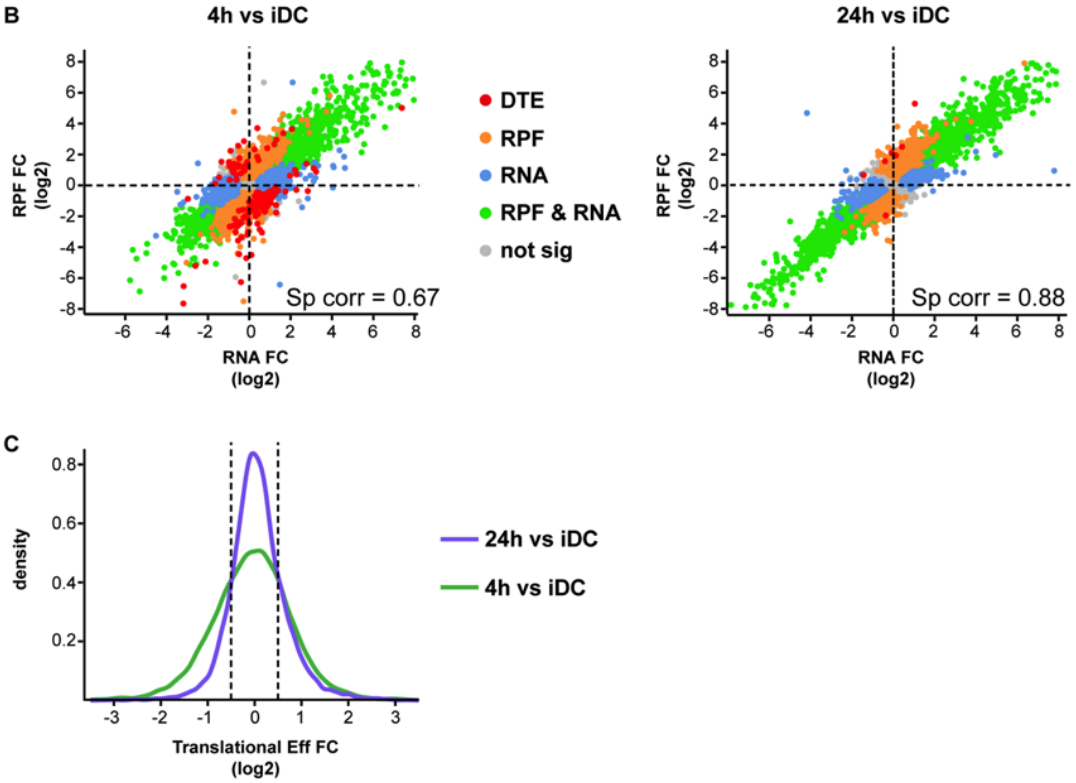

Figure 3.6 Differential expression of genes during DC maturation.

(A) Numbers of differentially expressed genes (DEG) at the level of translatome (RPF), transcriptome (RNA) and translational efficiency (RPF/RNA) are plotted. (B) Correlation between changes in transcriptome and translatome upon induction of DC maturation are plotted. Genes showing significant homo-directional changes (both RPF and RNA) are shown in green. Genes showing significant changes only at the level of translatome and transcriptome are shown in orange and blue, respectively. Genes without any significant changes are plotted in grey, and genes significant for changes at the level of translational efficiency are plotted in red. (C) Cumulative distribution of translation efficiency changes over the course of DC maturation is plotted.

In order to examine the coupling between transcription and translation during DC maturation, RNA-FC against RPF-FC for both time points (4h/iDC and 24h/iDC) were plotted (Figure 3.6B). This analysis revealed that the changes in gene expression at the RNA and RPF were much more correlated for 24 h DC (Spearman correlation = 0.88) than in comparison to 4 h DCs (Spearman correlation = 0.67). Differential gene expression analysis detected a total of 5352 genes that showed significant changes at 4 h time-point, while at 24 h time-point 5661 genes were detected. This includes expression changes at the level of RPF, RNA and RPF/RNA.

To further analyze changes in translation and transcription during DC maturation, genes were sorted into three categories. The main objective here was to investigate the reason for reduced correlation between RNA and RPF fold changes at the 4 h time-point. First, genes that showed significant changes at the level of both transcriptome (RNAseq) and translatome (RPFseq) were analyzed. This category would contain genes that exhibit homo-directional changes, *i.e* genes showing similar changes at the level of the transcript as well as at the translatome level. The second and third category would be genes showing significant changes only at the RNA or at the translatome level (RPF). Spearman correlation was then calculated between RNA and RPF fold changes for both the time-points (4h/iDC and 24h/iDC) post induction of DC maturation. Within each category, Spearman correlation was calculated separately for up- and down-regulated genes respectively. For example, in the second category, genes were split into up (positive change) or down (negative change) regulated based on RNA fold changes. Similarly, for the third category, genes were separated based on RPF fold changes, while in the first category, genes were separated if they show similar changes at both the levels.

First, the number of genes that showed homo-directional changes in expression at both RNA and RPF levels were identified (Figure 3.6A). Surprisingly, at 4 h time point only ≈ 40% of DEG showed significant changes at both levels (RNA and RPF), while at 24 h time point ≈ 60% DEG show similar homo-directional changes. Spearman correlations between RNA and RPF fold changes were quite high especially at the 24 h time point, around 0.9 for both up and down regulated genes. While correlation values were slightly

lower at the 4 h time point, 0.87 and 0.77 for up- and down-regulated genes, respectively (Figure 3.7, top). Higher correlation values are not surprising; since this category contains genes that exhibit homo-directional changes at both the levels.

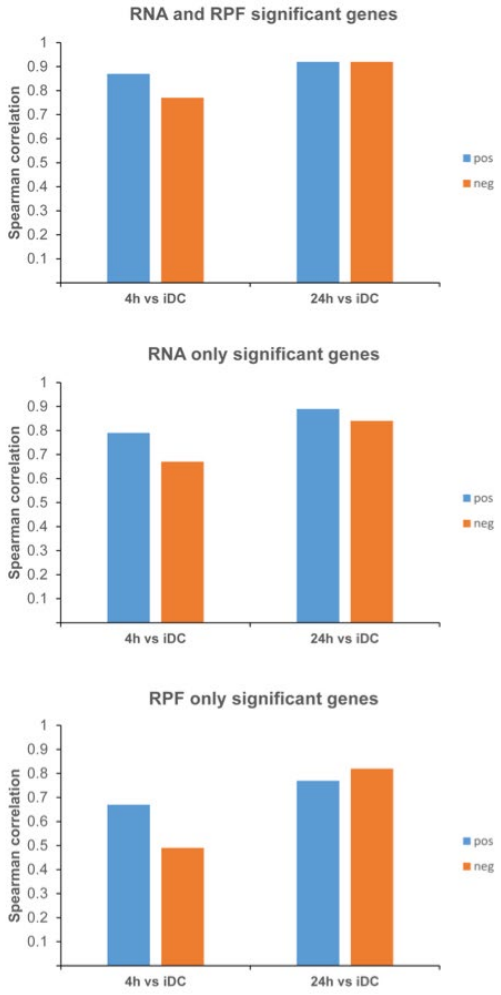

Figure 3.7 Correlation between RNAseq and RPFseq fold changes.

(Top) Spearman correlations for genes showing significant fold changes at the level of both RNAseq and RPFseq. Similarly, Spearman correlation was calculated for genes showing statistically significant changes either at the RNA (middle) or at the level of translatome (bottom).

To find out what families of transcripts are homo-directionally regulated, these set of genes were subjected to gene set enrichment analysis using the WebGestalt online tool (J. Wang et al., 2017). To mention some, pathways

such as ‘Cytokine-cytokine interaction’, ‘IL-17 signaling pathways’, ‘NOD-like receptor signaling pathway’ and ‘TNF signaling pathway’ are up regulated during the course of DC maturation (Figure 3.8, top). Also, these pathways are amongst the top up-regulated pathways at the 24 h time point as well (Figure 3.8, bottom). These pathways are activated in response to the pro-inflammatory cytokines present in the cytokine mixture to induce DC maturation. Therefore, it can be inferred these pathways are strongly up regulated and this up-regulation persists in the 24 h time-point as well.

Interestingly, some of the transcripts that are down-regulated during the 4 h time point, encode for proteins that take part in DNA repair (belong to pathways such as ‘Mismatch repair’ and ‘Base excision repair’). It should be noted that iron-sulfur cluster containing proteins play a critical role in DNA repair and replication, although the down regulation of these genes in the context of DC maturation is not clear. Transcripts that code for proteins involved in ‘Phosphatidylinositol signaling’ and ‘Inositol phosphate metabolism’ are also down regulated at the 4 h time-point. Phosphoinositides play a critical role in many signaling pathways influencing cell migration, endocytosis and membrane lipid dynamics. Importantly they are also part of the PI3K-Akt pathway, and this pathway has been implicated in the activation of rapid cap-dependent protein synthesis during the early stages (4 h time-point) of DC maturation.

Multiple pathways involved in lipid metabolism such as ‘Cholesterol metabolism’, ‘Glycerophospholipid metabolism’ and ‘Ether lipid metabolism’ are strongly repressed at the 24h time-point. Twenty-four transcripts encoding for four proteins (ATP synthase (n=6), cytochrome c oxidase (n=5), NADH:ubiquinone oxidoreductase (n=5), ubiquinol-cytochrome c reductase (n=3), succinate dehydrogenase complex iron sulfur subunit B (n=1)) involved in the oxidative phosphorylation pathway are significantly down-regulated at the 24h time-point (Figure 3.8, bottom). Down-regulation is observed at the level of both transcriptome and translatome and is much stronger at the 24h time-point (Figure 3.9).

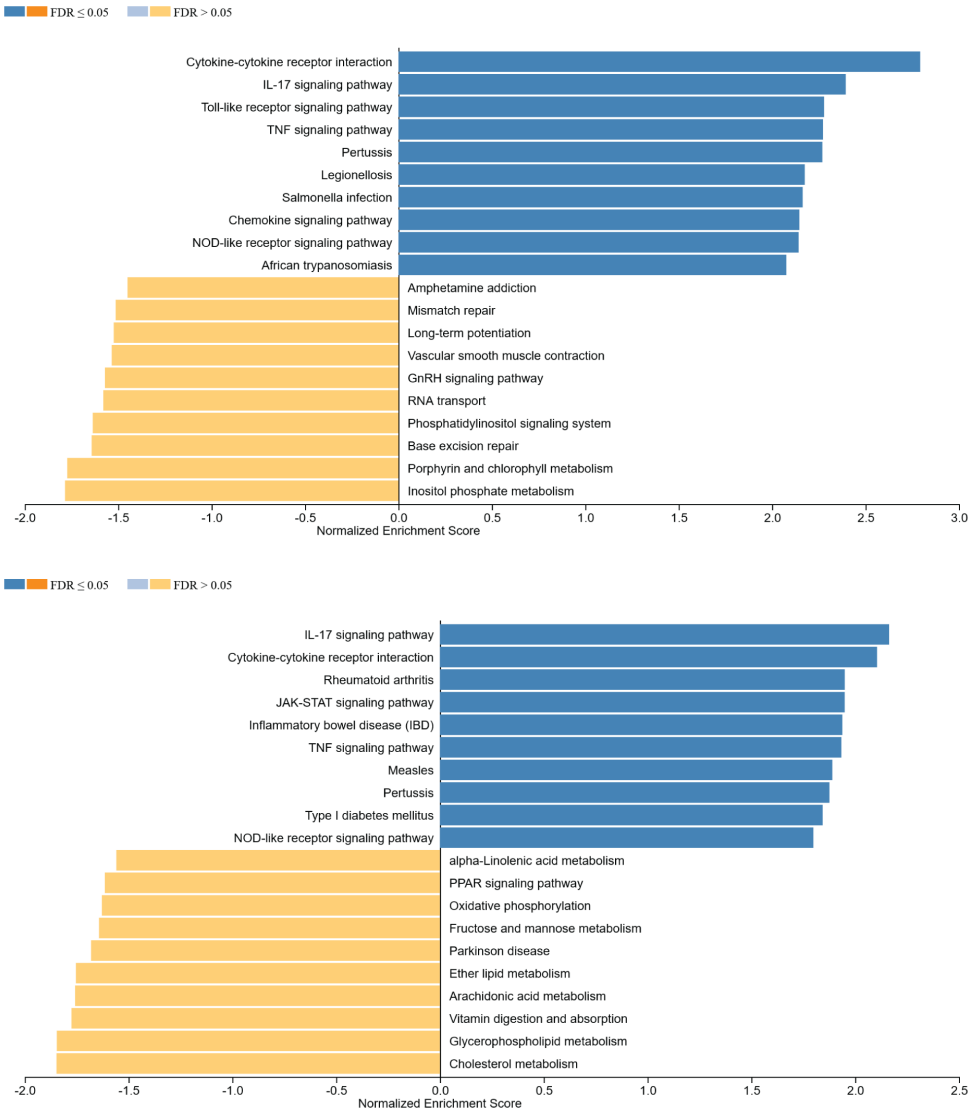

Figure 3.8 Pathways exhibiting homo-directional during DC maturation.

Pathways identified by gene set enrichment analysis (GSEA) using genes that showed significant changes at the level of both transcriptome (RNAseq) and translatome (RPFseq). Pathways shown in blue or yellow correspond to up- or down-regulated upon DC maturation, and the darkness of the color depicts the false discovery rate (FDR). Up and down regulated pathways at the 4 h (top) and 24 h (bottom) time point are shown here.

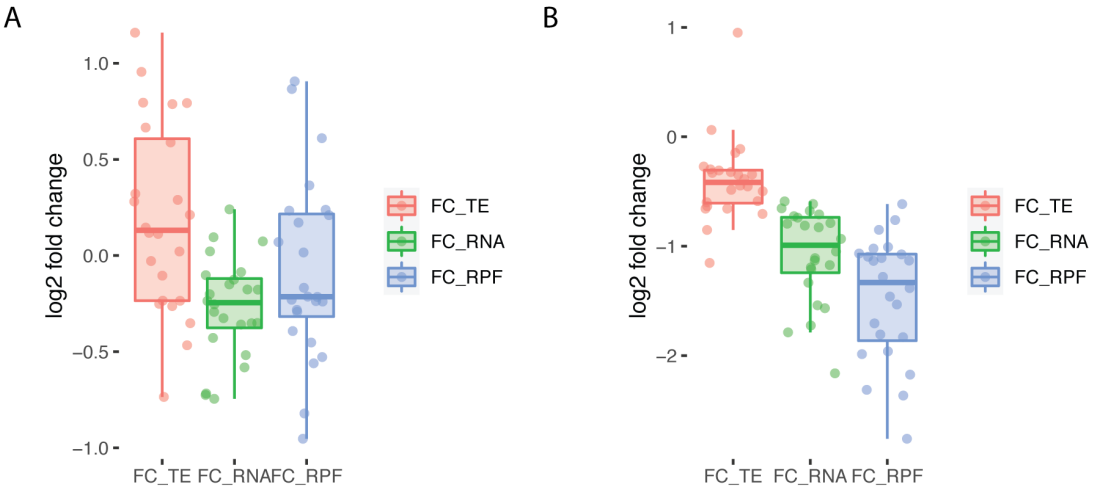

Figure 3.9 Changes in transcripts encoding for proteins involved in oxidative phosphorylation pathway.

Twenty four transcripts encoding for mitochondrial ATP synthase, cytochrome c oxidase, ubiquinol-cytochrome c reductase and NADH:ubiquinone oxidoreductase core subunits are significantly repressed during the 24 h time-point. Repression is at the level of both transcriptome and translatome. Box plots show the distribution of translational efficiency, RNA and RPF fold changes at the 4 h (left) and 24 h time-point (right). Points represent individual genes.

Performing similar analysis for genes that showed significant changes only at the RNA-level, correlation values were 0.89 and 0.84 for up and down regulated genes at the 24 h time-point, while at the 4 h time point, genes exhibited less correlation between RNA and RPF fold changes with values of 0.79 and 0.67 for up and down regulated genes (Figure 3.7, middle).

For genes that show significant changes only at the translatome level, correlation values were 0.77 and 0.82 at the 24 h time point for up and down regulated genes respectively. While for the 4 h time point, correlation values were 0.67 and 0.49 respectively (Figure 3.7, bottom). This is indeed surprising especially at the 4 h time point for significantly down regulated genes, and this shows that there are strong changes at the level of translation, which has not been reflected at the level of RNA. Especially at the 4 h time point, genes that showed significant changes only at the translatome are preferentially repressed or engaged by the ribosomes. In order to find out what families of transcript are enriched in this gene set, GSEA was performed. With the

exception of transcripts encoding for ribosomes (RPF up regulated, translationally engaged), this analysis did not provide any other family or pathway that was statistically enriched. This means that ribosomal transcripts are translationally engaged at the 4 h time point, and this observation is in accordance with previous studies (Ceppi et al., 2009; Lelouard et al., 2007).

3.1.5 Changes in translation over the course of DC maturation

In order to find out translationally engaged or repressed genes during the course of DC maturation, GSEA was performed with translational efficiency values. Here, all genes that had a base mean expression level of 50 or greater was used, regardless of whether the gene exhibited significant fold changes at the level of RNA and/or at the translatome level. At the 4 h time-point this GSEA analysis revealed five sets of transcripts that showed positive change in translational efficiency (Figure 3.10, top).

These sets of transcripts encode for ribosomal proteins, antigen processing, amino acid biosynthesis, tyrosine metabolism and ‘alcoholism’ (Figure 3.10, top). Almost all the genes under the ‘alcoholism’ family encode for histones. Translational up-regulation of transcripts encoding for ribosome and antigen processing and presentation is well in accordance with previous polysome profiling analysis of DC maturation (Ceppi et al., 2009). Apart from the above-mentioned gene families, the glycolysis pathway is translationally engaged at the 4 h time point. When plotting the fold changes for translational efficiency, RNA and RPF, it could be clearly seen that there is translational engagement for these transcripts at the 4 h time point (Figure 3.11). Among the pathways that are repressed it is important to note that PI3K-Akt signaling pathway is one of them (Figure 3.10, top).

In line with previous studies, temporal up-regulation of ribosomal and antigen processing and presentation transcripts were also evident. At the 24 h time point, top two repressed transcript families are ribosome and glycolysis respectively (Figure 3.10, bottom). This was also evident when plotting the distribution of translational efficiency; RNA and RPF fold changes at the 24 h time point (24h/iDC) (Figure 3.12). Among the five families of transcripts that were up-regulated at the 4 h time point, translational repression at the 24 h time point was much stronger for ribosomal transcripts (Figure 3.12). Transcripts encoding for antigen processing and presentation do not show much translational repression at the 24 h time point. This makes sense, since DCs need to still present the processed antigen at this time point.

The number of genes that showed statistical for differential translational efficiency (RPF/RNA, DTE) at 4 h time point (157 genes) is also higher in

comparison to 24 h time point (11 genes). In order to find out how translational efficiencies (TE) were affected during the course of DC maturation, the change in TE was plotted for both 4 h and 24 h time-point respectively. This distribution revealed that at the 4 h time-point the change in TE exhibited broader distribution than in comparison to the 24 h time-point (Figure 3.6C). In accordance with all previous analysis, it can be inferred that there is more translational regulation at 4 h post maturation than during later stages of DC maturation.

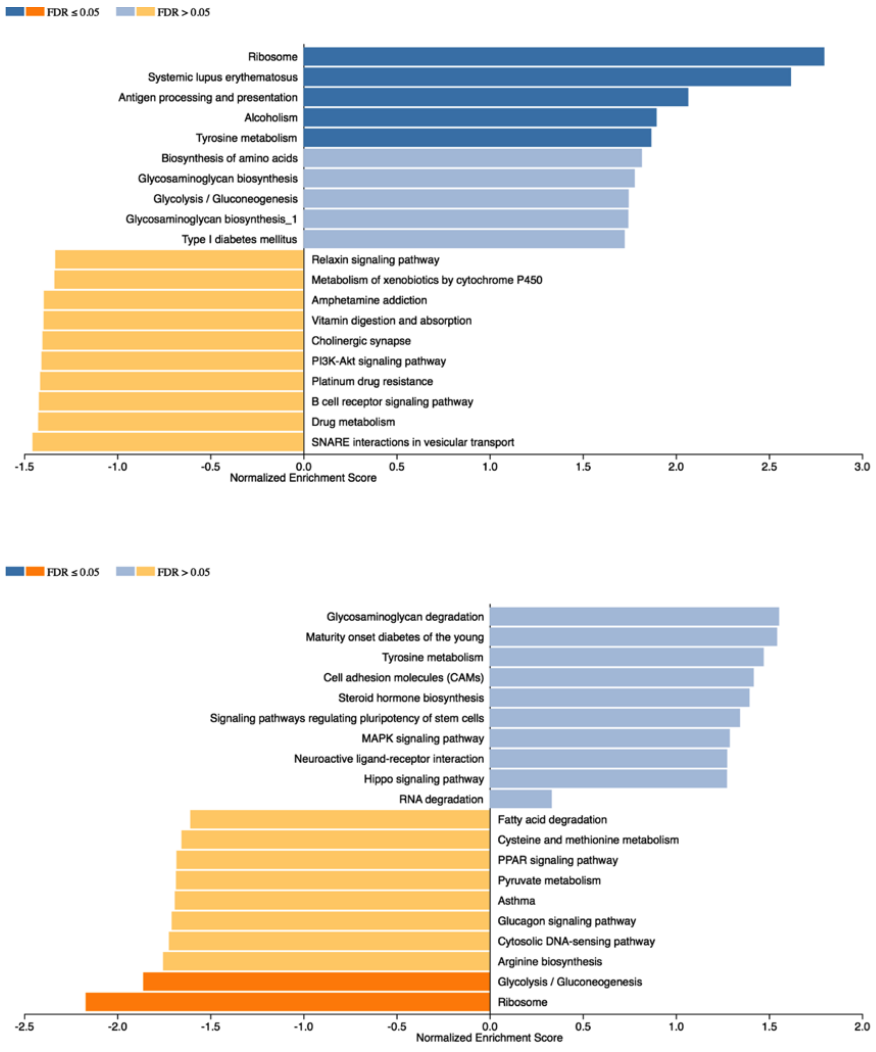

Figure 3.10 Pathways enriched for translational efficiency changes over the course of DC maturation.

GSEA was performed with translational efficiency values. Pathways shown in blue or yellow correspond to enhanced or repressed translational efficiency. Analysis was performed for both the 4 h (top) and 24 h (bottom) samples. Intensity of the color depicts false discovery rate of the identified pathways.

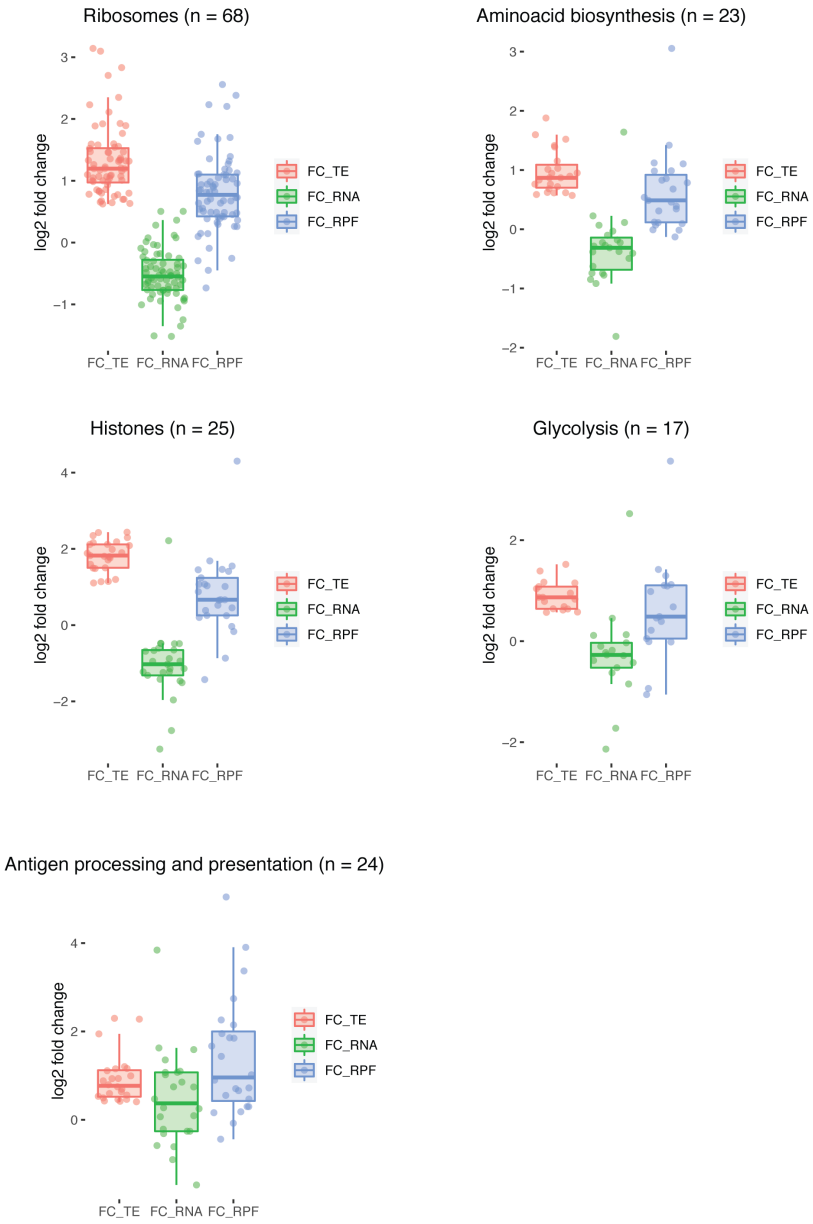

Figure 3.11 Translationally upregulated pathways at the 4 h time-point during DC maturation.

Transcripts that encode for ribosomes, histones, amino acid biosynthesis, antigen processing and presentation and glycolysis are translationally up regulated at the 4 h time-point. Shown here are the distributions of translational efficiency (red), RNAseq (green) and RPFseq (blue) fold changes (4h/iDC) respectively.

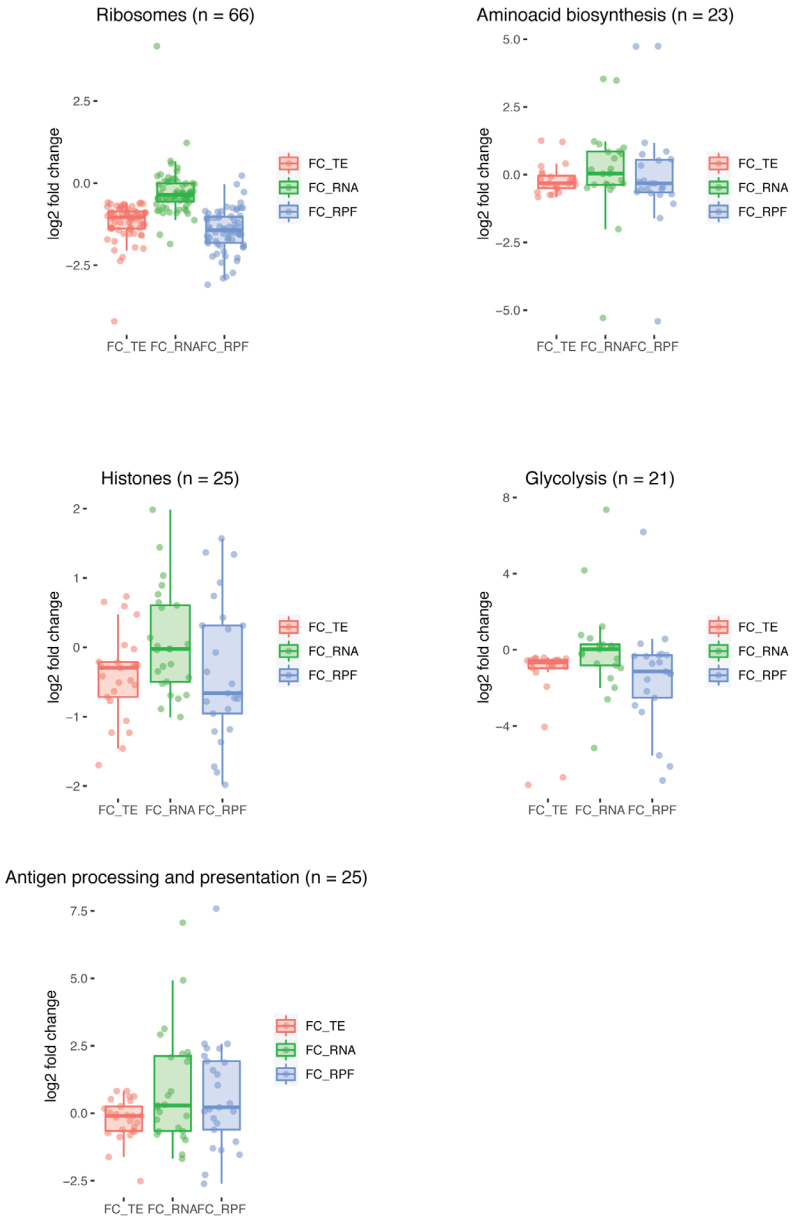

Figure 3.12 Pathways that are repressed translationally at the 24 h time point.

Plotted are the distributions of translational efficiency (red), RNA (green) and RPF (blue) fold changes for transcripts encoding for ribosomes, histones, amino acid biosynthesis, glycolysis and antigen processing and presentation.

3.1.6 Accumulation of ribosomes in untranslated regions during dendritic cell maturation

Since ribosome profiling involves sequencing of fragments protected by 80S monosomes, it is assumed that the majority of RPFs map to coding sequences. Therefore, it was surprising to observe RPFs mapping to 5'-UTR regions at 4 h as well as at 24 h time point (Figure 3.13). Additionally, an

increased number of RPFs mapped to 3'-UTR at 24 h time-point. As mentioned before, the ribosome-profiling protocol employed here involved a sucrose gradient step after RNAse-I treatment in order to enrich 80S monosomes and subsequent downstream processing of this fraction for RPFseq library preparation. Hence, the RPFs mapping to UTRs are likely originated from fragments protected by the 80S monosomes. Comparison of ribosome density on untranslated regions and CDS across all samples revealed that elevated ribosome density on UTRs is apparently a global effect rather than for specific genes. This is evident from the number of genes showing significantly increased ribosome density for 5' UTR. It should also be mentioned that the 5' UTR displays a progressive increase in ribosome density during the course of DC maturation, while, the 3' UTR shows increased ribosome density only at 24 h time point (Figure 3.13).

Plotting the 5' UTR ribosome density against the corresponding CDS ribosome density revealed no strong correlation for iDC and the 4h time-point, while the 24 h time point showed weak correlation (Spearman correlation-0.24) (Figure 6.2). Metagene analyses of ribosomal footprints around AUG codons in the 5' UTR were performed for all samples to test for active translation in the 5' UTR during DC maturation, And a global alignment of ribosomal footprint was performed similar to regions around the canonical stop codon, where three-nucleotide periodicity was observed (Figure 3.4). However, performing a similar analysis with start codons in the 5' UTR exhibited only weak three-nucleotide periodicity for 4h DC, while iDC and 24 h DC samples did not show any periodicity (data not shown). Therefore, the current state of analysis does not provide strong evidence for active translation in the 5' UTR.

Recently, a growing number of ribosome profiling studies have reported on the presence of small ORFs (coding for less than 100 aa) in the non-coding regions of the genome. However, the validation of these small peptides is quite challenging, since ribosome profiling has to be performed in the presence of translation initiation inhibitors (such as lactimidomycin or harringtonine). Furthermore, the evidence for corresponding peptides has to be supported by mass spectrometry studies. This can be investigated in future

studies specifically focused on identification and characterization of novel small ORFs during DC maturation.

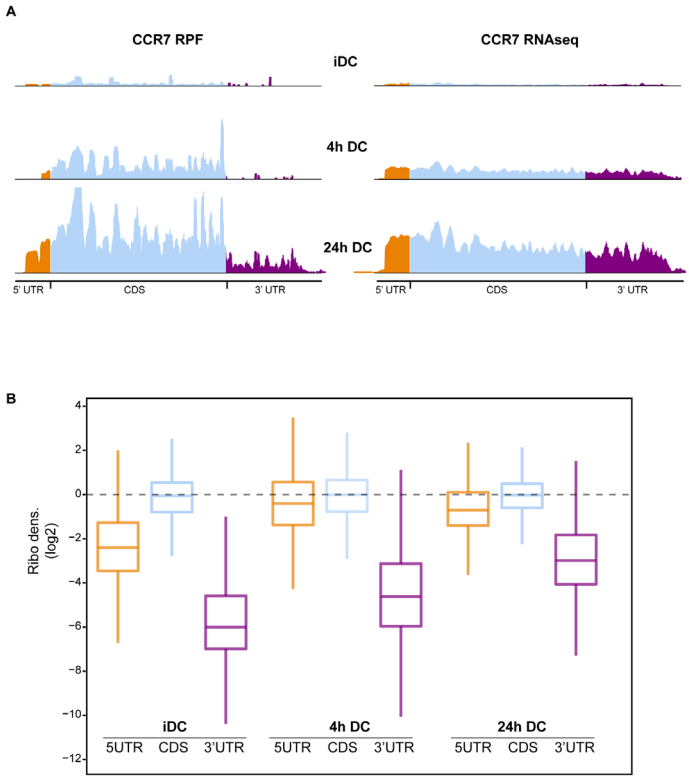

Figure 3.13 Increase in ribosome density in the UTRs over the course of DC maturation.

(A) As an example, ribosome occupancy (RPF, left) and RNA coverage (RNA, right) is shown for the gene CCR7. Coverage over 5' UTR, CDS and 3' UTR is shown in orange, light blue and purple, respectively. 5' UTR ribosome occupancy increases over the course of DC maturation, while 3' UTR shows increased ribosome occupancy at a later time point. (B) Ribosome density is ribosome occupancy normalized for RNA amounts, and is plotted here for 5' UTR, CDS and 3' UTR, respectively. Globally CDS ribosome density median does not change much over the course of maturation, while 5' UTR shows increase in ribosome density after induction of maturation. Interestingly, at the last time-point (TLRdc_24h) 3' UTR shows increased ribosome density.

3.1.7 Ribosome recycling defect in mature dendritic cells

Similar to 5' UTR, the increase in ribosome density in the 3' UTR also showed no correlation to the corresponding CDS. The accumulation of ribosomes in the 3' UTR at 24 h could be a result of defects in translation termination leading to stop codon readthrough. However, a stop codon metagene plot of

RPFs showed that ribosomes entering 3’ UTR lose their three-nucleotide periodicity, a typical feature of RPFs generated from translating 80S, therefore rendering this explanation unlikely (Figure 3.14A). Correspondingly, expression levels for the genes encoding for release factors eRF1 and eRF3 showed only slight changes in their expression levels.

Using rabbit reticulocyte *in vitro* translation system, it has been shown before that post termination ribosomal complexes (*i.e* after canonical peptide release by eRF1), in the absence of ABCE1 can diffuse along the mRNA into the 3’ UTR and are able to rebind to codons cognate to the P-tRNA which they still carry. Similarly, a recent publication (D. J. Young et al., 2015) by the Green group showed that Rli (ABCE1 in mammals) depletion in yeast leads to accumulation of ribosomes in the 3’ UTR. Interestingly, these ribosomes are shown to reinitiate translation in the 3’ UTR by a frame-independent non-canonical mechanism. In fact, the gene coding for ABCE1 showed a slight decrease of one-third at 4 h and three-fold down regulation at 24 h at the level of both RPF- and RNAseq respectively (Figure 3.14D). Further, the down regulation of ABCE1 during DC maturation was validated at RNA and protein levels by qRT-PCR (Figure 3.14C) and western blot analysis (Figure 3.14E).

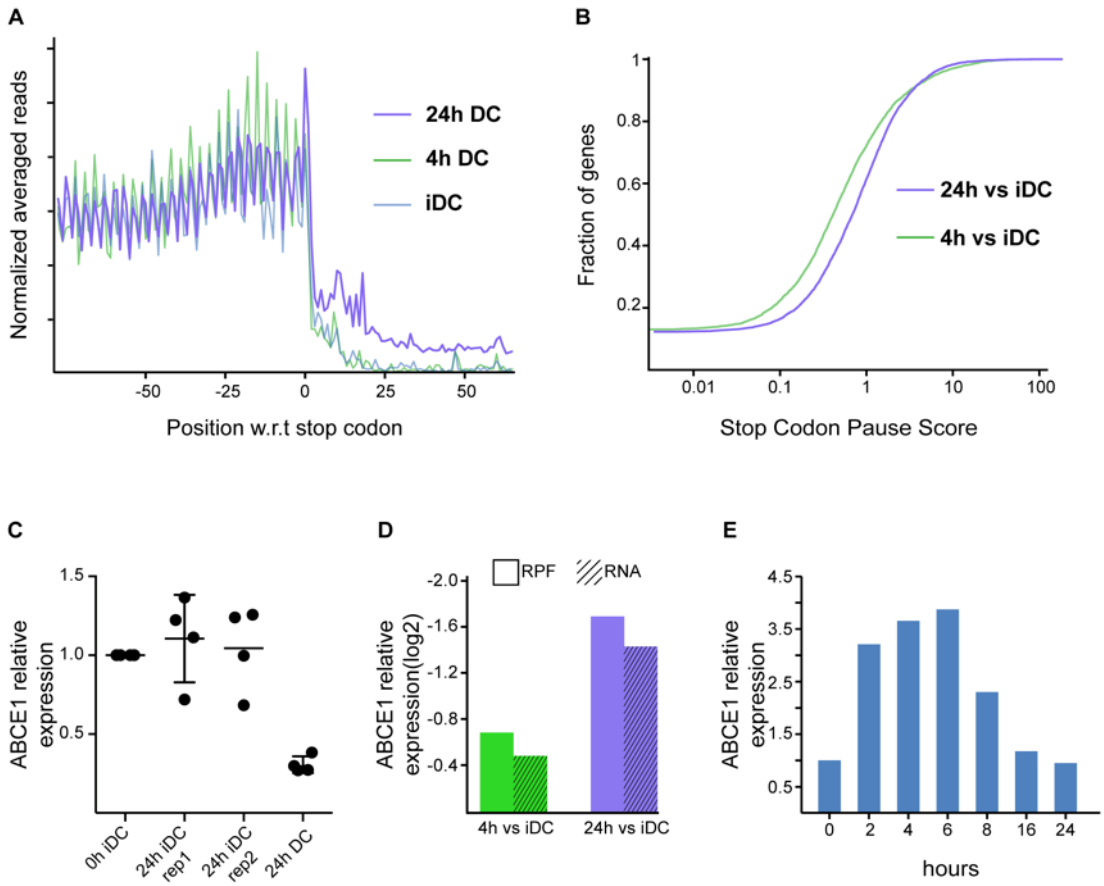

Figure 3.14 Down regulation of ABCE1 in mature dendritic cells.

(A) Metagene analysis reveals ribosome occupancy well past the stop codon into the 3' UTR for 24 h DC sample. Modest increase in ribosome occupancy can be seen over the stop codon for the 24 h time-point. (B) Stop codon pause score was calculated for 4 h/iDC and 24 h/iDC. This analysis revealed that at later stage of DC maturation, ribosomes indeed dwell longer at the stop codon. (C) ABCE1 mRNA levels were quantified using qPCR, and It is down regulated after induction of maturation. As a control, iDCs were cultured for 24 h without adding the cytokine mixture for maturation, and ABCE1 levels does not show much difference compared to the 0 h time-point. (D) ABCE1 shows slight decrease in expression at the transcriptomic and translatome level for the 4 h time-point, while a stronger down regulation is seen at both levels for the 24 h time-point. (E) ABCE1 protein levels were estimated after induction of DC maturation by western blotting. It can be seen that indeed at the protein level, ABCE1 expression is repressed strongly as the maturation progresses.

The consequence of ABCE1 down-regulation should lead to increased ribosome occupancy at canonical stop codons as a result of defective post-termination ribosome recycling. Therefore, a pause score was calculated over canonical stop codons for iDC and 24 h DC samples. The analysis

demonstrated that indeed in 24 h DC sample, as a result of post-termination recycling defect, ribosomes occupy the stop codon much longer than in comparison to iDC. Stop codon pause scores (Figure 3.14B) are normalized to their corresponding CDS expression levels, therefore the observed change in pause score is not the effect of differential CDS expression.

In contrast to the study conducted in yeast (D. J. Young et al., 2015), the non-recycled ribosomes in 24 h DC do not show any hint of translation reinitiation in the 3' UTR. This is evident, as ribosomes pass by number of stop codons in the 3' UTR, and also 3' UTR stop codons do not display any detectable level of ribosome occupancy (Figure 3.15). Overall, the reduction of ABCE1 levels results in increased occupancy of non-recycled ribosomes over canonical stop codons and also in the 3' UTR.

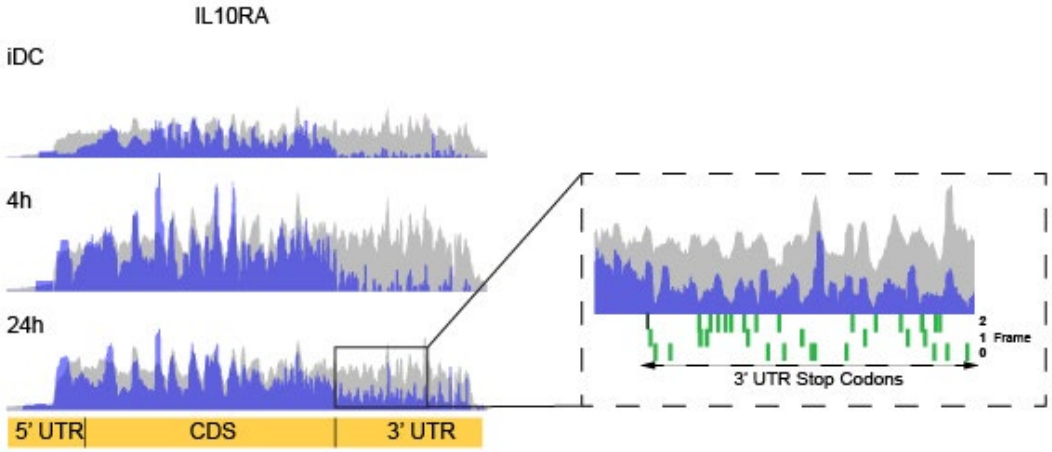

Figure 3.15 Stop codons in the 3' UTR does not show increased ribosome occupancy.

As an example, ribosome occupancy (blue) and RNA coverage (gray, background) of the gene IL10RA is shown here. Corresponding features of this gene are shown below in yellow. At the 24 h time-point, the IL10RA gene shows increased ribosome occupancy in the 3' UTR, due to the down-regulation of ribosome recycling factor ABCE1. As a zoomed-in view, a part of 3' UTR is shown. The canonical stop codon of the gene is shown in red, while stop codons in the 3' UTR are shown in green. It can be seen that 3' UTR stop codons do not show increased ribosome occupancy, indicating absence of re-initiation or any active translational activity by the ribosomes stuck in the 3' UTR.

3.1.8 Ribosome density in 3’ UTR shows strong correlation to the 3’ UTR GC content

To investigate further if any additional features contributed to increased ribosome density in the 3’ UTR, length and GC content of 3’ UTR were compared to their corresponding ribosome densities. Plotting ribosome densities against the length of gene features across all samples (iDC, 4 h and 24 h) did not yield any conclusive result.

An interesting observation was made with respect to the GC content. Not surprisingly, the GC content of CDS and their corresponding ribosome density did not show any correlation. Despite this, CDS ribosome density of 4 h DC sample showed a mild correlation to GC content, which might be likely due to changes in expression and/or translation levels during DC maturation. For 5’ UTR, there was neglectable correlation for iDC sample, while 4 h and 24 h DC sample showed a slightly positive correlation. As mentioned before, the biological relevance for ribosome occupancy of 5’ UTR is not clear. Calculating the correlation for 3’ UTR GC content and corresponding ribosome density showed a mild correlation for iDC (Spearman correlation, $r = 0.26$), but progressively became stronger over time ($r = 0.66$ for 24 h DC sample, Figure 3.16)

What explains this strong correlation between GC content and 3’ UTR ribosome density? A simple explanation would be that, 3’ UTRs with high GC content have a higher propensity to form folded secondary structures. As a result of ABCE1 down-regulation during DC maturation, non-recycled ribosomes diffusing along the 3’ UTR would be slowed down and sequestered by 3’ UTRs with higher GC content.

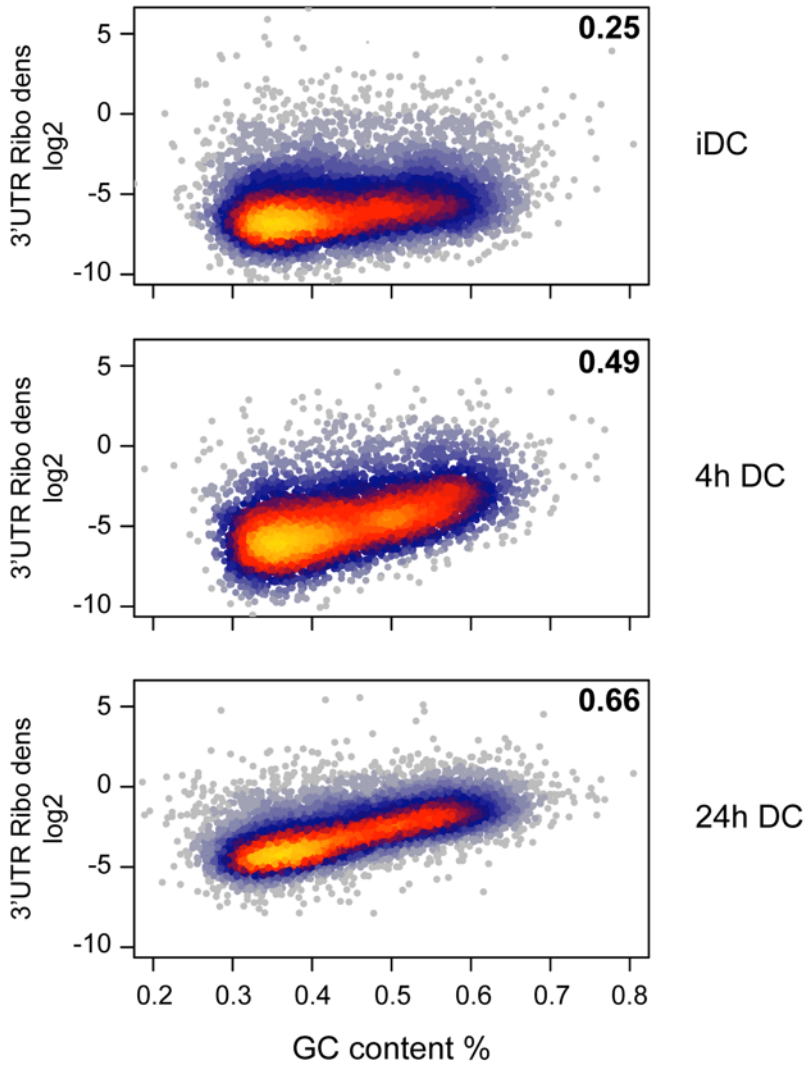

Figure 3.16 Correlation between 3'UTR GC content and ribosome density.

During the course of DC maturation, ribosome density in the 3'UTR exhibited progressively stronger correlation to its GC content.

In conclusion, mammalian ribosomal profiling has been successfully established, and has been used to study translational regulation in maturing dendritic cells. Certain sets of pathways or genes were homo-directionally regulated during DC maturation. Especially, twenty-four transcripts encoding for proteins involved in oxidative phosphorylation pathway were repressed both at the level of RNA and translatome. In line with previous studies, transcripts encoding for ribosomal proteins, antigen presentation and processing were translationally up regulated during the early stage of DC

maturation, while being repressed at the 24 h time point. Further, 5’ UTR showed gradual increase in ribosome occupancy. Interestingly, the ribosome-recycling factor ABCE1 is down regulated over the course of DC maturation, leading to accumulation of post termination 80S-ribosomal complexes in the 3’ UTR. This accumulation of ribosomes in the 3’ UTR is strongly correlated to its GC content.

3.2 Selective ribosome profiling of the ribosome-Ski complex

In this project, the structure and function of ribosome-bound Ski complex was explored. Ribosome-Ski complexes were structurally investigated using cryo-electron microscopy and functionally characterized by *in vivo* selective ribosome profiling.

3.2.1 The Ski complex interacts with ribosomes *in vivo*

In order to examine whether Ski proteins interact with the ribosomes *in vivo*, yeast strains expressing TAP tagged versions of Ski7 and Ski3 were used. Lysates from these modified yeast strains were subjected to sucrose gradient centrifugation and fractionated for polysome analysis (Figure 3.17A). Dr. Christian Schmidt (Group of Prof. Dr. Roland Beckmann) performed the polysome analysis, purification and structural analysis of native ribosome-Ski-complexes discussed in this part. Collected fractions were further analyzed by western blotting, and positions of Ski3-TAP and Ski7-TAP in the sucrose gradient were monitored using α-TAP antibody. Surprisingly, most of the signal for Ski7-TAP was confined to lower molecular weight fractions (upper-part) of the gradient, while Ski3-TAP was detected throughout ribosomal fractions (Figure 3.17A). In order to exclude the possibility of Ski3 co-migrating with ribosomes due to possible non-specific interaction with mRNA, polysome analysis was performed with RNAse-A treated lysates. RNAse-A treatment collapsed the polysomes to a single 80S monosome peak, and Ski3-TAP was detected only in this fraction (Figure 3.17A). Possibly, mRNA overhangs created upon RNAse-A treatment led to enrichment of Ski3-TAP on the 80S monosome fraction.

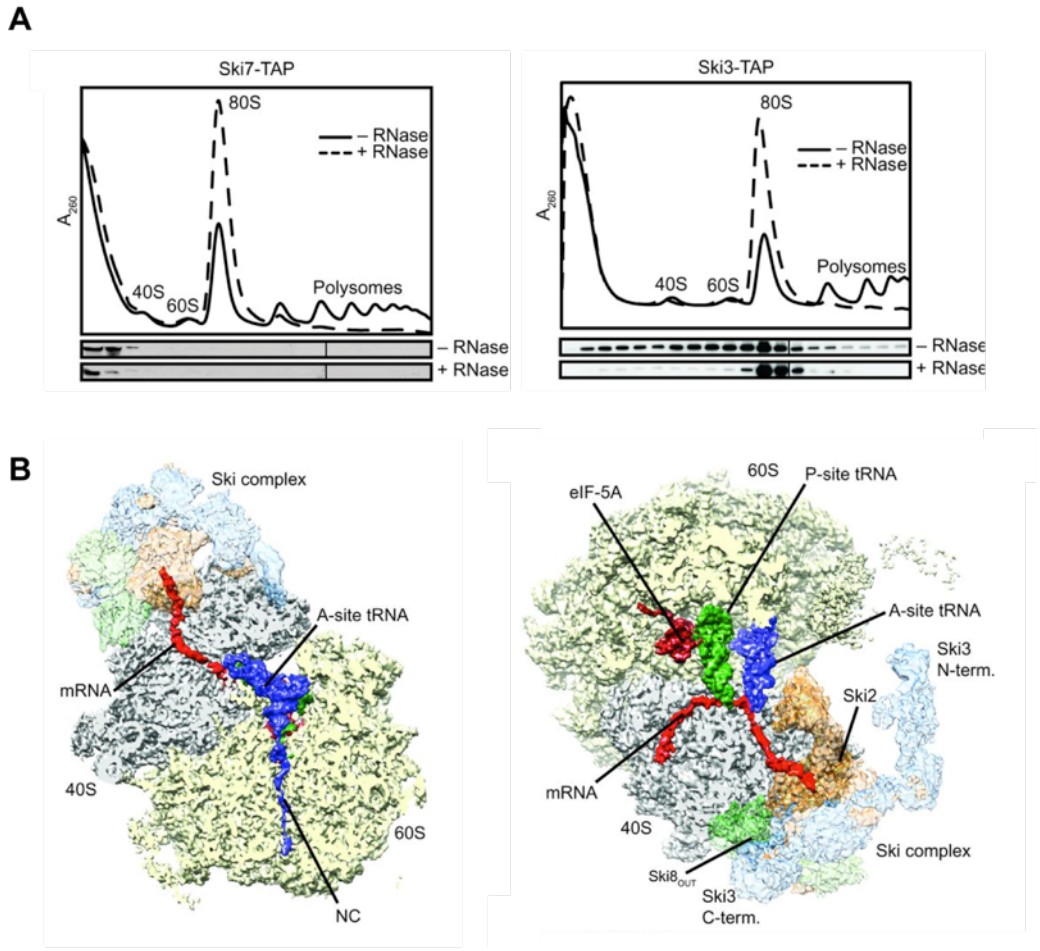

Figure 3.17 Ski complex interacts with 80S monosomes.

(A) Sucrose gradient polysome profiles of yeast lysate containing TAP tagged Ski7 or Ski3 protein and with and without RNAse-A treatment. (B) Cryo-EM maps of the Ski complex-bound 80S ribosome (front and top view). Ribosomal subunits, A-, P-site tRNAs, the nascent chain and mRNA are shown as segmented densities.

This result suggested that the Ski complex but not Ski7 interacts with ribosome *in vivo*. Additionally, Ski-complex and Ski7 were tested for their function in NSD using non-stop reporter assays (Performed by Quentin Defenouillere, Alain Jacquier lab). The non-stop reporter construct had a TAP-tag, and was expressed in strains lacking *SKI7* and either *DOM34* or *HBS1*. Non-stop ribosomal complexes were purified using the TAP-tag, and further quantified using label-free mass spectrometry. This analysis further confirmed that Ski-complex is recruited to the non-stop ribosomal complexes in the absence of Ski-7 and either Dom34 or Hbs1.

Moreover, native ribosome-Ski-complexes were purified via Ski3-TAP for cryo-EM structure determination and selective ribosome profiling. The cryo-EM analysis performed by Dr. Christian Schmidt revealed ribosomal particles containing indeed the entire Ski complex as additional density. Refinement of these particles led to a 3.8 Å structure of the 80S-Ski-complex, enabling to build a near complete atomic model of the ribosome and the Ski complex. The structure revealed a ribosome programmed with tRNAs in the A and P sites and the presence of a nascent polypeptide chain indicating that Ski-bound ribosome are indeed stalled during translation. The Ski complex binds exclusively to the small ribosomal subunit on the mRNA entry site (Figure 3.17B) forming multiple interactions with 40S subunit proteins and rRNA. Strikingly, density for 34-nts of mRNA was observed extending from the mRNA channel into the Ski2 helicase core (Figure 3.17B) indicating that the Ski complex indeed directly interacts with mRNA overhangs as suggested by the RNAse experiment (Figure 3.17). Refer to this publication for further structural details (Schmidt et al., 2016).

3.2.2 Selective ribosome profiling of the native ribosome-Ski-complex

Analysis of the cryo-EM structure revealed that the mRNA overhang extending from the 3’ end of the ribosome might serve as a signal for recruitment of the Ski-complex to the translational machinery. In order to characterize this interaction and to gain insights about *in vivo* mRNA substrates of the Ski-complex, selective ribosome profiling of the 80S-Ski-complex has been performed. The overall strategy is depicted in the Figure 3.18. Ribosome profiling (RPFseq) gives global information about the position of the ribosomes *in vivo*, while RNAseq provides data on the mRNA abundance. Since the Ski-complex is known to be involved in the exosome-mediated mRNA turnover, RNAseq was done for the purified ribosome-Ski-complexes (Ski-80S-RNAseq) and also for the background lysate (control-RNAseq) sample.

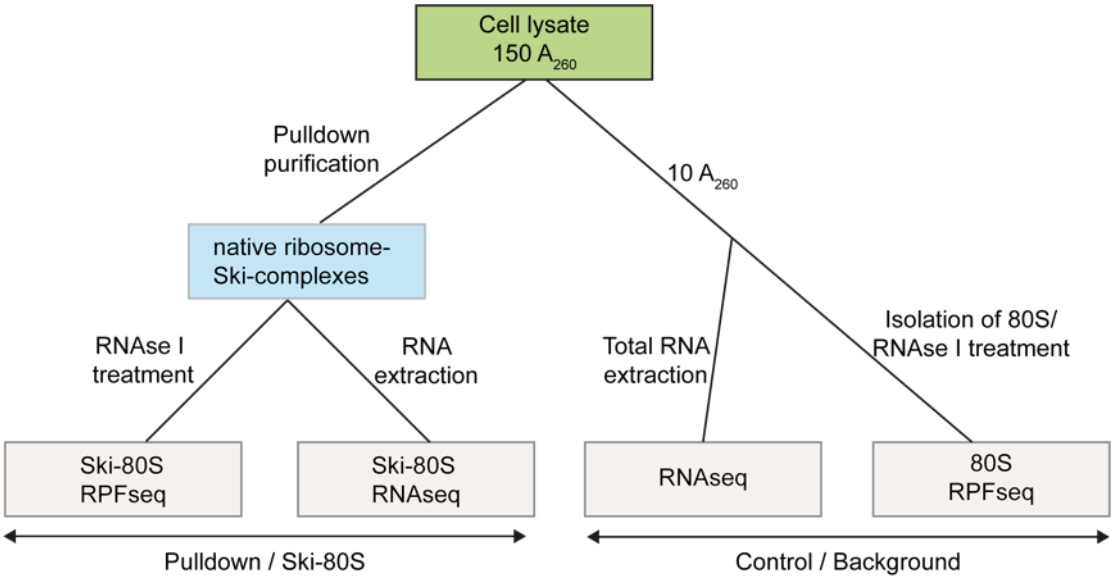

Figure 3.18 Schema for selective ribosome profiling of the native Ski-80S complexes.

Sample preparation overview for ribosome profiling from Ski3 TAP tagged strain. Control or background sample is prepared directly from the cell lysate. Pull-down or Ski-80S sample is generated from purified native Ski-80S complexes. Isolation of 80S step is excluded for ribosome profiling of Ski-80S complexes, since most of the purified Ski-80S complexes contained 80S monosomes.

Native ribosome-Ski-complexes for selective ribosome profiling (Ski-80S-RPFseq) have been purified using the exact same method used for cryo-EM sample generation. Preparation of background RPFseq (80S-RPFseq), which served as a control here, involved an extra step of 80S isolation after nuclease digestion using sucrose gradient centrifugation. Also, as mentioned before in the previous section, this step was performed for human dendritic cell ribosome profiling. This 80S isolation step, however, has been omitted for Ski-80S-RPFseq, since the purified 80S-Ski-complexes predominantly contained monosomes. Libraries were prepared using the protocol developed for dendritic cell ribosome profiling. Sequenced libraries were clipped of the 3' end adapter, and further removed of reads mapping to the non-coding parts (rRNA, tRNA, snRNA and snoRNA) of the yeast genome. Unless otherwise mentioned only uniquely mapped reads were used for further analysis.

In total 677,621 and 790,797 reads that uniquely map to the yeast genome were obtained for control- and pullout-RPF, respectively. It is a well-known fact that the length distribution of yeast ribosomal footprints exhibits a

sharp peak at 28 nts (Ingolia et al., 2009; Weinberg et al., 2016). Not surprisingly, approximately 40% of control-RPF footprints were of length 28 nts (Figure 3.19, top). Interestingly, footprint length distribution of pullout-RPFseq peaked at 30 nts but also showed a sub-population of footprints (15%) of length between 36 – 40 nts (Figure 3.19, bottom). As seen in the structural analysis (Figure 3.17) mRNA overhangs bind to the Ski2 helicase core leading to a protection of this fragment, thus explaining the longer footprints in the Ski-RPF data. This observations also agree with previous biochemical data showing that the Ski-complex protects mRNA fragments of 9 - 10 nucleotides *in vitro* (Halbach et al., 2013). Taken together, this work shows that the Ski-complex binds to the ribosome *in vivo* and channels mRNA extending from the mRNA tunnel into its helicase core.

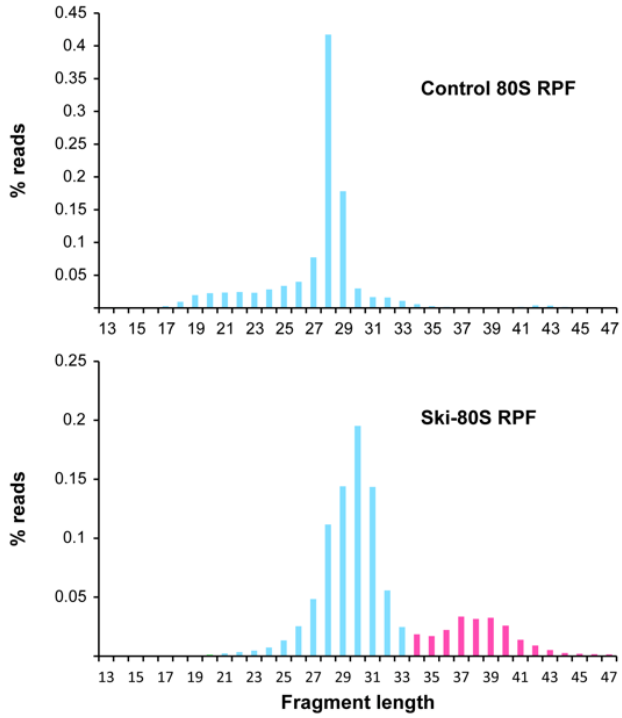

Figure 3.19 Length distribution of ribosomal footprints from 80S-Ski-complexes and control 80S monosomes.

(Top) Length distribution of control-RPFseq footprints exhibiting a sharp peak at the expected length of 28 nts (light blue). (Bottom) Length distribution of RPFs from purified 80S-Ski-complex showing a peak at 30 nts bases (light blue), but also a smaller population of longer length fragments between 35 – 40 nts (dark pink).

3.2.3 The Ski-complex interacts with the 40S subunit on the mRNA entry site

Examination of the structural data showed that the Ski-complex predominantly interacts with the 40S subunit on the mRNA entry site. In order to examine whether this interaction is reflected in RPFseq data, ribosomal footprints were aligned and summed with respect to start and stop codon. 5' and 3' end of ribosomal footprints was generated upon nuclease digestion by the 40S mRNA exit and entry side respectively.

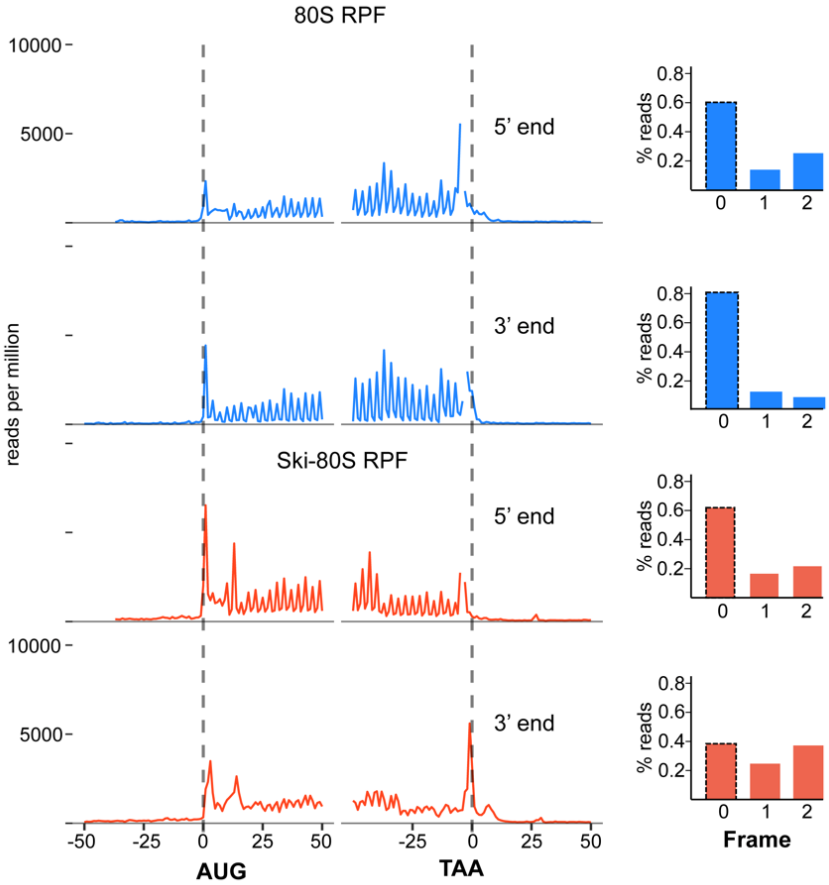

Figure 3.20 Ski complex interacts with the 40S subunit on the mRNA entry side *in vivo*.

(Left) 5' and 3' end metagene plot of ribosomal footprints around start and stop codon, respectively. It can be observed for control RPFseq (top) that there is 3-nt periodicity for both footprint ends (Ingolia et al., 2009). However, Ski-80S footprints exhibit periodicity only for 5' end, while 3-nt periodicity is disturbed at the 3' end, implying 3' end periodicity for Ski-80S footprints are lost due to the interaction of the Ski complex with the ribosome on the mRNA entry site. (Right) Shown are the percentages of reads within the three reading frames (0, 1 and 2).

Moreover, there are two main advantages analyzing yeast ribosomal footprints generated upon RNAse-I digestion. First, RNAse-I does not have cutting bias and therefore ribosomal footprints display clear three-nucleotide periodicity, representing ribosomal movement of one codon at a time. Second, since the majority of yeast ribosomal footprints are of a single length (28 nts), consequently these footprints all display strong single reading frame preference (Ingolia et al., 2009). Reading frame preference simply denotes that the footprint ends predominantly map to one of the three bases of the codon. On that account, the number of footprints mapping into any of the three bases was calculated for both control and Ski-80S-RPFseq datasets. This analysis was performed for 5'- and 3'-ends of the footprint. Inspecting the 5' end, both footprints display three-nucleotide periodicity and strong preference for one of the reading frames. However, examining the 3' end, it can be seen that only control footprints predominantly map to a single reading frame and also exhibit three-nucleotide periodicity. While 3' end analysis of footprints derived from ribosome-Ski-complexes does not show three-nucleotide periodicity, and also do not map predominantly to single reading frame. Therefore, this analysis shows that the Ski-complex in fact interacts with the 40S subunit on the mRNA entry site. Notably, this is in accordance with the structural data.

3.2.4 The Ski-complex interacts with ribosomes stalled during NSD

The Ski-complex is known to function with the exosome in NSD, targeting the stalled ribosomes in the mentioned pathway (Frischmeyer et al., 2002; van Hoof et al., 2002). As previously demonstrated, ribosomes involved in NSD should give rise to footprints with consecutive A's in the 3' end (Guydosh & Green, 2014). Ribosomal footprints containing only stretches of A's cannot be mapped to the yeast genome and therefore were discarded. Interestingly, both in the control- and Ski-RPFseq there were footprints that could be mapped back to the yeast genome after being trimmed of poly-A stretches from the 3' end. Most of the poly-A trimmed footprints map at the junction between 3' UTR and the poly-A tail (Figure 3.21A). Notably, these footprints were initially classified as 'unmapped' by the mapper, meaning these

footprints could be mapped uniquely only after poly-A stretches have been trimmed. Similar reads in the control- and Ski-RNAseq were also analyzed.

Calculating the number of poly-A trimmed footprints revealed an about four-fold enrichment in the Ski-RPFseq (Figure 3.21B). As many as 20 A's have been clipped from the 3' end (Figure 3.21C), and this implies that the poly-A stretch could reach the A-site of the ribosome, for being translated into lysine residues and subsequent ribosomal stalling as described before (Inada & Aiba, 2005; Ito-Harashima et al., 2007; Koutmou et al., 2015). Similar inspection in the RNAseq data showed that poly-A trimmed reads are more than fivefold enriched in the background control-RNAseq (Figure 3.21B). This implies that control-RNAseq has more intact mRNAs with poly-A tails than in the Ski-RNAseq. However, ribosome-Ski-complexes are enriched on fewer numbers of poly-A containing mRNA reads. Overall, this indeed confirms that the ribosomes involved in NSD are targeted by the Ski-complex *in vivo* (Frischmeyer et al., 2002; Ito-Harashima et al., 2007; Van Hoof et al., 2002).

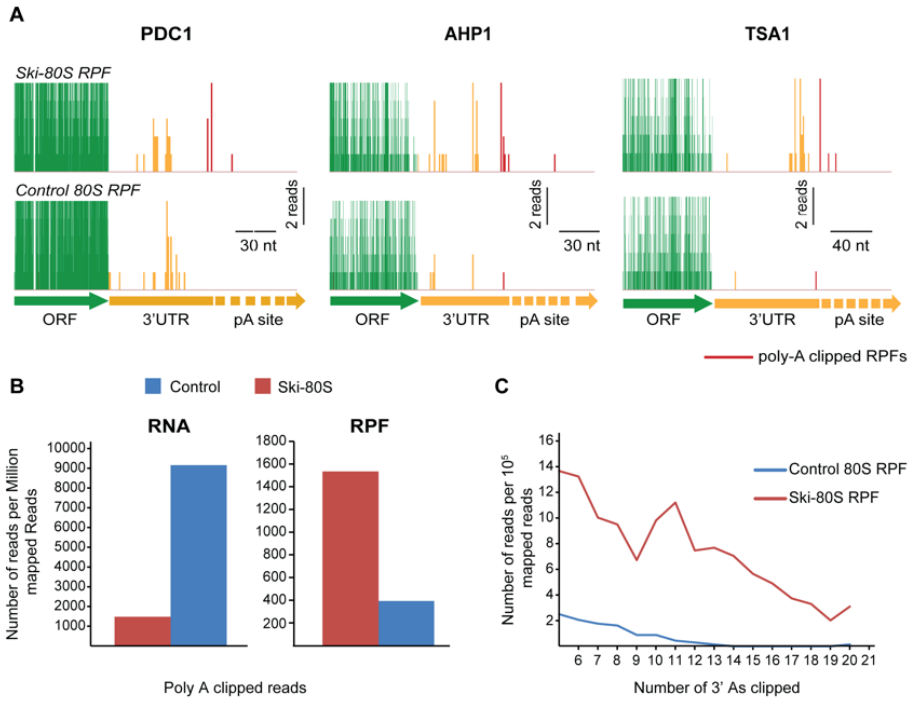

Figure 3.21 Ski-complex targets ribosomes stalled in NSD.

A) Footprints mapping to ORF (green), 3' UTR (yellow) and at poly-adenylation site (poly-A) (red) are plotted. Reads that map to poly-A sites could be mapped after poly-A trimming. **(B)** Proportion of poly-A containing reads in control and pull-down RPFseq and RNAseq data respectively. **(C)** Numbers of consecutive A's present in the 3' side of the footprints derived from Ski-80S (red) and 80S ribosome profiling data (blue).

3.2.5 Ribosome-Ski-complex is involved in 3'-5' mRNA degradation

Since Ski-80S-RNAseq contained fewer poly-A containing reads, reads mapping to 3' UTR and ORFs were calculated. Plotting the read ratio (Ski/control) for both regions revealed that the Ski-RNAseq dataset contained almost three-fold fewer reads that map to 3' UTR (Figure 3.22B, orange), while there is not much difference between the datasets for reads mapping to the ORF (Figure 3.22, green). Even though there is high correlation for ORF mapping reads, there is a striking difference in their coverage pattern. A couple of examples are shown in Figure 3.22A. It can be clearly seen that there are more reads that map to 5' ends of the transcript in the Ski-80S-RNAseq dataset in comparison to control-RNAseq. In order to verify whether this trend is observed across the genome, each coding transcript was divided into ten equal segments.

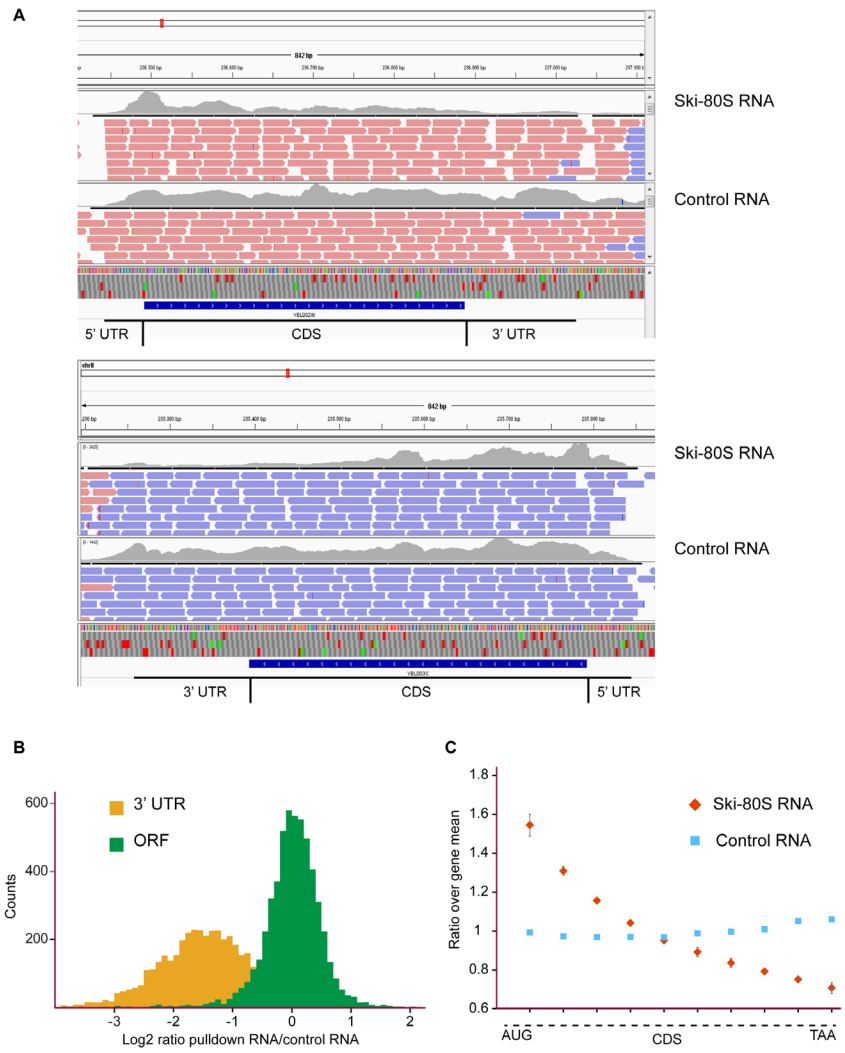

Figure 3.22 Characteristics of pull-down and control RNAseq reads.

(A) IGV browser (Thorvaldsdóttir et al., 2013) screenshots showing pull-down and control RNA coverage for a couple of genes. Evident is the difference in distribution of RNA coverage between pullout and control RNA. Pull-down RNA shows asymmetric coverage with more reads mapping to the 5' end of the transcript. **(B)** Histogram showing ratio of pull-down RNA over control-RNA for 3' UTR (4427 genes) and ORF respectively (5521 genes). **(C)** RNA coverage within the ORF (5814 genes). Genes were split into ten segments, and each segment mean was normalized with its corresponding gene mean. Plotted is the mean of normalized segment mean across the yeast genome.

Further, each segment's mean coverage was normalized to their corresponding gene mean. Then for each segment, this normalized mean was averaged across the genome and plotted (Figure 3.22C). A total of 5814 genes were included in this analysis. This analysis revealed that for control-RNAseq, each segment's mean does not deviate much from its corresponding

gene mean. This implies that transcripts sequenced in the control-RNAseq are complete and intact as expected. However, Ski-RNAseq showed asymmetric coverage with greater number of reads mapping to the 5’ end and coverage gradually decreasing towards the 3’ end. Mean coverage at the 5’ end was 1.6x gene mean, while the depleted 3’ end showed coverage of 0.6x gene mean. Overall, analysis of RNAseq data points to the fact that those transcripts engaged by ribosome-Ski-complexes are in the process of undergoing 3’-5’ mRNA degradation. This observation also fits well with the fact that Ski-RNAseq contained fewer reads containing poly-A stretches (Figure 3.21B), and also reads mapping to the 3’ UTR.

3.2.6 Transcripts with shorter half-lives are enriched in ribosome-Ski-complexes

In case the ribosome-Ski-complex is really involved in 3’-5’ mRNA degradation of canonical transcripts, it can be assumed that mRNAs with shorter half-lives are enriched in the Ski-pulldown, since shorter half-life transcripts are turned over faster and consequently engage more often with degradation machineries. In order to examine whether this hypothesis is true, RNAseq and RPFseq read ratios (Ski/control) were compared to mRNA half-lives. A majority of yeast transcripts are short-lived in comparison to their generation time (Geisberg et al., 2014). Nevertheless, two subsets of transcripts with shorter (< 5 min, 1052 genes) and longer half-lives (> 20 min, 596 genes) were used for analysis. The cumulative fraction of genes for both subsets was plotted against either RNAseq or RPFseq read ratios. While the RNAseq read ratio did not show any enrichment for shorter half-life transcripts (Figure 3.23A), a similar analysis with RPFseq revealed that indeed ribosome-Ski-complexes engage more often with short-lived transcripts (Figure 3.23B). As this analysis was done only with a subset of transcripts, we wanted to examine whether this trend holds true across the genome.

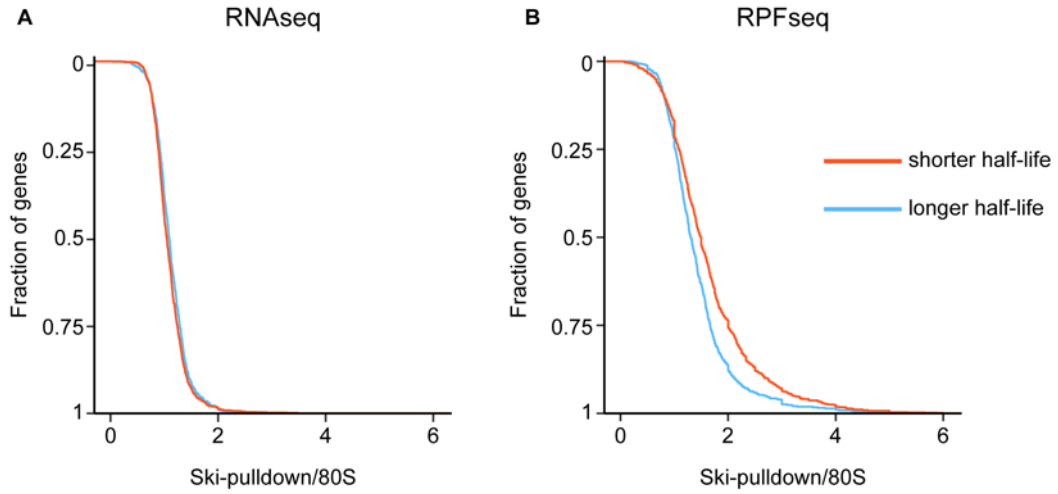

Figure 3.23 80S-Ski-complex footprints show enrichment for shorter half-life mRNAs.

A) Cumulative plot of RNA ratio (Ski pull-down/80S) were plotted for genes with longer half-life (greater than 20 min, n = 596 genes) and shorter half-life (less than 5 min, n = 1052 genes). **(B)** Cumulative plot for footprint ratio. With higher ratios for lower half-life mRNA compared to longer half-life mRNA species suggests Ski complex might be involved in the turnover of canonical mRNA in 3' – 5' direction.

To that end, percentages of non-optimal codons in transcripts were calculated. A recent study characterized 61 sense codons into optimal- and non-optimal codons, and transcripts with increased non-optimal content tend to have significantly reduced half-life (Presnyak et al., 2015). Accordingly, to investigate whether Ski-RPFseq is enriched for substrates with reduced half-life, the Spearman correlation between codon content and RPFseq read ratio (Ski/control) was calculated. This analysis was performed across the genome for 3765 coding genes. 25 codons showed positive correlation (Ski-enriched), and strikingly 21 of them are non-optimal codons (Figure 3.24). Therefore, it can be concluded that the ribosome-Ski-complex engage more often with shorter half-life transcripts *in vivo*. Notably, it is important to point out that only the footprint data showed enrichment for short-lived mRNAs. Probably this phenomenon can be explained by the fact that there could be multiple numbers of ribosomes associated with any single transcript. Thereby, this enrichment can be seen only at the level of the translatome (RPFseq) but not at the transcriptomic (RNAseq) level.

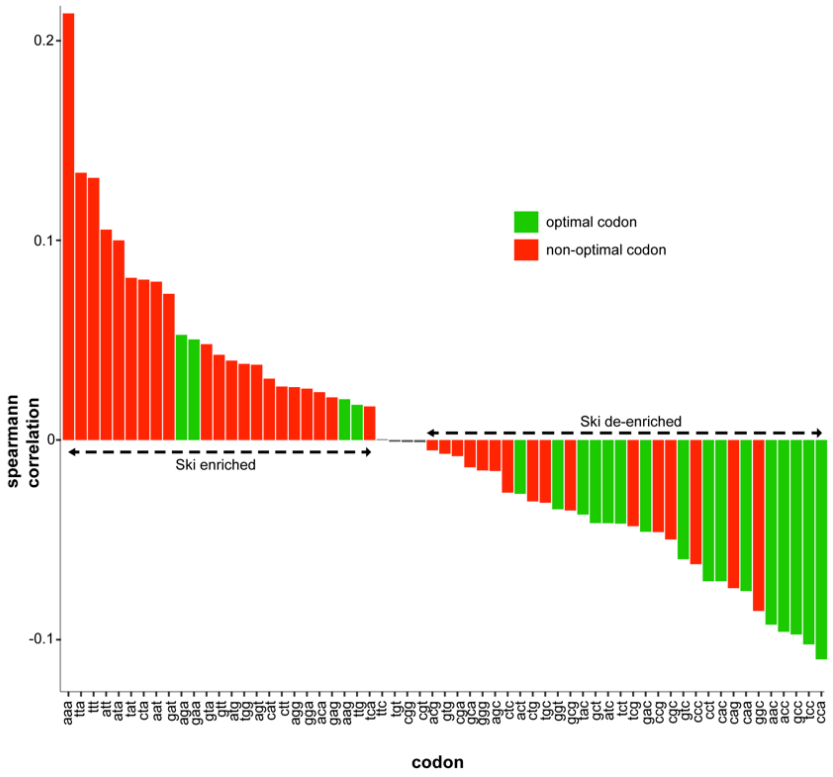

Figure 3.24 Enrichment of Ski-80S footprints on transcripts with increased non-optimal codon content.

Spearman correlation of codon content and Ski/80S footprint ratio across the genome (n = 3765 genes). Codons with positive and negative correlation were termed as Ski enriched and de-enriched respectively. Bars are colored whether codons are characterized as optimal (green) or non-optimal (red) as described in this study (Presnyak et al., 2015).

In conclusion, selective ribosome profiling of ribosome-80S-Ski-complexes revealed a sub-population of longer footprints. This is in accordance with the structural data that the 3' end mRNA overhangs might serve as a signal for Ski-complex recruitment. Also, analysis of poly-A clipped ribosomal footprints showed that the Ski-complex is recruited to non-stop stalled ribosomal complexes. Finally, RNAseq reads from Ski-80S complexes showed strong asymmetric distribution in comparison to background RNAseq, with more reads mapping to the 5' end of the transcript. This hinted at the possibility that the ribosomal-Ski-complexes might be involved in the 3'-5' degradation of canonical transcripts. Accordingly, shorter half-life transcripts

with more non-optimal codon content showed enrichment for Ski-80S ribosomal footprints.

3.3 Cryo-EM structure of a 80S ribosome stalled by the mammalian XBP1u arrest peptide

This part of the thesis deals with early targeting steps of the main UPR transcription factor in mammals – XBP1u to the ER membrane. As outlined in chapter 1.2.8, targeting of *XBP1u* mRNA involves translation of an arrest peptide, that also contains a hydrophobic SRP targeting sequence at its N-terminus. In this study, first the molecular mechanism of XBP1u arrest peptide (XBP1u-AP) mediated ribosome stalling was elucidated, via cryo-EM and single particle analysis of stalled XBP1u-RNC complex. The obtained structure was then compared with SRP-bound and Sec61-bound XBP1u-RNC to examine, if and how binding of these ligands affects the structure of the arrest peptide, e.g. if SRP or Sec61 can act as a force sensor to relive stalling. This may eventually even play a role for activation of IRE1α to initiate splicing of the *XBP1*-bound mRNA on the ER.

3.3.1 Generation of stable XBP1u- ribosome-nascent-chain complex (XBP1u-RNC)

Since the wildtype XBP1u-AP has weaker arrest potency, and stalls the ribosome only transiently (Yanagitani et al., 2011), the more stable S255A mutant has been used. It has been previously shown to be an efficient ribosome staller, and thus would allow to purify homogenously stalled ribosomal complexes for structural analysis (Yanagitani et al., 2011). The human full-length XBP1u construct was modified to express only the HR2 domain and the AP of XBP1u with N- terminal (3x-Flag, 8x-His tag and 3C-cleavage site) and C-terminal (HA tag) tags for purification and detection purposes (Figure 3.25A).

The rabbit reticulocyte lysate (RRL) *in vitro* translation system was used for generating stalled XBP1u-RNC. RRL is a well-established mammalian *in vitro* translation system, and previously (Braunger et al., 2018; A. Brown et al., 2015a; Shao et al., 2016) it has been successfully used for generating ribosomal complexes for cryo-EM structural analysis.

In vitro translation was initiated with the addition of capped mRNA to RRL. The stalled XBP1u-RNC was affinity-purified via the N-terminal His_8-tag (See materials and methods for details). The final sample was subjected to SDS-PAGE and CBB staining, and a clear ribosomal protein pattern similar to

control 80S ribosomes was observed (Figure 3.25B). Typically, a 1 ml translation reaction yielded stalled XBP1u-RNCs of concentration between 3 – 4 pmol, which was then subjected to cryo-EM analysis. Cryo-EM data was collected on a Titan Krios TEM with a Falcon II direct electron detector, and further processing was carried out with RELION.

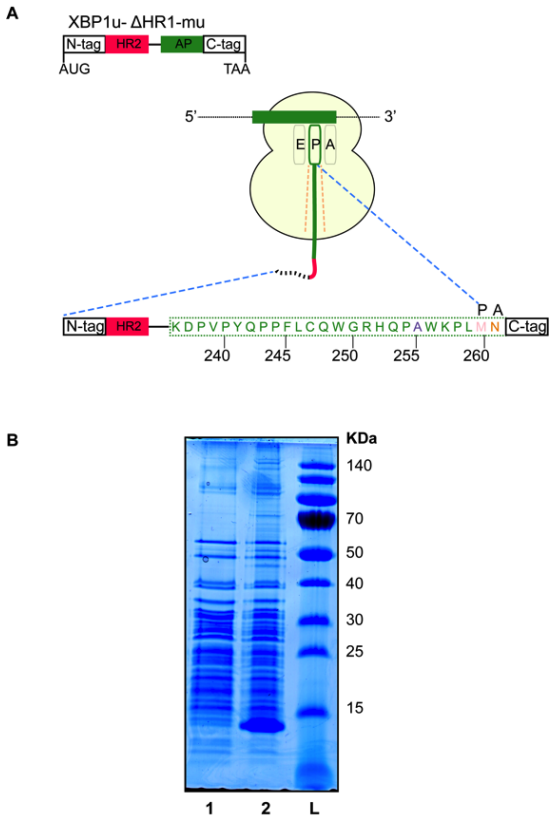

Figure 3.25: Generation of the stalled XBP1u-RNC complex.

(A) Schematic representation of the construct used for generating the stalled XBP1u-RNC complex. The XBP1u arrest peptide sequence is shown in green, while the HR2 domain is shown in red. A- and P-site positions are also denoted above the arrest peptide sequence. XBP1u-AP is numbered according to full length XBP1u. The S255A mutation used in this study is also shown purple. **(B)** Simply Blue stained gel after SDS-PAGE of purified XBP1u-RNC complex. Control 80S ribosomes (lane 2), purified XBP1u-RNC complex (lane 1), and stained protein molecular weight markers (lane L).

3.3.2 Cryo-EM analysis of the paused XBP1u-RNC

Processing of the cryo-EM dataset yielded a total of 531952 ribosomal particles, and an initial 3D refinement led to a density (electron potential map) of 6.6 Å with densities for P- and E-site tRNA. Further 3D classification resulted in two ribosomal subpopulations with a majority of them in the post state (54% with P-, E-site tRNA) and a smaller class in the hybrid state (18%

with A/P-, P/E- site tRNA) denoted as class-5 and class-4, respectively (Figure 3.26). After this initial 3D-classification step only 28% of the ribosomal particles were not programmed (absence of P-tRNA). The post state ribosomal class was further enriched by 3D classification for the presence of P-tRNA (with 60S mask). The particles of this enriched post state class were Bayesian polished (correcting for beam induced movement) before a final round of 3D refinement with a large subunit mask.

The overall resolution of the post state XBP1u-RNC was 3 Å (Figure 3.27A) with the local resolution of the ribosomal core reaching up to 2.5 Å. After initial sorting, the hybrid class was directly Bayesian polished before final 3D refinement, which yielded in a final density of average resolution 3.1 Å (Figure 3.27B). A model for the XBP1u stalled ribosome nascent chain was obtained by fitting a previously published rabbit ribosome model (PDB 5LZV) into the cryo-EM map. After initial fitting of the model in Coot, it was further refined in real space (using Phenix; Adams et al., 2010) and in reciprocal space (using REFMAC; Murshudov et al., 2011). Dr. Jingdong Cheng built the initial model of the XBP1u nascent chain in the ribosomal exit tunnel. Validation of the model was done by first calculating a Fourier shell correlation (FSC, model vs. full-map Figure 3.27) between the model and the cryo-EM map. In order to check for overfitting of the model during refinement, atoms of the final model were randomly displaced by 0.5 Å. Then this displaced model was refined against the first half of the map from the gold standard determination. After refinement, a new FSC is calculated with this model against the first-half (FSC_{work}, model vs. half-map1) and second-half map (FSC_{test}, model vs half-map2) (Figure 3.27). The discrepancy between these FSC curves should indicate overfitting. This procedure showed that the XBP1u-RNC atomic models for both post and rotated state do not display overfitting bias.

In both classes of stalled XBP1u-RNCs, the density for the XBP1u-AP in the exit tunnel was observed extending from the CCA end of the peptidyl-tRNA (Figure 3.28). In the upper parts of the tunnel, closer to PTC, the XBP1u-AP in the post state complex was resolved to between 3 – 3.5 Å (Figure 3.29A,B), while in the lower parts of the tunnel, owing to flexibility it was not well resolved with resolution lower than 4 Å (not shown).

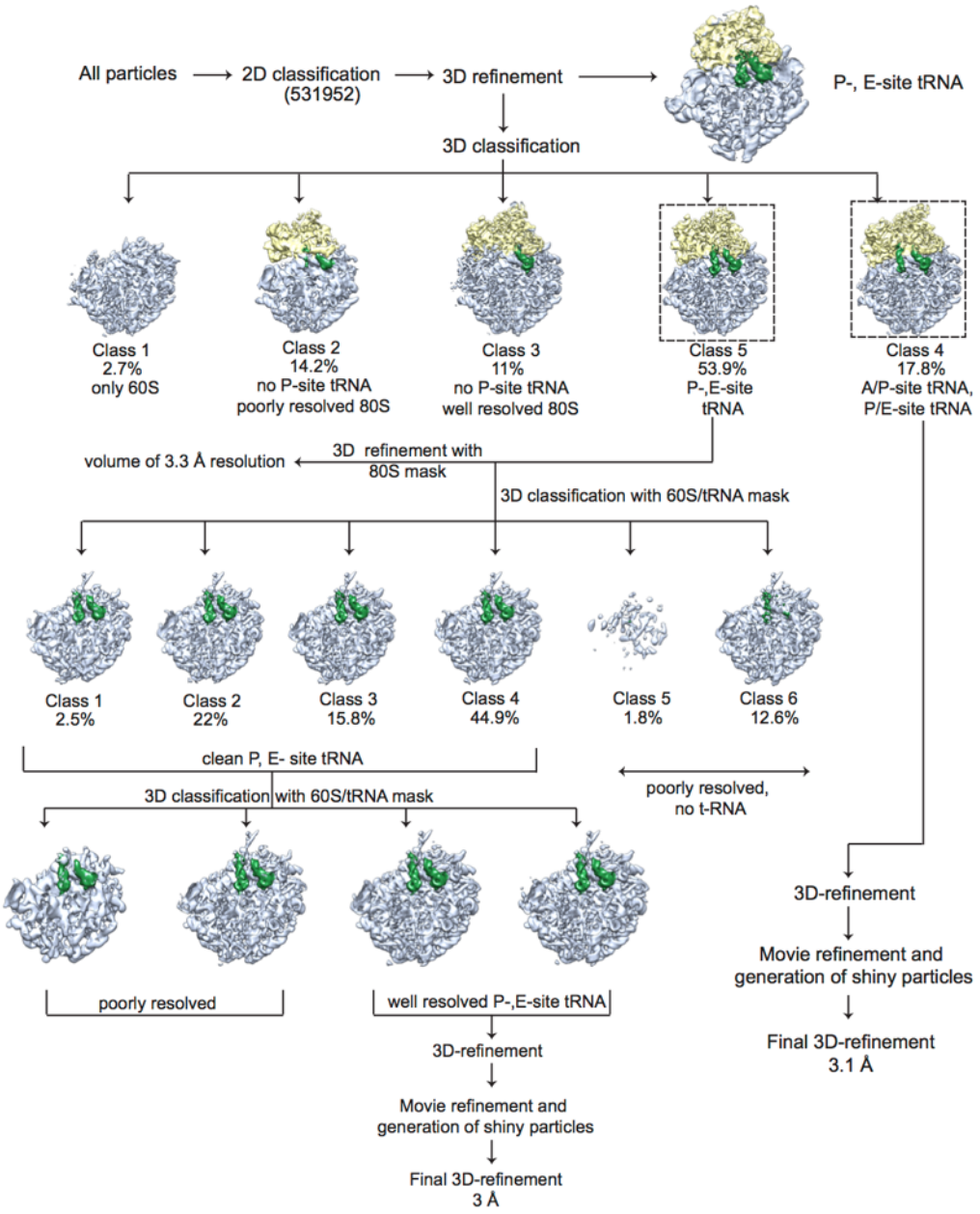

Figure 3.26: Cryo-EM processing scheme of XBP1u-RNC dataset.

In silico 3D classification and entire processing of the dataset was performed in Relion 2.1 (Kimanius et al., 2016). Initial 3D-classification was done without a mask. Further sorting resulted in a post state XBP1u-RNC class with 223,773 particles. The hybrid state subset comprising 94,923 particles was directly Bayesian polished from first 3D-classification to generate shiny particles for final 3D-refinement.

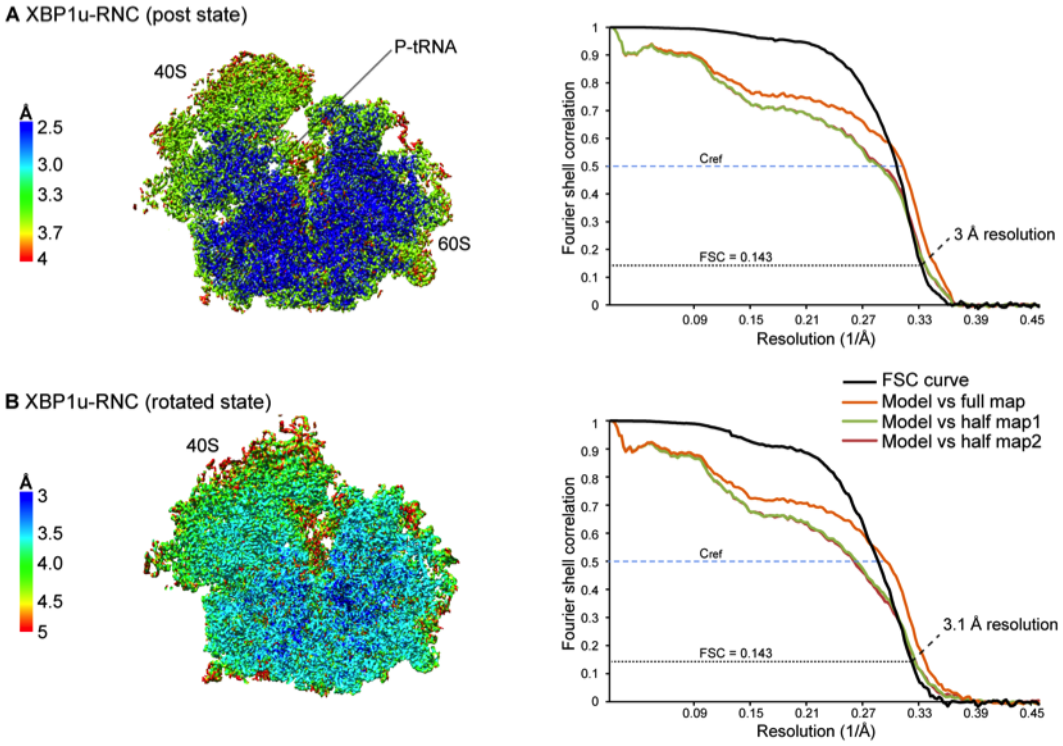

Figure 3.27: Resolution of XBP1u-RNC's.

Cross-section of **(A)** post and **(B)** hybrid state XBP1u-RNC maps colored according to their local resolution (left panel). (Right panel) Fourier shell correlation (FSC) curve of the final map (black) indicating average resolutions are shown (FSC=0.143, dashed black line). FSC curves calculated between final full-map and model (orange), as well as the self (green) and the cross-validated (brown) correlation curves (indicating resolution, FSC = 0.5 C_{ref}, dashed blue line) for the respective maps are plotted here.

3.3.3 XBP1u nascent chain in the ribosomal exit tunnel

With well-resolved density for the nascent chain in the upper parts of the tunnel, the complete XBP1u-AP pausing motif comprising 25 residues (Met260 – Asp236) was modeled. This model allowed deciphering the role of XBP1u-AP in inhibiting ribosomal function. In both the paused ribosomal states, the last residue attached to the P-tRNA is Met260, which is also the penultimate amino acid of the XBP1u nascent chain. Most of the nascent chain is in an extended conformation, except for residues located in the upper part of the tunnel where the XBP1u-AP forms a turn in close proximity to the ribosomal active center (Figure 3.30).

The turn is comprised of eight residues (Trp249 – Trp256), which is the latter half of the pausing motif. It is only four residues away from the ribosomal peptidyl transferase center (PTC) and located above the constriction site, the narrowest region in the ribosomal peptide exit tunnel. The turn's proximity to ribosomal active site suggests its critical role in inhibiting ribosomal peptidyl transferase function. Even though the XBP1u-AP is well resolved in both the ribosomal classes, the AP resolution in the post state complex was better than in rotated state. Therefore, further discussion and analysis is pertained to post state XBP1u-AP.

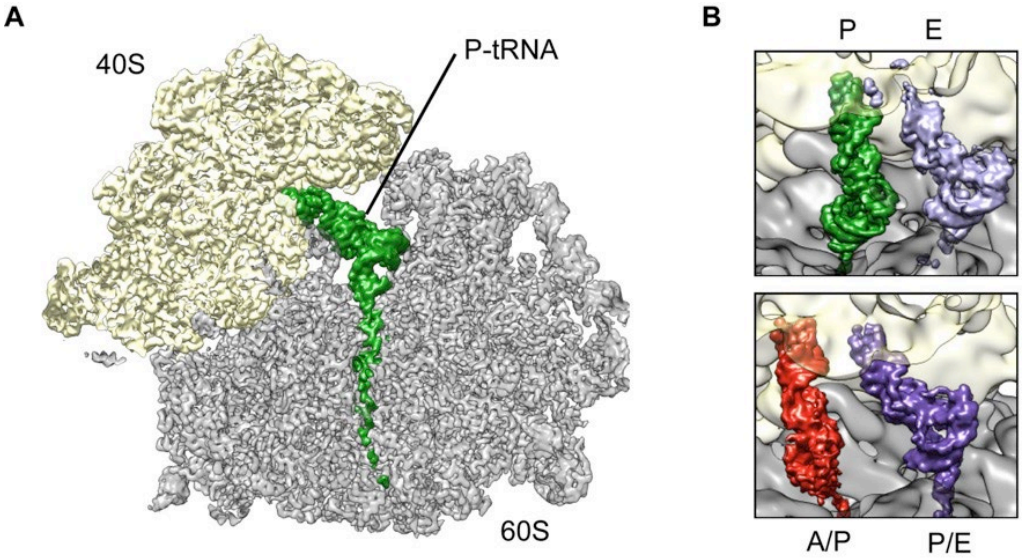

Figure 3.28: Cryo-EM reconstruction of XBP1u-RNC.

(A) Cross-sectional view focusing on the XBP1u-AP in the ribosomal exit tunnel. The XBP1u-AP is attached to the CCA end of P-tRNA, and the density spans a major portion of the exit tunnel. **(B)** Close-up view on tRNAs in the XBP1u-RNC reconstruction. Post state (top panel) P- and E- site tRNAs are shown in green and pink. Hybrid state (bottom panel) A/P- and P/E- tRNAs are shown in red and purple.

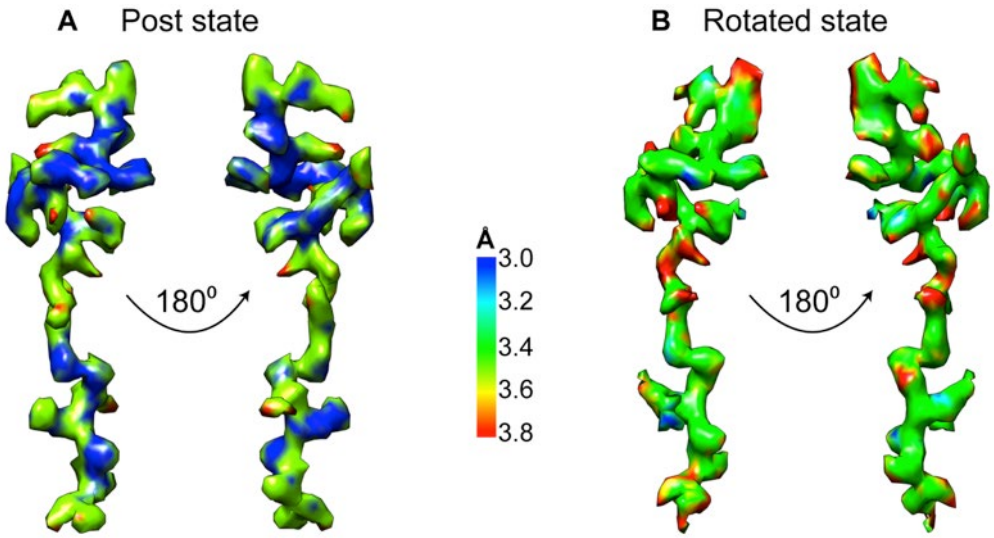

Figure 3.29: Local resolution of the XBP1u-AP in the ribosomal exit tunnel.

Displayed are the isolated XBP1u-AP densities in post **(A)** and hybrid (B) state XBP1u-RNC. Nascent chain densities is colored according to estimated local resolution.

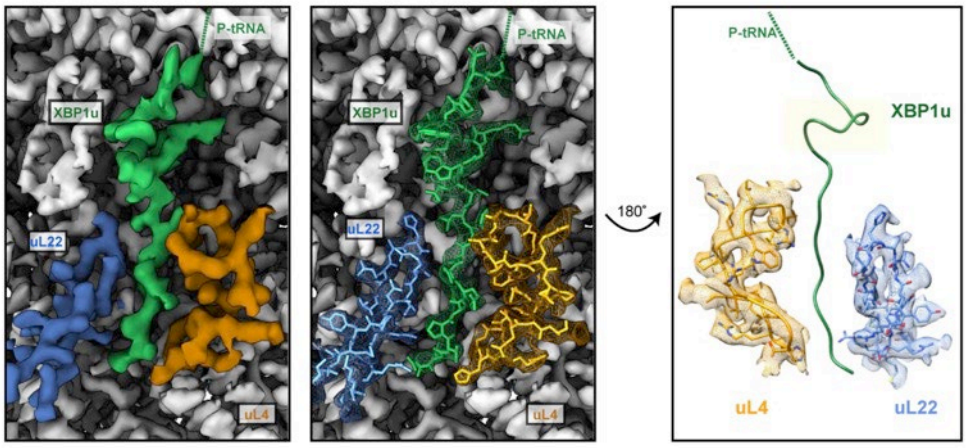

Figure 3.30: XBP1u-AP in the ribosomal exit tunnel.

View on the XBP1u-AP (green) in the ribosomal exit tunnel; also shown is the constriction site formed by uL4 (orange) and uL22 (blue). The rest of the tunnel and 60S subunit is shown in grey. Left to right: Cross-sectional view with solid density, same view with respective models (density shown as mesh), and a 180° rotated view without the ribosomal tunnel showing only the XBP1u nascent chain, uL4 and uL22 (density shown as transparent mesh).

3.3.4 Interactions of the XBP1u nascent chain with the ribosomal exit tunnel

XBP1u-AP interacts with the ribosomal peptide exit tunnel. In the lower part of the tunnel, the constriction site protein residues Arg71 and Ser87 (Figure 3.31J-L) of uL4 and Arg128 of uL22 (Figure 3.31K) make contact via hydrogen bonds with the backbone of the XBP1u-AP. In the same region Tyr241 of XBP1u-AP stacks on C2794 of the 28S rRNA (Figure 3.31H).

The turn that is bordered by bulky tryptophan residues (Trp249 & Trp256) protrudes into a hydrophobic crevice in the tunnel, causing the displacement of the base G3904 (Figure 3.31E). The corresponding base in prokaryotes is A2058, which along with A2059 has been described as critical for macrolide binding (Hansen et al., 2002) and drug mediated ribosomal stalling (Arenz, Ramu, et al., 2014). Moreover, in the case of TnaC leader peptide induced ribosomal stalling, it has been shown that this base can sense the free L-tryptophan (Martínez et al., 2014). It is likely that this region in the ribosomal tunnel has evolved in eukaryotes to play a similar role to sense nascent chains as previously shown for prokaryotic ribosomes (Cruz-Vera et al., 2011; Tanner et al., 2009). Positively charged Arg251 of XBP1u forms a salt bridge with the phosphate group of A4388 (Figure 3.31F), while Gly250 and Gln253 makes contact with the tunnel via hydrogen bonds with the 28S rRNA bases A3908 and U4555, respectively (Figure 3.31G,I). These are the interactions made with the tunnel by the residues forming the turn.

When analyzing the nascent chain interactions within close proximity to the PTC, Lys257 stacks onto U4532 (Figure 3.31D) that is next to U4531 (U2585 in E*. coli*). Met260 of the nascent chain makes a hydrophobic interaction with U4531 (Figure 3.31C). These two interactions of the nascent chain might hinder the movement of U4531, which is critical for PTC activity (Youngman et al., 2004).

Apart from nascent chain interactions with the tunnel, two intramolecular interactions within the nascent chain lead to stabilization. Tyr249 of XBP1u stacks onto Gln248 (Figure 3.31B), while Arg251 makes a hydrogen bond with Lys257 (Figure 3.31A). All these interactions eventually contribute to the stability of the XBP1u nascent chain leading to its unique conformation within the tunnel.

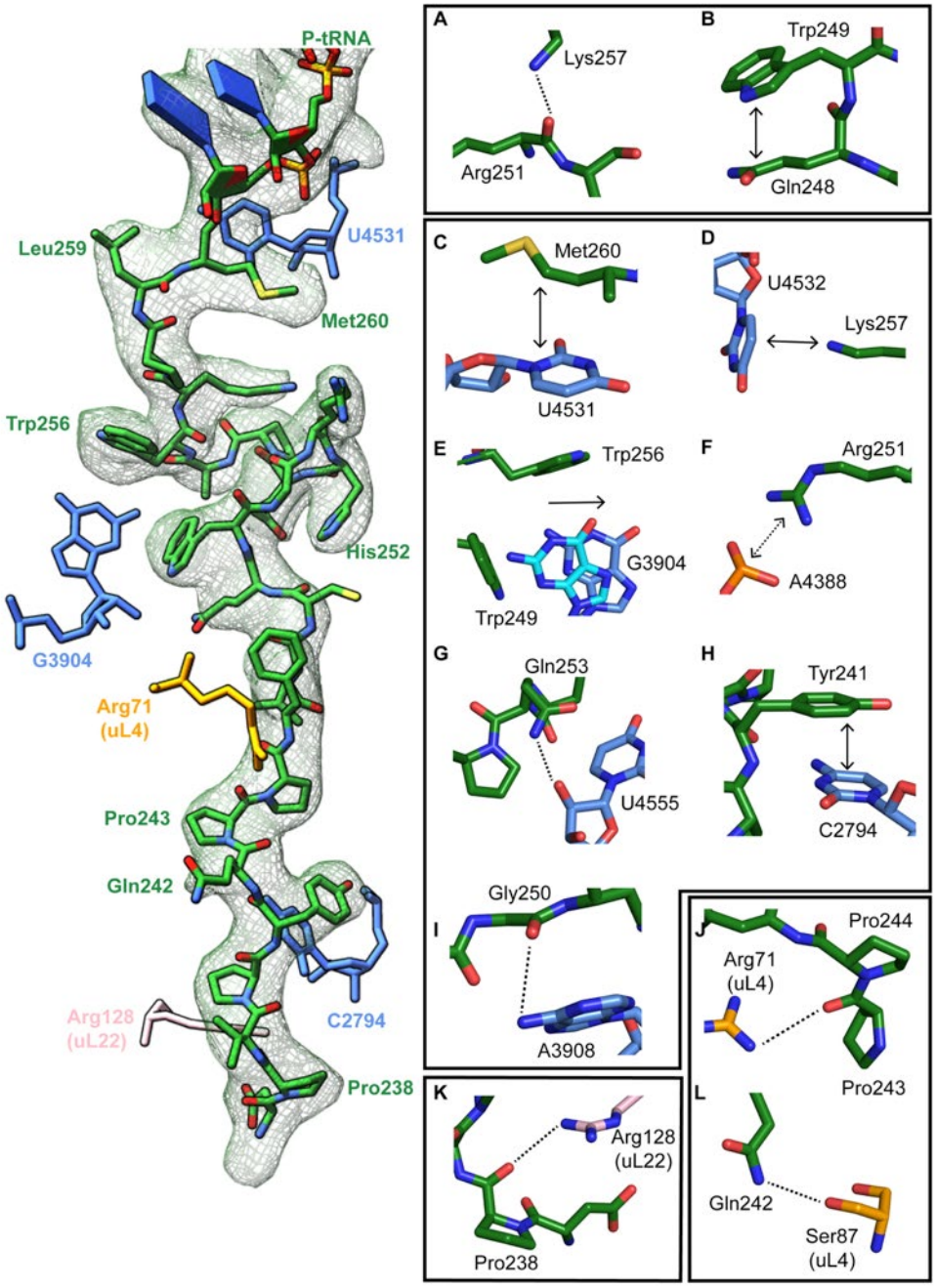

Figure 3.31: Interactions of the XBP1u nascent chain with the ribosomal exit tunnel.

(Left panel) XBP1u-AP density (shown as transparent mesh), and the corresponding model in green. Important interacting rRNA and protein residues are shown as well. (Right panel) **(A)** Lys257 of XBP1u (green) contacts Arg251 of XBP1u via an internal hydrogen bond. **(B)** Trp249 of XBP1u internally stacks against Gln248. **(C)** Met260 of XBP1u makes a hydrophobic interaction with U4531 of 28S rRNA (blue). **(D)** Amino group of Lys257 of XBP1u stacks against U4532 of 28S rRNA. **(E)** Trp249 and Trp256 of XBP1u displaces G3904 of 28S rRNA. **(F)** Arg251 of XBP1u forms a salt-bridge with the phosphate group of the base A4388 of 28S rRNA. **(G, I)** Gln253 and Gly250 of XBP1u are in hydrogen bonding distance with U4555 and A3908 of 28S rRNA respectively. **(H)** Tyr241 of XBP1u stacks 28S rRNA

base C2794. **(J, L)** Pro244 and Gln242 are in hydrogen bonding distance with Arg71 and Ser87 (orange) of uL4 ribosomal protein. **(K)** Pro238 of XBP1u is in hydrogen bonding distance with Arg128 (pink) of constriction site uL22 protein.

3.3.5 Inhibition of peptidyl transferase activity by XBP1u nascent chain

Precise positioning of the PTC bases is critical for ribosome's peptidyl transferase function (Wilson et al., 2016). Often ribosomal arrest peptides distort the geometry of rRNA bases involved in PTC activity, thereby inhibiting ribosomal function. Some of the bases involved in peptidyl transferase activity are U4531 (U2585 in E. *coli*), U4452 (U2506) and A4548 (A2602), and these bases are severely distorted by ribosomal arrest peptides to stall ribosomal activity as shown in cryo-EM reconstructions of other stalled ribosomal complexes (Arenz, Meydan, et al., 2014; Matheisl et al., 2015; Su et al., 2017). Of the three bases, the most critical one is U2585 (U4531 in rabbit) shown to be critical for peptidyl transferase function and peptide release (Youngman et al., 2004).

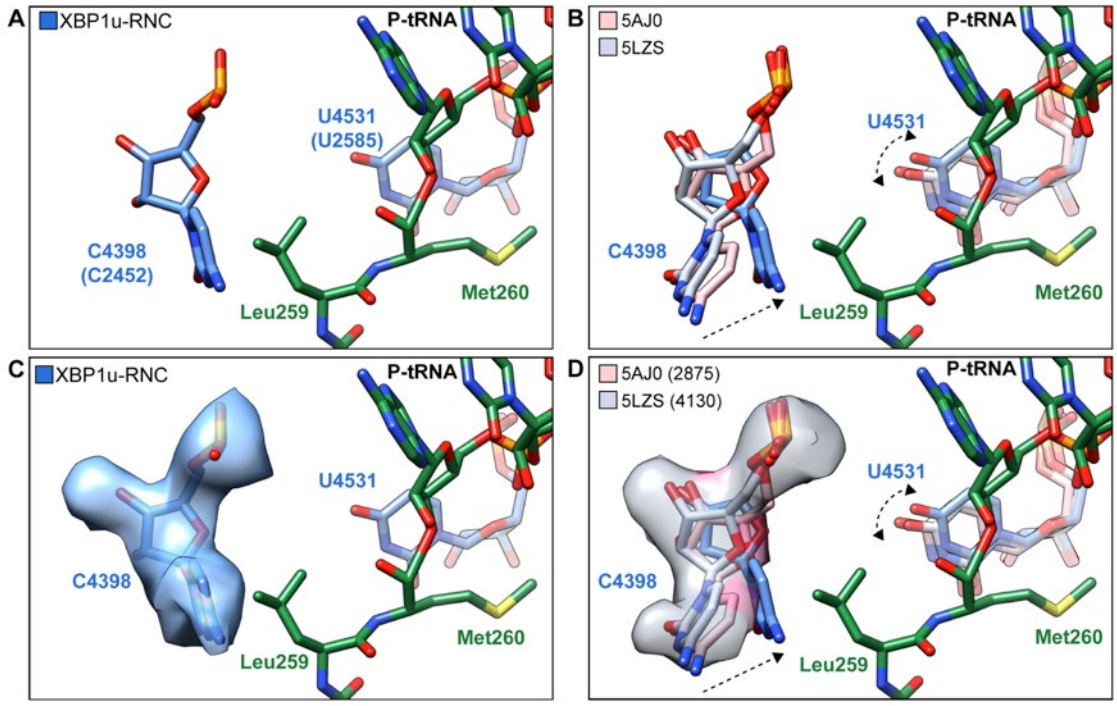

Figure 3.32: Position of critical PTC bases C4398 (C2452) and U4531(U2585).

(A) Position of 28S rRNA base C4398 (C2452 in E. *coli*) in XBP1u-RNC (blue) stabilized by Leu259 of XBP1u-nascent chain (green). Un-induced state of U4531 of 28S rRNA is also shown. **(B)** Comparison of 28S rRNA bases C4398 and U4531 of XBP1u-RNC with human post-state 80S reconstruction (Behrmann et al., 2015) (PDB ID: 5AJ0) and didemnin treated rabbit 80S (Shao et al., 2016) (PDB ID: 5LZS). This depicts the movement of base C4398 in XBP1u-RNC, while U4531 is unperturbed. **(C – D)** Same view and models as in **(A – B)**, but with corresponding densities: XBP1u-RNC (blue), human post state 80S (soft-pink, EMDB ID: 2875) and rabbit 80S (soft-blue, EMDB ID: 4130).

To begin with, the conformation of the base U4531 was compared to that in a post state 80S human ribosome (Behrmann et al., 2015). In comparison, U4531 (U2585 in *E. coli*) is in typical un-induced state before A-site tRNA accommodation (Figure 3.32A-D), which has been shown before for prokaryotes (Martin Schmeing et al., 2005). U4531 (U2585) moves down into induced state upon A-site tRNA accommodation. Even though U4531 interacts with Met260 of the XBP1u nascent chain, we find that U4351 will not be hindered to transit into induced state upon A-site accommodation. Therefore, it is clear that the state of base U4531 is not perturbed.

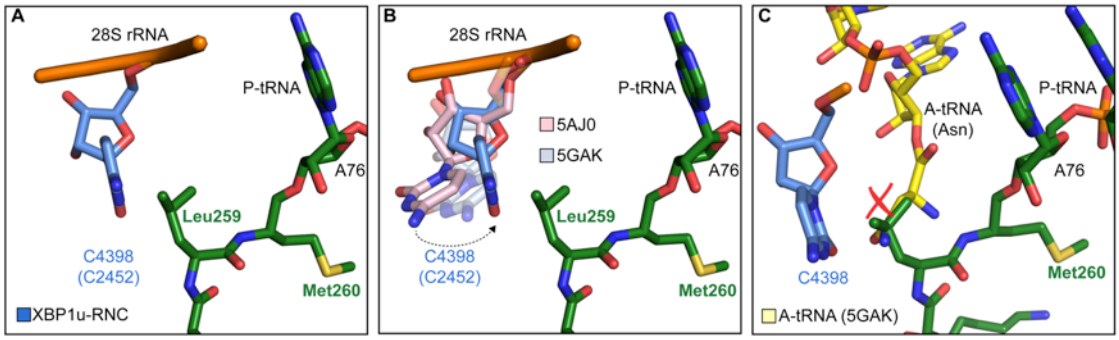

Figure 3.33: Inhibition of peptidyl transferase activity by XBP1u nascent chain.

(A) View of the base C4398 in XBP1u-RNC (blue), stabilized by Leu259 of XBP1u-AP (green). **(B)** Comparison of C4398 in XBP1u-RNC with human post-state 80S (Behrmann et al., 2015) (soft-pink, PDB ID: 5AJ0) and with yeast 80S with A-, P- site tRNA and eIF-5A (Schmidt et al., 2015) (soft-blue PDB ID: 5GAK). Premature closed conformation of C4398 in XBP1u-RNC a similar position as seen in yeast 80S model, but without the presence of an A-site tRNA. **(C)** Model of incoming Asn-tRNA (A-site) would clash with Leu259 of XBP1u-AP. Premature closure of A-site cleft by C4398 of 28S rRNA, and the prevention of A-site tRNA accommodation by Leu259 of XBP1u is the mechanism behind ribosome arresting activity of XBP1u-nascent chain.

Looking at other PTC bases, we find that C4398 is in closed conformation. C4398 is a part of a so called A-site crevice (Gürel et al., 2009) and is also implicated in peptidyl transferase function. Closed conformation of this base is observed only after A-site accommodation as seen in the reconstruction of yeast 80S ribosomes with A-, P- site tRNA and eIF-5A (Schmidt et al., 2015). Leu259 of the XBP1u nascent chain stabilizes this premature closed conformation of C4398 (Figure 3.33A,B), and unlike Met260, mutating Leu259 to Alanine almost completely abolishes stalling (Yanagitani et al., 2011). Moreover, Leu259 in its final unique conformation would clash with the incoming Asn-tRNA (Figure 3.33C).

Therefore, the underlying mechanism behind the stalling activity of XBP1u-AP is to prevent the accommodation of incoming A-site tRNA. Accordingly, there are no ribosomal classes with accommodated A-site tRNA in our dataset.

3.3.6 Cryo-EM structure of XBP1u-RNC with SRP and Sec61

For effective splicing of XBP1u mRNA mediated by IRE1α, the arrested XBP1u-RNC needs to be localized to the ER membrane where it presumably inserts into the Sec61 protein-conducting channel (PCC). The targeting of the stalled XBP1u-RNC to the ER membrane is mediated by SRP (Kanda et al., 2016; Plumb et al., 2015), which is recruited non-canonically by the moderately hydrophobic HR2 domain of XBP1u. In order to investigate this special mode of SRP recruitment and to analyze XBP1u-AP state upon SRP recognition and ER targeting, purified XBP1u-RNCs were *in vitro* reconstituted with dog SRP (see materials and methods for details) or canine high salt/puromycin treated rough microsomes. The *in vitro* reconstituted ER targeting/translocation complexes were subjected to cryo-EM analysis.

Classification of the dataset for the presence of SRP and further refinement yielded 80S XBP1u-RNC (post state) with SRP bound to it (Figure 3.34). Average resolution of the final reconstruction was 3.7 Å (Figure 3.35), and SRP was itself resolved locally between 5 – 10 Å probably owing to its flexibility. Characteristic L-shaped density of the SRP, extending from the ribosomal inter-subunit space to S-domain contacting the exit tunnel was observed (Figure 3.36A). The recently published engaged state mammalian SRP model (Voorhees & Hegde, 2015) fitted well with the observed density. Individual domains of SRP were manually inspected and fitted in Coot (Emsley & Cowtan, 2004).

When analyzing the hydrophobic groove of SRP54 M-domain, which is known to mediate the recognition of signal sequences, a clear rod like density was observed (Figure 3.36B). An adequate hydrophobic stretch available for recognition by SRP would be the HR2 domain, and therefore the density can be assigned to this domain. This indicates that the HR2 domain of XBP1u forms a helical structure upon recognition by SRP and this mode of interaction is identical to that of M-domain mediated recognition of canonical signal sequences. Moreover, XBP1u-AP density was also well resolved in this SRP-bound paused complex. Therefore, this enabled to *de novo* model the AP, and compare its conformation in the exit tunnel between SRP bound and unbound stalled XBP1u-RNC. Surprisingly, the comparison revealed that the conformation of the XBP1u-AP in the exit tunnel was unperturbed suggesting

that the paused state of the complex is maintained upon recruitment of SRP by the stalled XBP1u-RNC.

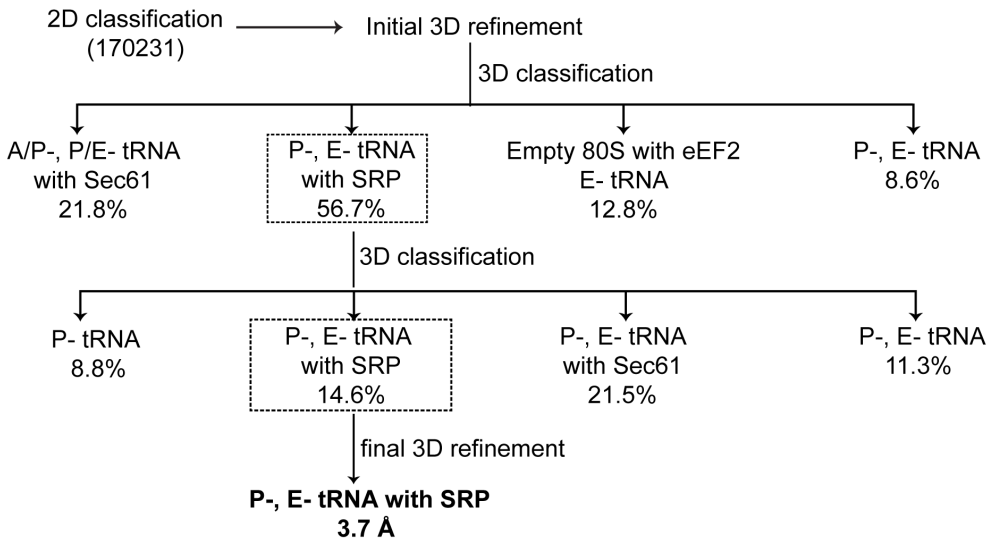

Figure 3.34: Cryo-EM dataset processing scheme of XBP1u-RNC-SRP.

3D-classification for presence of SRP with XBP1u-RNC resulted in a subpopulation of 24875 ribosomal particles bound to SRP in post state, which was further refined to a final resolution of 3.7 Å.

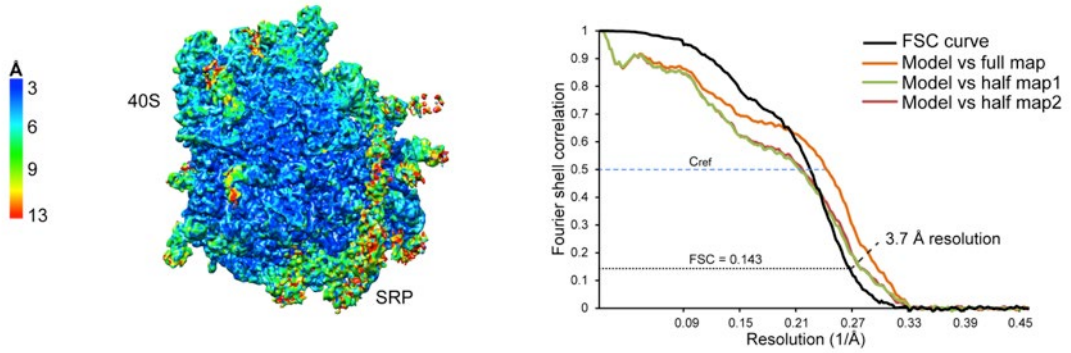

Figure 3.35: Local resolution and model validation of XBP1u-RNC-SRP.

Final volume of XBP1u-RNC-SRP colored by local resolution. SRP was resolved between 5 – 10 Å, while the overall average resolution of the complex was 3.7 Å. FSC curve of the final map indicating average resolution (black) (FSC = 0.143, dashed black line). FSC curve between model and full-map (orange), and self-validation (green) and cross-validation (brown) FSC curves (indicating resolution, C_{ref} = 0.5) are plotted here.

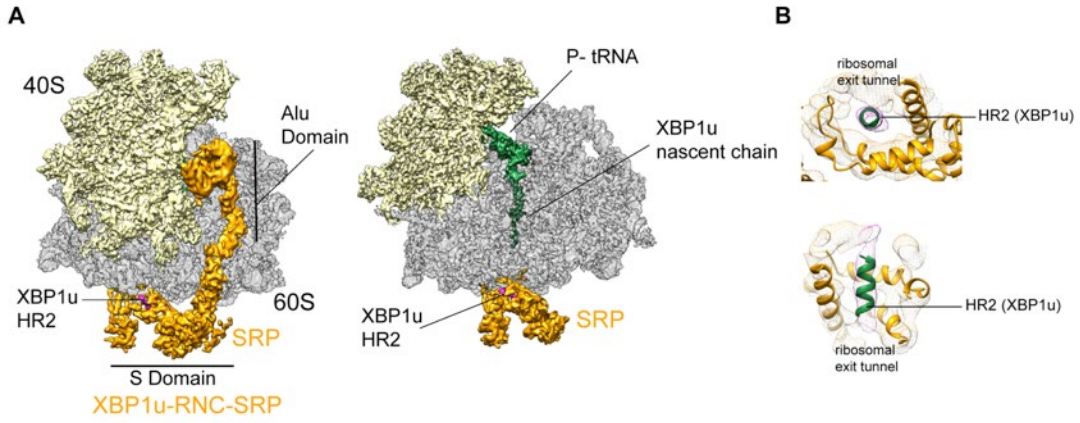

Figure 3.36: Cryo-EM structure of *in vitro* reconstituted XBP1u-RNC with SRP.

(A) View of SRP (orange) interacting with the XBP1u-RNC, also shown is the HR2 domain (purple) of the XBP1u nascent chain bound to the SRP54 M-domain. Same view: with a cross-sectional slice to elucidate the presence of XBP1u-nascent chain (green) in the ribosomal tunnel. **(B)** Close-up top and lateral views of SRP54 M-domain interacting with the HR2 domain (purple). The HR2 domain forms a helical structure when being recognized by SRP.

Purified XBP1u-RNCs were incubated with canine high salt/puromycin treated rough microsomes (see experimental methods for details) to generate the XBP1u-RNC-Sec61 complex. The final sample was obtained after solubilization of the membranes with digitonin and was subjected to cryo-EM

analysis (Figure 3.37). A clear density for Sec61 was observed at the tunnel exit, and also for the XBP1u-AP in the exit tunnel (Figure 3.39). The overall resolution of the complex was 3.9 Å, while Sec61 showed a modest resolution of around 8 Å (Figure 3.38). A recently published Sec61 model (Braunger et al., 2018) was fitted into the observed density, and the state of the lateral gate was inspected. The lateral gate of the translocon was in closed state, when comparing the position of TM2 and TM7 with other known Sec61 structure (idle state) (Voorhees & Hegde, 2015). No extra density was observed upon searching near the lateral gate for the HR2 domain of XBP1u (Figure 3.39). Given the moderate hydrophobicity of the HR2 domain only 10% of the ER targeted complex engage successfully with the Sec61 channel and get integrated into ER membrane as shown previously before (Plumb et al., 2015). This could explain why no extra density for HR2 was observed. HR2 likely only makes transient or weak interactions with the translocon. Taken together in the *in vitro* reconstituted ER targeting complex, the Sec61 is in the idle state, and HR2 domain probably can interact with Sec61 but cannot engage productively.

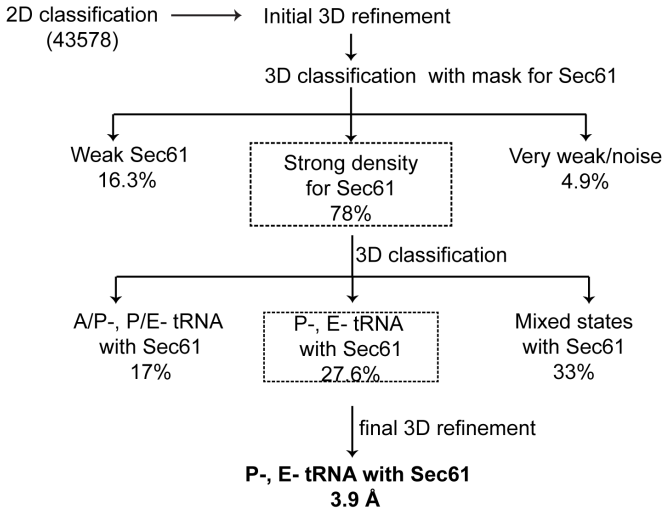

Figure 3.37: *In silico* sorting of XBP1u-RNC-Sec61 cryo-EM dataset.

Processing of XBP1u-RNC-Sec61 dataset yielded a final population of 12749 ribosomal particles in post-state bound to Sec61 (see methods for more details).

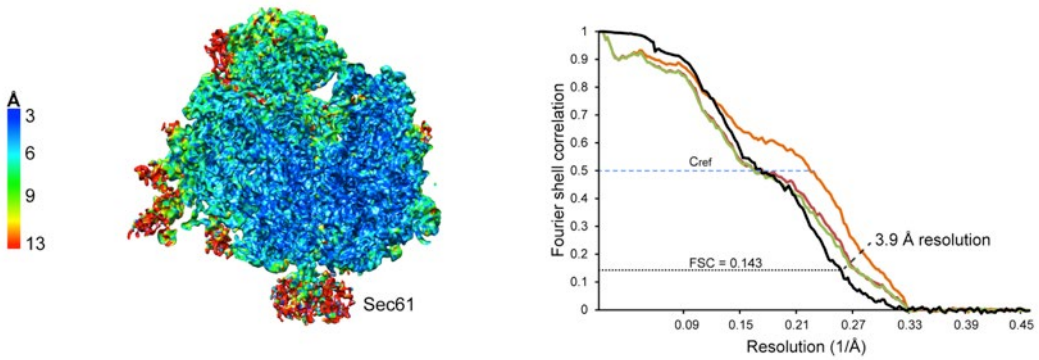

Figure 3.38: Average resolution and model validation for XBP1u-RNC-Sec61.

Final density of *in vitro* reconstituted XBP1u-RNC-Sec61 complex colored according to its local resolution. On the right, showing FSC curve (black) for final volume indicating the average resolution of the complex (FSC = 0.143). Also plotted model validation FSC curves: final map against the model (orange), self-validation (green) and cross-validation (brown) respectively.

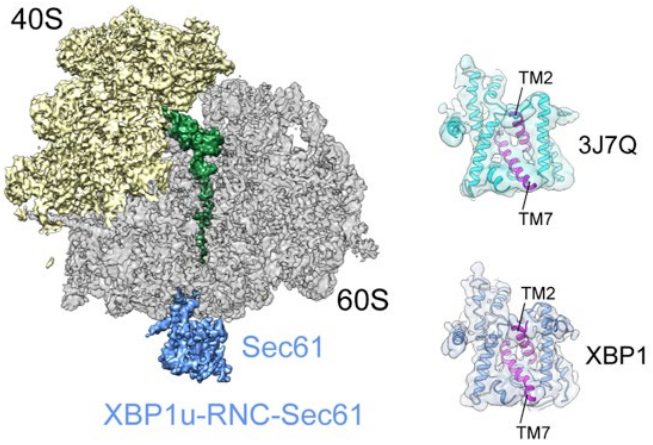

Figure 3.39: Cryo-EM structure of *in vitro* reconstituted XBP1u-RNC-Sec61.

(Left) Cross-sectional view of Sec61 (blue) bound to the stalled XBP1u-RNC. XBP1u-nascent chain and P-tRNA in green, while 40S and 60S ribosomal subunits shown in yellow and grey respectively. (Right) Analysis of Sec61 lateral gate forming TM2 and TM7 helices. Comparing it to another known idle-state translocon (Voorhees et al., 2014), shows that Sec61 bound to paused XBP1u-RNC is in idle-state. Also evident is absence of density for HR2 domain of XBP1u-nascent chain.

Next, the conformation of XBP1u-AP in XBP1u-RNC-Sec61 was compared with structures of XBP1u-RNCs alone or with SRP. The comparison revealed that XBP1u-AP state was indistinguishable, and RMSD's between the structures is less than 1 Å (Figure 3.40). This suggests that the paused state is maintained through ER targeting and even after being localized to the ER membrane. Therefore XBP1u-AP does not act as a force sensitive switch in UPR i.e., the paused state of XBP1u-RNC is unlikely to be released by the force exerted by Sec61.

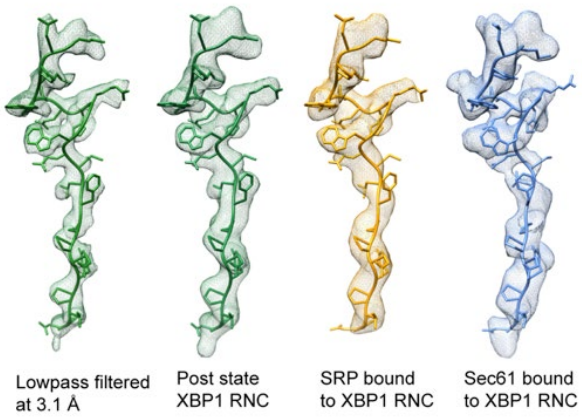

Figure 3.40: XBP1u nascent chain states with XBP1u-RNC (alone), XBP1u-RNC with SRP and Sec61.

(Left to Right) Shown are XBP1u-nascent chain densities (mesh) also with their respective models. XBP1u-nascent density from RNC alone (green, low-pass filtered at 3.1 Å), followed by Gaussian filtered densities of XBP1u-nascent chain from RNC alone (green), RNC with SRP (orange) and Sec61 (blue) respectively. State of XBP1u-nascent chain is unaltered from pausing to being targeted to Sec61 on the ER membrane.

In conclusion, structural analysis of the XBP1u-AP within the ribosomal exit tunnel revealed that it makes several interactions with the tunnel wall. Further, it forms a turn near the ribosomal active site. Surprisingly, the ribosomal pausing of XBP1u-AP is mediated by minimal distortion of the peptidyl-transferase center. Leu259 of the XBP1u-AP stabilizes the premature closed confirmation of C4398, and it prevents the accommodation of the incoming A-site tRNA. Cryo-EM structures of the XBP1u-RNC reconstituted with SRP and rough microsomes show that the state of XBP1u-AP within the exit tunnel is unperturbed during the ER targeting of the paused XBP1u-RNC. While the HR2 domain is recognized by SRP, but fails to engage productively with the Sec61 translocon. Therefore, XBP1u-AP cannot function as a force sensor.

4 Discussion

In the thesis presented here, translational regulation has been explored in three different biological contexts.

The first study involved investigating translational control during dendritic cell maturation. This was done mainly using ribosome profiling, which has been successfully established in the Beckmann lab. Analysis of ribosome profiling data revealed that there is more translational regulation during the early stages of DC maturation. Further, in line with previous studies transcripts encoding for ribosomal proteins, antigen processing and presentation were translationally up regulated during early stages of DC maturation (Ceppi et al., 2009; Lelouard et al., 2007). Globally, 5' UTRs showed increased ribosome occupancy during DC maturation. Unexpectedly, at the 24 h time point down-regulation of ABCE1 led to accumulation of post termination ribosomal complexes in the 3' UTR.

4.1 Translational regulation in maturing dendritic cells

Previously, gene expression changes during DC maturation were studied using RNAseq and proteomic approaches (Buschow et al., 2010). Further polysome profiling was used to get insights into translational control during DC maturation (Ceppi et al., 2009). But polysome profiling suffers from a major limitation. Genes that were detected showing significant changes in translation did not provide positional information of ribosomes on the transcript. With polysome profiling it would not have been possible to detect the presence of ribosomes in the 3' UTR during the later stages of maturation.

The depth of the generated data enabled to identify gene families that showed either homo-directional changes or significant changes only at the level of RNA or RPF. Here ribosome profiling with RNAseq enabled to identify in total more than 5000 differentially expressed genes (DEG) at the level of transcriptome (RNA), translatome (RPF) and RPF/RNA (normalized changes). Such analysis shed light on transcriptional and translational control of gene expression during DC maturation. Overall, transcriptional changes correlated with translatome changes, although correlation was slightly reduced at the 4 h time point (Figure 3.6B). Translation efficiency changes showed a much

broader distribution at the 4 h time point (Figure 3.6C). In order to further investigate this reduced correlation at the 4 h time point, DEGs were sorted into three classes, either showing homo-directional changes (i.e significant changes at the level of both RNA and RPF) or showing significant changes only at the level of RNA or RPF, respectively. Here genes at the 4 h time point showed again less correlation between RNA and RPF fold changes (Figure 3.7). Changes at the level of RNA were not reflected at the level of RPF indicating post transcriptional regulatory mechanisms during the early stages of DC maturation. A likely explanation for these observations could be provided by the context of functional changes that define the process of DC maturation.

DC maturation is marked by rapid changes in cellular morphology and the ability to migrate, to uptake and to process foreign antigens etc. (Mellman & Steinman, 2001). Such changes require quick strategies to alter gene expression patterns. Translational regulation provides the advantage to rapidly modify the proteome, and therefore it makes sense that more translational regulation was observed at the 4 h time point.

Some of the homo-directionally up regulated pathways include the ‘cytokine-cytokine receptor interaction’, the ‘IL-17 signalling pathway’, the ‘TNF signaling pathway’ and the ‘NOD signaling pathway’. This is not entirely surprising, since these pathways are activated upon engagement by cytokines used for DC maturation. Also, previous RNAseq studies of DC maturation showed these pathways to be up regulated (Buschow et al., 2010), establishing them as maturation markers for DC.

Genes that showed significant changes only at the level of RPF provided insights into translational control during DC maturation. As with previous DC maturation studies (Ceppi et al., 2009), here as well transcripts encoding for ribosomal proteins, antigen presentation and processing and amino acid metabolism are translationally engaged at the 4 h time point (Figure 3.10). One possible explanation for this translational up-regulation at the 4 h time point is the need for increased protein synthesis capacity, and the immediate need to uptake and process foreign antigens. Interestingly, this translational up-regulation is temporal and ribosomal protein transcripts are down-regulated at the 24 h time point.

Apart from these known gene families, transcripts encoding for histones and proteins involved in the glycolysis pathway were also temporally engaged by the ribosomes (Figure 3.11). Currently, the significance of histone mRNA's being translationally up regulated in the context of DC maturation cannot be explained yet.

Although it was not observed in previous polysome profiling analyses, recently it has been shown that metabolic regulation plays a critical role in DC maturation (Wculek et al., 2019). One of the key metabolic pathways that is activated in the early phase of DC maturation is glycolysis (Krawczyk et al., 2010). Sustained activation of the glycolytic pathway is dependent on the cytokine stimulation used for DC maturation. Further, glycolysis is activated via the Akt/PI3K pathway and is essential for ER and Golgi body biogenesis in the mature DCs (Everts et al., 2014). Glycolysis and mitochondrial oxidative phosphorylation are tightly regulated *in vivo*, as these are the key pathways for cellular energy generation. In this study, transcripts for the glycolytic pathway were only temporally engaged by ribosomes, while transcripts encoding for proteins involved in oxidative phosphorylation showed to be strongly repressed during later stages of maturation. OXPHOS transcripts were down regulated at the level of both transcriptome and translatome (Figure 3.9). It could be speculated that lower translational efficiency of glycolytic transcripts might be enough to replenish cellular energy resources in terminally differentiated mature DCs.

4.2 Down regulation of ABCE1 in mature dendritic cells

During DC maturation increased ribosome occupancy was observed in both the 5' and 3' UTRs (Figure 3.13). This is a rather surprising observation. Occurrence of ribosomes on the 5' UTR may be related to a previous study, where it has been shown that there is a switch in the mode of translation initiation from cap-dependent to cap-independent mechanism (Lelouard et al., 2007). This switching is primarily due to the phosphorylation of eIF2α, which is generally an outcome of stress response. After switching, translation initiation through presence of endogenous IRES elements in the 5' UTR bas been previously described (Lelouard et al., 2007). However, this could not be verified with the ribosome profiling data generated here. Yet, it seems likely

that the DCs undergo cellular stress during the maturation process, causing ribosomes to accumulate in the 5'-UTR region.

Surprisingly, also the 3' UTR showed increased ribosome occupancy during the later stages of DC maturation (Figure 3.13). The profiling data suggested that this correlated with down-regulation of ABCE1, and consequently leading to accumulation of post-termination 80S ribosomes in the 3' UTR. One of the immediate consequences of this would be the reduced availability of free ribosomes in the cytosol to initiate translation. Another interesting observation was that, ribosomal mRNAs were down-regulated at the 24 h time point. Similar down-regulation of ABCE1 was observed in terminal differentiation of erythroid cells (Mills et al., 2016). However, in erythroid cells, in order to replenish free ribosomes in the cytosol for translation initiation, the Dom34/Hbs1 rescue system was up-regulated. In a yeast study (D. J. Young et al., 2015), diminished levels of Rli1 (ABCE1 homolog) resulted in the accumulation of 80S ribosomes over the stop codon, and as well as in the 3' UTR. Unexpectedly, they also observed that the non-recycled 80S ribosomes re-initiate translation in a frame independent manner in the 3' UTR. These re-initiation events lead to generation of small peptides, and the study provided multiple lines of evidence supporting this claim. Similar to erythroid cells, the yeast study also showed the critical importance of Dom34/Hbs1 mediated recycling 80S ribosomes stuck in the 3' UTR. Such a similar up-regulation of Dom34/Hbs1 rescue system was not observed in the mature DCs. Therefore, in order to reduce the translational activity in mature DCs, ribosomes are sequestered to the 3' UTR and further synthesis of new ribosomal proteins is getting repressed as well. What causes the down regulation of ABCE1 in mature DCs?

ABCE1 is an iron-sulfur cluster containing protein, and the biogenesis of these clusters happens in the mitochondria. Therefore, one of the possible reasons could be that mitochondrial integrity is compromised during DC maturation. Transcripts encoding for OXPHOS are strongly repressed, and there is a strong connection between OXPHOS down regulation and mitochondrial dysfunction. Another explanation for ABCE1 downregulation may be the generation of reactive oxygen species (ROS) during cytokine stimulation (Herb et al., 2019; Yang et al., 2007). Metals are sensitive to ROS

generated within the cells and may affect incorporation of Fe-S clusters into proteins causing reduced levels.

Taken together, the ribosome profiling work presented here provides novel insights into the DC maturation process. Apart from previously known gene families that were translationally regulated during DC maturation (Ceppi et al., 2009), here it has been shown that transcripts involved in lipid metabolism, glycolysis and oxidative phosphorylation are regulated as well. Down-regulation of ABCE1 leads to accumulation of post-termination ribosomes in the 3' UTR, and this would eventually reduce the rate of translation initiation. Reduced translation, and coupled with down-regulation of glycolysis and oxidative phosphorylation might cause decreased metabolic activity, which can possibly serve as a signal for programmed death in these terminally differentiated DCs.

4.3 The Ski complex interacts with the 80S ribosome

The second part of this thesis dealt with the relationship between the ribosome and the Ski proteins. Based on structural similarity between the C-terminal region of Ski7 and the translational GTPase Hbs1 (Van Hoof et al., 2002), it has been proposed that Ski7 might be the factor recognizing the ribosomes stalled in NSD *in vivo*. It was further believed that Ski7 can recruit the Ski complex and the exosome for turnover of non-stop mRNAs. Here, however it has been demonstrated that the Ski complex and not Ski7 interacts with ribosomes *in vivo*.

4.4 Characteristic features of *in vivo* Ski complex interaction with the 80S ribosome

Footprints generated from the purified 80S-Ski complexes contained a four-fold excess of poly-A containing footprints than the background 80S (Figure 3.21). Poly-A clipped footprints predominantly mapped to poly-adenylation sites across the transcriptome. These footprints were generated from ribosomes stalled while translating poly-A stretches. In contrast, RNAseq analysis showed that the purified 80S-Ski complex harbored less poly-A containing reads, and fewer reads mapping to the 3'UTR, as well (Figure 3.22). The primary reason for this enrichment observed only at the

translatome level is due to the protection of non-stop intermediates by the ribosomes stalled during NSD. Such ribosomes were already previously shown to be recognized by the exosome/Ski machinery (Frischmeyer et al., 2002; Ito-Harashima et al., 2007; Van Hoof et al., 2002), providing the most likely explanation for their enrichment in the purified 80S-Ski complexes.

Moreover, 80S-Ski RNA showed asymmetric read distribution with more reads mapping to the 5' end of the transcript, while, background RNA displayed a uniform distribution of reads (Figure 3.22). Since the Ski complex plays a major role in 3'-5' mRNA decay mediated by the exosome, these data showing an observed asymmetric pattern can be well explained by an enrichment of transcripts undergoing 3'-5' mRNA decay in the 80S-Ski complexes.

4.5 The Ski complex bridges translational and mRNA degradation machineries

Ski complex interaction with the 80S resulted in longer footprints than the expected footprint length of around 27 – 29 nts (Figure 3.19). Metagene analysis of the 5' end of 80S-Ski footprints revealed three-nucleotide periodicity, while similar analysis with the 3' end showed marked reduction in this periodicity (Figure 3.20). This is consistent with structural studies by the Beckmann lab, showing that the Ski complex contacts ribosomes on the mRNA entry site. This explains how, complete trimming by RNase I on the 3' end may be prevented. Overall, these data confirm that mRNA overhangs serve as a signal for Ski complex recruitment to the ribosome.

Interestingly, the 5' end of the 80S-Ski footprints exhibits three-nucleotide periodicity and a substantial fraction of these footprints map to the coding region (Figure 3.20). This signifies that the Ski complex is being recruited to actively translated ribosomes. But it raises the question why so many 80S-Ski footprints are mapping to the coding region or how within the coding region substrates are generated for Ski complex recruitment to the ribosomes?

One of the possible reasons is the pervasive presence of prematurely poly-adenylated transcripts within the yeast transcriptome (Ozsolak et al., 2010). These prematurely polyadenylated mRNAs are non-stop substrates

and ribosomes get stuck while translating over poly-A stretches. A recent ribosome profiling study has shown that such stalling events leads to ribosome-phased endonucleolytic cleavage to degrade non-stop transcripts (Guydosh & Green, 2017). Further, they observe that these cleavage events occur hundreds of nucleotides upstream of the stalling site, within the coding region of the transcripts. Potentially, every single yeast transcript could contain certain amount of prematurely poly-adenylated substrates. Therefore, it could be envisaged that ribosomal stalling triggered endonucleolytic cleavage might generate mRNA overhangs for Ski complex recruitment. But there was no correlation observed (data not shown) between footprint ratio (Ski vs background) and the percentage of premature poly-A mRNA amounts (normalized for canonical poly-A mRNA levels). Although premature poly-A substrates might be predominantly decayed via 3'-5' pathway this does not completely explain the presence of Ski footprints mapping to the ORFs.

Analysis of 80S-Ski selective ribosome profiling data showed that mRNAs with shorter half-lives displayed higher ratio of Ski footprints (Figure 3.23) and this correlated with non-optimal codon content of the transcripts (Figure 3.24). Thus, another possible scenario that might explain accumulation of reads in 5' UTR regions could be that the Ski complex is involved in cotranslational degradation of canonical mRNAs in 3'-5' direction. Notably, also Xrn1, the main decay factor for mRNAs in the 5'-3' direction was recently shown to be involved in cotranslational decay. (Hu et al., 2009; Pelechano et al., 2015; Tesina et al., 2019).

Cotranslational decay activity of Xrn1 allows complete translation of the substrate mRNA before being degraded, while cotranslational interaction of the Ski complex with the ribosome would not allow further translation. Possibly degradation from the 3' end could prevent the full-length synthesis of defective protein products, which could cause harmful consequences for the cell. Xrn1 degrades from the 5' end, thereby, could allow multiple ribosomes to finish translation. Accordingly, Xrn1 has been shown to be associated with polysomes, degrading decapped mRNAs (Hu et al., 2009). But how does Ski complex engage with ribosomes in the context of canonical mRNA turnover? Possibly, during canonical mRNA turnover, exosome together with the Ski complex might start to rapidly degrade from the 3' end. Upon reaching the

coding region, here then Ski complex could encounter translating ribosomes. A recent study has identified that sub-population of Ski complex interacts with a protein named Ska1 to form Ski-Ska1 complex (E. Zhang et al., 2019). They further show that this complex with exosome is sufficient to decay 'ribosome free regions' of mRNAs. Interestingly, they observe that Ska1 prevents Ski complex association with 80S ribosomes, however, the structural obtained in the Beckmann lab suggests that Ski complex interaction with ribosome displaces the auto-inhibitory domain of Ski2, thereby threading mRNA overhangs into the Ski2 helicase channel.

Once the Ski complex is bound to translating ribosomes with the 3' overhang, it can then proceed to extract the mRNA. It has been shown *in vitro* that the mammalian Ski complex proceeds to extract mRNA in the 3'-5' direction (Zinoviev et al., 2020). Ski complex mediated mRNA extraction is an ATP-dependent process and can extract from both pre- and post-translocation ribosomal complexes. Further, they show that the Ski mediated extraction renders stalled ribosomal complexes (both pre- and post-translocation) to be split and recycled via the A-site factors Pelota/Hbs1 and ABCE1 (Zinoviev et al., 2020). Since the Ski complex and the translational machinery is evolutionarily conserved, it could be speculated that Ski bound yeast 80S complexes are recycled via the same pathway.

Taken together analysis of Ski-80S complexes by selective ribosome profiling data confirms that indeed ribosomes stalled in NSD are targeted by the Ski complex apart from turnover of non-stop transcripts, Ski complex might also be involved in involved in turnover of canonical transcripts in the 3'-5' direction, especially if those messages have a high content of non-optimal codons.

4.6 XBP1u arrest peptide in the ribosomal tunnel

XBP1u is a central player in the unfolded protein response (UPR), and it contains a functionally critical ribosomal arrest peptide. IRE1α splices *XBP1u mRNA* on the ER membrane to generate the active transcription factor XBP1s. XBP1u uses the SRP pathway to localize itself on the ER membrane in the vicinity of IRE1α. XPB1u-AP arrests translational elongation, and this activity is absolutely essential for SRP recruitment by the moderately

hydrophobic HR2 domain. Interestingly, in comparison to other ribosomal stallers, XBP1u-AP induces only brief arrest in translation. Cryo-EM study presented here provided valuable insights into the functioning of XBP1u-AP.

To date, only several bacterial AP structures in the ribosomal tunnel have been solved, but until the start of the thesis, there has been only a single structure of mammalian ribosome staller: the “CMV-staller”. Here, stalling is mediated by CMV *gp48* uORF2 (cytomegalovirus leader peptide upstream open reading frame 2) to inhibit translation termination (Matheisl et al., 2015). The structural work presented here is the first cryo-EM structure of a well-characterized mammalian ribosome arresting peptide in the exit tunnel.

The high-resolution cryo-EM structure of the XBP1u arrest peptide obtained in this study provided insights into its role as a ribosomal staller. As observed in previously studied APs, XBP1u AP distorts the PTC minimally to inhibit translation. XBP1u-AP forms a turn in the upper-part of the tunnel near the PTC, and Leu259 of the XBP1u-AP prevents accommodation of the incoming t-RNA to prevent further peptide bond formation.

In the upper part of the tunnel, where XBP1u forms a turn, in the same region other stallers can form secondary structures like α-helices to inhibit PTC activity of ribosomes (Figure 4.1C,E). In the distal part of the tunnel, the conformation of the nascent chain is like a mammalian nascent chain in the tunnel (Figure 4.1B).

Ribosomal arrest peptides can stall ribosomes at a specific site (Ishii et al., 2015) or in some cases they can have multiple stall sites (Chiba & Ito, 2012; Tsai et al., 2014) within the arrest peptide. The high-resolution cryo-EM reconstructions, revealed that the first amino acid attached to P-tRNA in both post and rotated state complexes is methionine, corresponding to Met260 within the XBP1u arrest peptide (Figure 3.31), indicating that XBP1u arrest peptide has a specific stall site. Interestingly, bioinformatic analyses of mouse embryonic cell ribosome profiling data have also predicted ribosomes stall with Met260 in the P-site (Ingolia et al., 2011).

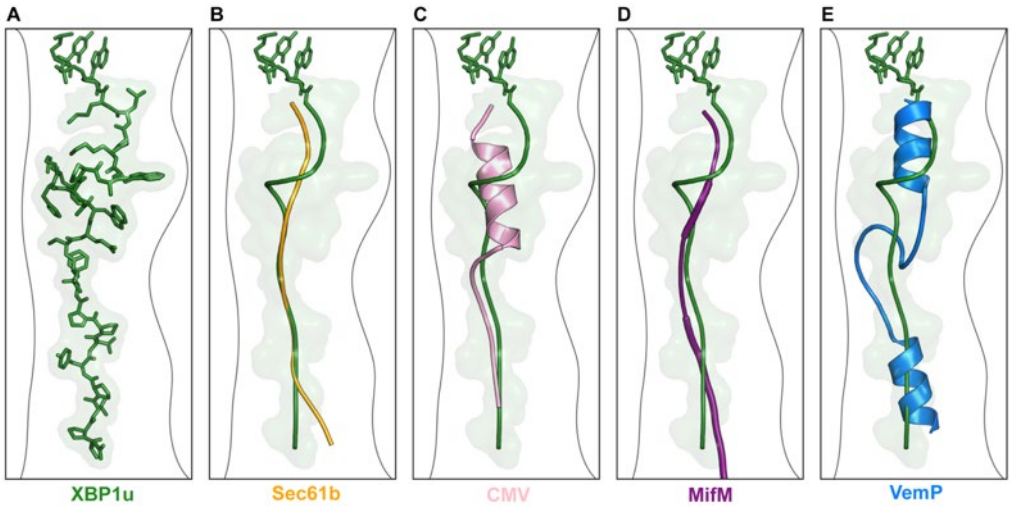

Figure 4.1: Comparison of XBP1u-AP in the ribosomal exit tunnel to other known ribosomal stallers.

(A) XBP1u-AP (green) shown as surface and model in the ribosomal tunnel. (B) Comparison of XBP1u-AP with a model of nascent chain from rabbit 80S (Voorhees & Hegde, 2015) (orange, PDB ID: 3JAG). (C – E) XBP1u-AP compared with other known ribosomal stallers such as CMV uORF2 (Matheisl et al., 2015) (pink, PDB ID: 5A8L), MifM (Sohmen et al., 2015) (purple, PDB ID: 3J9W) and VemP (Su et al., 2017) (cornflower blue, PDB ID: 5NWY). Positional overlap of the turn formed by XBP1u-AP and α-helical structures by CMV and VemP in ribosomal exit tunnel.

4.7 Minimal distortion of PTC by XBP1u arrest peptide

Bases, that coordinate PTC activity need to be precisely positioned for PTC functioning. Important bases involved in PTC include A4548 (A2602), U4452 (U2506) and U4531 (U2585), and of these U4531 coordinates both translation elongation as well as termination. Since U4531 (U2585) being the critical one, it is often severely perturbed by ribosomal arrest peptides or in some cases prevented to move into the induced state. Surprisingly U4531 is unperturbed in XBP1u-RNC, while another PTC base C4398 (C2452 in E. *coli*) is in a premature closed conformation stabilized by Leu259 of XBP1u-AP. Therefore, XBP1u-AP prevents accommodation of A-site tRNA to induce ribosomal stalling, similar to some of the previously described arrest peptides (Arenz, Meydan, et al., 2014; Sohmen et al., 2015; Su et al., 2017), albeit in a unique manner.

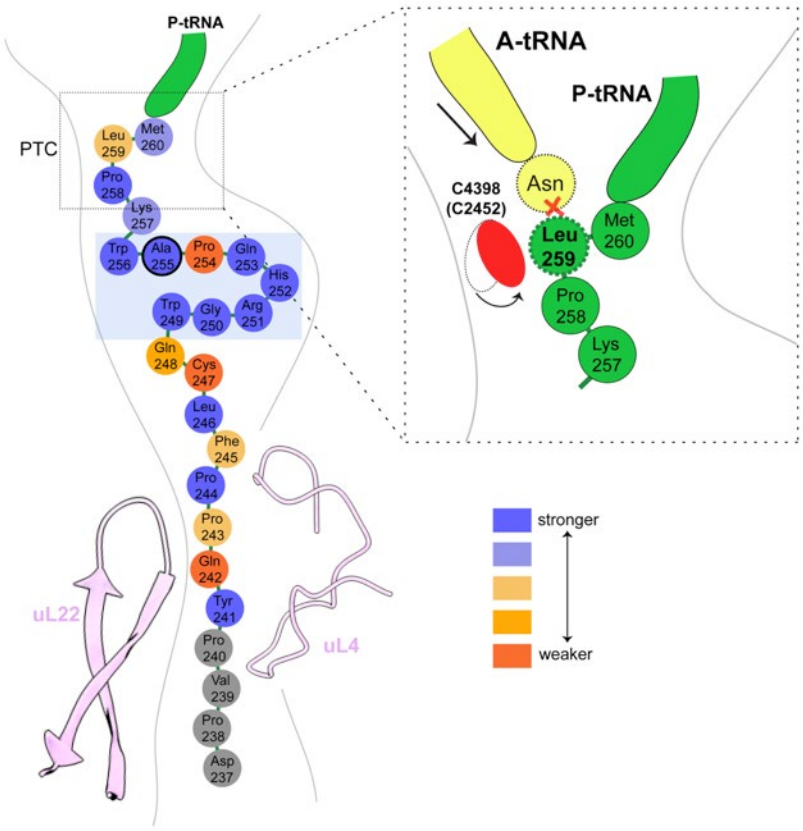

Figure 4.2: Schematic representation of XBP1u-AP in the ribosomal exit tunnel.

Schematic representation of the XBP1u nascent chain within the tunnel, and the unique conformational turn is highlighted. Residues of the nascent chain are colored based on the number of residues that could be mutated for a particular position to increase the potency of XBP1u-AP. Coloring is based on Figure 4.1C. Inset, shows PTC as a cartoon where the perturbed base C4398 (red) is highlighted, also shown is incoming A-site tRNA (yellow) where it would clash with Leu259 (green) of XBP1u-AP.

4.8 XBP1u nascent chain does not function as a force sensor in UPR

Cryo-EM structures of XBP1u-RNC with SRP and Sec61 revealed that HR2 is recognized as a canonical signal sequence but fails to engage the translocon Sec61. This observation is consistent with previous efforts (Kanda et al., 2016; Plumb et al., 2015). Even if a minimal force is exerted on the nascent chain, there is a possibility that the arrested state can be released given that the perturbation of PTC by XBP1u is minimal. In order for the AP to

experience a significant pulling force it has to be placed with a certain length from the hydrophobic segment: between the pausing site and the hydrophobic segment. As has been observed from the force profile analysis of XBP1u-AP, it experiences maximum pulling force at the length of 43 residues (Shanmuganathan et al., 2019), while XBP1u pausing site is at 53 residues from HR2 sequence. Therefore, it is very unlikely that XBP1u-AP will experience any significant force mediated by Sec61 while interacting with the HR2 domain.

4.9 Fate and role of XBP1u nascent chain in UPR

Since force mediated release of the arrested XBP1u-RNC complex is not likely *in vivo*, there can be two alternative scenarios envisioned regarding the fate of this stalled ribosomal complex. Arrest enhancing XBP1u-AP mutant (Ser255Ala) has been used for both structural and saturation mutagenesis in the study reported here, while wildtype XBP1u has a shorter half-life *in vivo*, as shown in a previous study (Yanagitani et al., 2011). Therefore, one likely scenario is that the stalling complex is released spontaneously *in vivo*. Second, the stalled complex might be targeted by the ribosomal quality control factors such as Pelota/Hbs1, acting in the A-site and potentially releasing the stall.

A recent ribosome profiling study surveyed for ribosomal collisions sites caused by ribosomal pausing within the human and zebrafish transcriptome. One of the prime candidate *in vivo* that showed several disome peaks was XBP1u. Strikingly, the highest peak representing the disome ribosomal footprint was at the predicted arrest site (P. Han et al., 2019). With the leading ribosome on the arrest site (Met260), they detect several disome peaks upstream of the pause site indicating queued colliding ribosomes. Further with biochemical experiments, they also show that XBP1u is decayed via ribosomal quality control (RQC) pathway. Therefore, unstressed cells seem to utilize the process of ribosomal collision to trigger decay of XBP1u via RQC.

In conclusion, XBP1u nascent chain interacts with the ribosomal exit tunnel to pause translation, while this pausing state allows HR2 domain to successfully recruit SRP. This sets the path for the paused complex to be targeted to ER on the Sec61 translocon, where during ER stress IRE1α can

splice *XBP1u mRNA* to generate *XBP1s mRNA*. In this context, the XBP1u nascent chain might have evolved as a timer, which provides a short window for IRE1α to access the mRNA to generate the active transcription factor XBP1s. In agreement with a function as a timer, the arrest phenotype as well as the arrest mechanism is rather weak. Compared to rather robust bacterial stallers like SecM and VemP, where the geometry of the PTC is perturbed at multiple sites, in case of XBP1u only one single base of the PTC is distorted, suggesting a rather quick reversal.

5 Outlook

Translation is one of the central and energy consuming processes of the cell. In order to conserve cellular resources regulation of translation is critical. Using ribosome profiling and cryo-EM, translational regulation has been explored in this thesis within three different biological contexts. The study presented here provides novels insights into translational regulation, but it also raises some interesting questions, which can be further explored.

During DC maturation increased ribosome occupancy was observed in the UTRs. One obvious question is, what exactly are the ribosomes doing there? Are the ribosomes involved in upstream initiation? This could be probably studied further by performing ribosome profiling in the presence of eukaryotic specific translation initiation inhibitors such as lactimidomycin and harringtonine. Identification of translation initiation sites upstream and more interestingly in the 3' UTRs during the later stages of DC maturation would provide insights into UTR mediated translational control during DC maturation. 3‘ UTRs harbor sites for RNA binding proteins (RBP), and these RBPs can further recruit effector proteins, which can affect the function and role of the encoded protein. Finally, it would be interesting to find out how long the mature DCs can tolerate with the ribosomes stuck in the 3' UTR, and whether the stuck ribosomes in the 3' UTR serve as a signal for triggering cellular death pathways in mature DCs.

Biologically, ribosome stalling has been exploited for various purposes, and the XBP1u-AP studied in this thesis plays a critical role in the UPR to alleviate ER stress. Cryo-EM analysis of the XBP1u-AP in the ribosomal tunnel showed that it minimally distorts PTC, thereby leading to transient arrest in translation. Mammalian ribosome profiling studies has shed light on amino acid sequences that can cause strong ribosomal arrest. It would be interesting to find amino acid stretches that can cause temporary arrest in translation and also can be structurally visualized to investigate the state of PTC in the arrested state. Probably such studies would be help to synthesize APs of varying strength to inhibit ribosomal activity.

6 Appendix

A

Number of genes significant for RNA, RPF or RPF/RNA change over 5' UTR

Analysis	RPF	RNA	RPF&RNA	RPF/RNA
4h vs iDC	1341	247	321	1225
24h vs iDC	2548	240	804	1704

B

Number of genes significant for RNA, RPF or RPF/RNA change over 3' UTR

Analysis	RPF	RNA	RPF&RNA	RPF/RNA
4h vs iDC	383	1185	119	191
24h vs iDC	988	643	563	4464

Figure 6.1 Identification of genes that showed differential ribosome occupancy and transcript fold change over the UTRs.

Number of genes that showed significant change in ribosome density (RPF/RNA), ribosome occupancy (RPF) and transcript levels (RNA) over the 5' UTR (A) and 3' UTR (B) was calculated using DEseq.

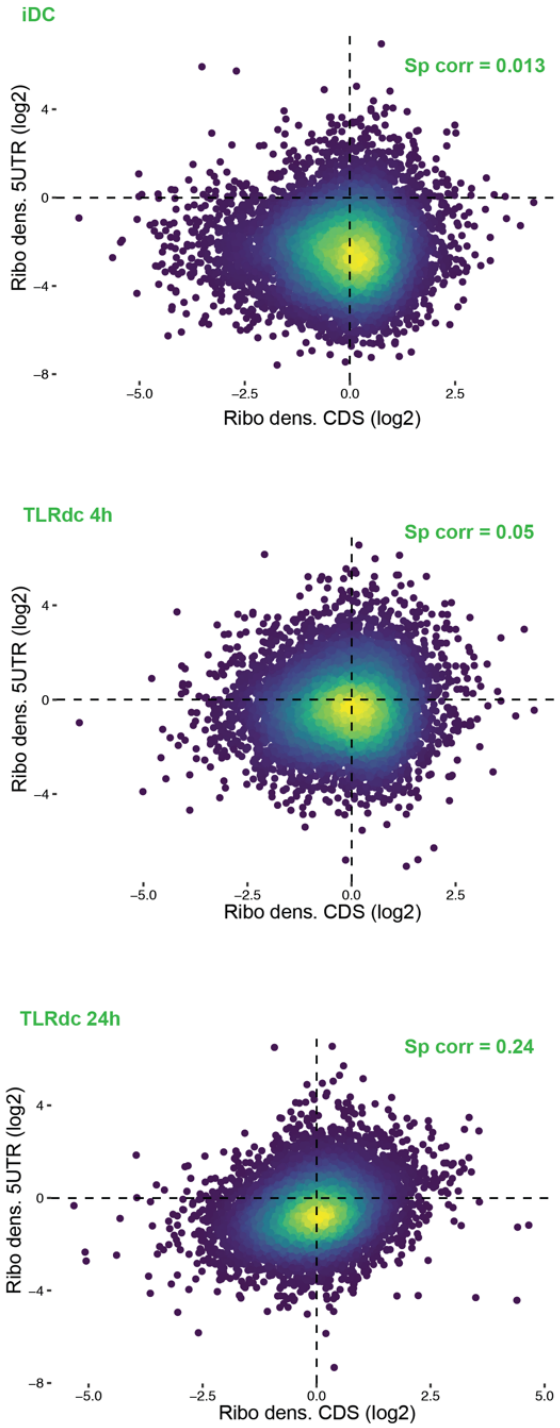

Figure 6.2 Correlation between 5' UTR ribosome density and CDS ribosome density.

Plotted is the ribosome density (RPF/RNA or Translational efficiency) of the 5' UTR against the ribosome density of CDS for all three points (iDC, 4h and 24h DC). There is a weak correlation only for the 24 h time-point (bottom) between 5' UTR ribosome occupancy and translation of the CDS.

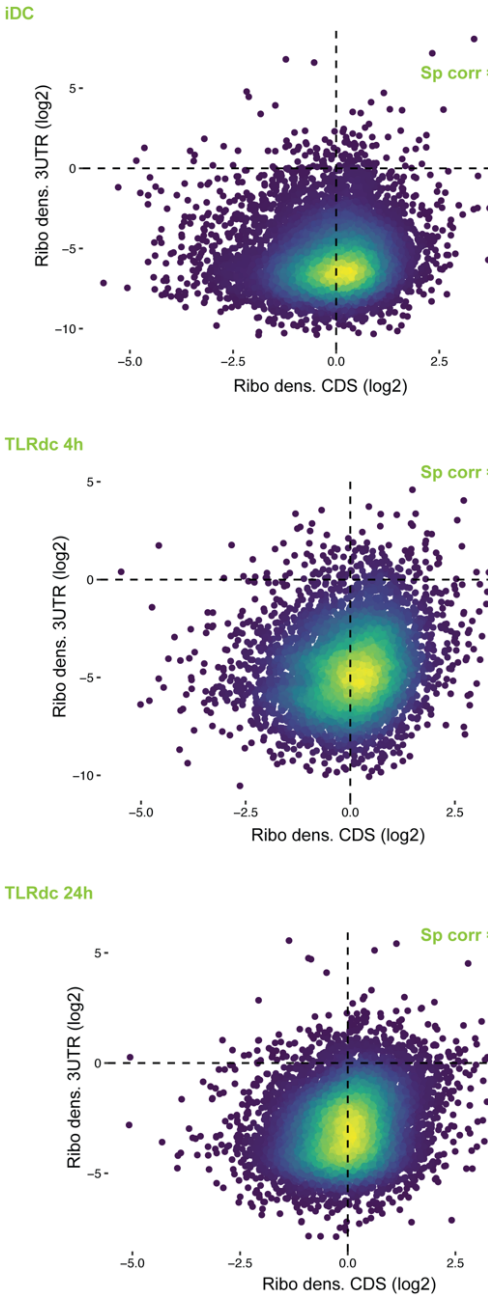

Figure 6.3 Correlation between 3' UTR ribosome density and CDS ribosome density.

3' UTR ribosome density is plotted against the ribosome density of CDS for all three time points: iDC (top), 4h (middle) and 24h (bottom) DC. Very weak correlation was observed for 4h and 24h time-point.

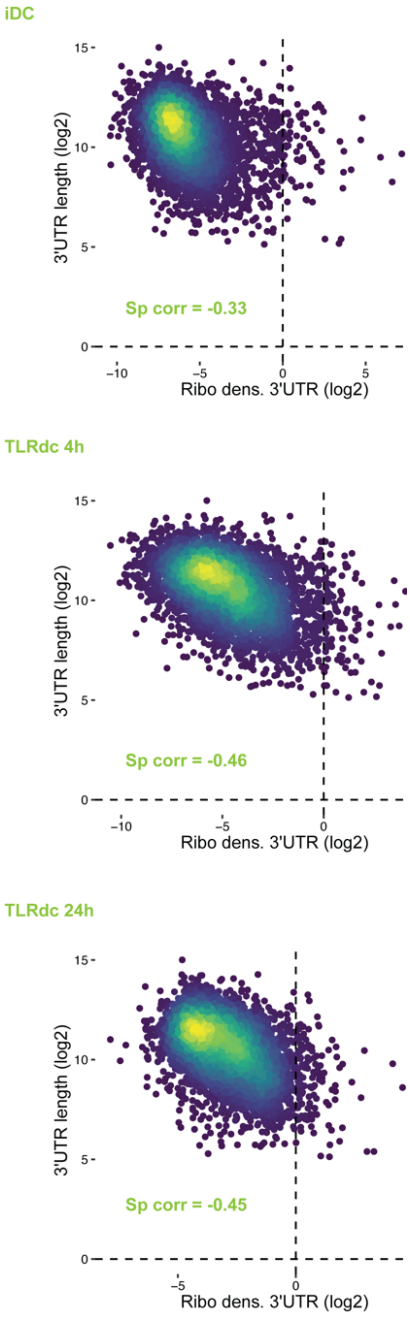

Figure 6.4 Correlation between 3' UTR length and 3' UTR ribosome density.

3' UTR ribosome density is plotted against its length for all three time points. Slightly strong negative correlation was observed for the 4 h and 24 h time points.

Table 6-1 Number of uniquely mapping reads

Sample	RNAseq	RPFseq	RPFseq (25-32)
iDC replicate 1	22491129	13762372	9888281 (71.8%)
iDC replicate 2	75603532	49027917	43622037 (88.9%)
TLRDC 4 h replicate 1	36626843	6878122	5212412 (75.7%)
TLRDC 4 h replicate 2	29526329	15448388	13194823 (85.4%)
TLRDC 24 h replicate 1	36578248	24233833	22380246 (92.3%)
TLRDC 24 h replicate 2	33832251	41786854	35672517 (85.3%)

Table 6-2 Percentage of reads mapping to the CDS

Sample	RPFseq (25 -32)	Percentage (%)
iDC replicate 1	8936271	90.3
iDC replicate 2	41720262	95.6
TLRDC 4h replicate 1	4565237	87.5
TLRDC 4h replicate 2	12415775	94
TLRDC 24h replicate 1	16003641	71.5
TLRDC 24h replicate 2	30831957	86.4

Table 6-3 Model and refinement statistics for XBP1u-ribosome nascent chain complexes

	XBP1u-RNC	XBP1u-RNC	XBP1u-RNC-SRP	XBP1u-RNC-Sec61
Ribosomal state	Post State	Rotated state	Post state	Post state
Microscope	FEI Titan Krios	FEI Titan Krios	FEI Titan Krios	FEI Titan Krios
Camera	Falcon II	Falcon II	Falcon II	Falcon II
Voltage (kV)	300	300	300	300
Pixel size (Å)	1.084	1.084	1.084	1.084
Electron dose (e-/Å^2)	28	28	28	28
Defocus range (μm)	0.5 - 2.5	0.5 - 2.5	0.5 - 2.5	0.5 - 2.5
Particles after 2D (no.)	531952	531952	170231	43578
Final particles (no.)	223773	94923	24875	12749
Model Composition				
Protein residues	11717	11673	12566	12239
RNA bases	5669	5797	5874	5668
Resolution (Å)	3	3.1	3.7	3.9
FSC threshold	0.143	0.143	0.143	0.143
Map CC (around atoms)	0.76	0.75	0.71	0.68
Map CC (whole unit cell)	0.73	0.72	0.68	0.66
Map sharpening B-factor (Å^2)	-71.2	-59.9	-105.54	-81.6
RMS Deviations				
Bond lengths (Å)	0.004	0.0038	0.0036	0.0035
Bond angles (°)	0.91	0.92	0.88	0.91
Validation				
MolProbity score	1.5	1.66	1.55	1.5
Clashscore	4.9	4.82	5.34	4.55
Poor rotamers (%)	0.23	0.20	0.16	0.13
Ramachandran Plot				
Disallowed (%)	0.03	0.09	0.05	0.02
Allowed (%)	3.60	5.67	3.84	3.87

Favored (%)	96.37	94.24	96.11	96.1

7 List of Abbreviations

A-tRNA	Aminoacyl-tRNA
ABCE1	ATP-binding cassette subfamily E member 1
AP	Arrest peptide
ATF6	Activating transcription factor
ATP	Adenosine triphosphate
Bip	Binding immunoglobulin protein
bZIP	Basic leucine zipper
CBB	Coomassie brilliant blue
CCR7	C-C chemokine receptor type 7
CD14	Cluster of differentiation 14
cDNA	Complementary DNA
CDS	Coding sequence
CHX	Cycloheximide
CMV	Cytomegalovirus
cryo-EM	Cryoelectron microscopy
DCs	Dendritic cells
DTT	Dithiothreitol
E-tRNA	Exit-tRNA
eIF	Eukaryotic initiation factor
EJC	Exon-junction complex
ER	Endoplasmic reticulum
eRF	Eukaryotic release factor
f_{FL}	Fraction full-length
FSC	Fourier shell correlation
GCN2	General control nonderepressible 2
GTP	Guanosine triphosphate
HLA-DR	Human leukocyte antigen DR-isotype
HR2	Hydrophobic region 2
HRI	Heme-regulated inhibitor
iDC	Immature dendritic cells

IFN-γ	Interferon-γ
IGR	Intergenic region
IL12	Interleukin 12
IRE1α	Inositol requiring enzyme 1α
IRES	Internal ribosome entry site
ITAF	IRES transactivating factors
LPS	Lipopolysaccharides
LSU	Large subunit
m7G	7-methylguanosine
miRNA	Micro RNA
mRNA	Messenger RNA
mTOR	Mechanistic target of rapamycin
ng	Nanogram
NGD	No go decay
NGS	Next generation sequencing
NMD	Nonsense mediated decay
NSD	Nonstop decay
ORF	Open reading frame
OST	Oligosaccharlytransferase
P-tRNA	Peptidyl-tRNA
Pab1	Poly-A binding protein-1
PAGE	Poly acrylamide gel electrophoresis
PCC	Protein conducting channel
PCR	Polymerase chain reaction
PERK	PKR-like endoplasmic reticulum kinase
PGE2	Prostaglandin E_2
PIC	Preinitiation complex
PIKK	Phosphatidylinositol 3-kinase-related kinase
PKR	Protein kinase R
PNK	Polynucleotide kinase
PPI	Protein-protein interaction
ProRP	Proximity specific ribosome profiling
PRR	Pattern recognition receptor

PTC	Peptidyl transferase center
RBP	RNA binding protein
RF	Release factor
RM	Rough microsomes
RNA	Ribonucleic acid
RNC	Ribosome nascent chain complex
RPF	Ribosome protected fragment
RQC	Ribosomal quality control
RRL	Rabbit reticulocyte lysate
rRNA	Ribosomal RNA
SDS	Sodium dodecyl sulfate
SecM	Secretion monitor
SeRP	Selective ribosome profiling
SL	Stem-loop
snoRNA	Small nucleolar RNA
snRNA	Small nuclear RNA
SRP	Signal recognition particle
SSU	Small subunit
TF	Trigger factor
TLR	Toll-like receptors
TM	Transmembrane segment
TNFα	Tumor necrosis factor-α
TOP	Terminal oligopyrimidine
tRNA	Transfer RNA
uORF	Upstream ORF
Upf	Upstream frame shifting
UPR	Unfolded protein response
UTR	Untranslated region
XBP1s	X-box binding protein-1 spliced
XBP1u	X-box binding protein-1 unspliced
µg	Microgram
µl	Microliter

8 References

Adams, P. D., Afonine, P. V., Bunkóczi, G., Chen, V. B., Davis, I. W., Echols, N., Headd, J. J., Hung, L. W., Kapral, G. J., Grosse-Kunstleve, R. W., McCoy, A. J., Moriarty, N. W., Oeffner, R., Read, R. J., Richardson, D. C., Richardson, J. S., Terwilliger, T. C., & Zwart, P. H. (2010). PHENIX: A comprehensive Python-based system for macromolecular structure solution. *Acta Crystallographica Section D: Biological Crystallography*, *66*(2), 213–221. https://doi.org/10.1107/S0907444909052925

Akashi, H. (1994). Synonymous codon usage in Drosophila melanogaster: natural selection and translational accuracy. *Genetics*, *136*(3), 927–935. https://doi.org/10.1093/genetics/136.3.927

Amrani, N., Ganesan, R., Kervestin, S., Mangus, D. A., Ghosh, S., & Jacobson, A. (2004). A faux 3'-UTR promotes aberrant termination and triggers nonsense-mediated mRNA decay. *Nature*, *432*(7013), 112–118. https://doi.org/10.1038/nature03060

Anders, S., Pyl, P. T., & Huber, W. (2015). HTSeq—a Python framework to work with high-throughput sequencing data. *Bioinformatics*, *31*(2), 166–169. https://doi.org/10.1093/bioinformatics/btu638

Anderson, J. S. J., & Parker, R. (1998). The 3' to 5' degradation of yeast mRNAs is a general mechanism for mRNA turnover that requires the SK12 DEVH box protein and 3' to 5' exonucleases of the exosome complex. *EMBO Journal*, *17*(5), 1497–1506. https://doi.org/10.1093/emboj/17.5.1497

Andreev, D. E., O'Connor, P. B. F., Zhdanov, A. V, Dmitriev, R. I., Shatsky, I. N., Papkovsky, D. B., & Baranov, P. V. (2015). Oxygen and glucose deprivation induces widespread alterations in mRNA translation within 20 minutes. *Genome Biology*, *16*, 90. https://doi.org/10.1186/s13059-015-0651-z

Araki, Y., Takahashi, S., Kobayashi, T., Kajiho, H., Hoshino, S. I., & Katada, T. (2001). Ski7p G protein interacts with the exosome and the ski complex for 3′-to-5′ mRNA decay in yeast. *EMBO Journal*, *20*(17), 4684–

4693. https://doi.org/10.1093/emboj/20.17.4684

Arenz, S., Meydan, S., Starosta, A. L., Berninghausen, O., Beckmann, R., Vazquez-Laslop, N., & Wilson, D. N. (2014). Drug-sensing by the ribosome induces translational arrest via active site perturbation. *Molecular Cell*, *56*(3), 446–452. https://doi.org/10.1177/0145721709355835.Continuous

Arenz, S., Ramu, H., Gupta, P., Berninghausen, O., Beckmann, R., Vázquez-Laslop, N., Mankin, A. S., & Wilson, D. N. (2014). Molecular basis for erythromycin-dependent ribosome stalling during translation of the ErmBL leader peptide. *Nature Communications*, *5*, 3501. https://doi.org/10.1038/ncomms4501

Arpat, A. B., Liechti, A., De Matos, M., Dreos, R., Janich, P., & Gatfield, D. (2020). Transcriptome-wide sites of collided ribosomes reveal principles of translational pausing. *Genome Research* , *30*(7), 985–999. https://doi.org/10.1101/gr.257741.119

B.Martoglio, S.Hauser, B. D. (1998). Cotranslational translocation of proteins into microsomes derived from the rough endoplasmic reticulum of mammalian cells. *Cell Biology: A Laboratory Handbook*, 265–273.

Barreau, C., Paillard, L., & Osborne, H. B. (2005). AU-rich elements and associated factors: are there unifying principles? *Nucleic Acids Research*, *33*(22), 7138–7150. https://doi.org/10.1093/nar/gki1012

Becker, T., Armache, J.-P., Jarasch, A., Anger, A. M., Villa, E., Sieber, H., Motaal, B. A., Mielke, T., Berninghausen, O., & Beckmann, R. (2011). Structure of the no-go mRNA decay complex Dom34-Hbs1 bound to a stalled 80S ribosome. *Nature Structural & Molecular Biology*, *18*(6), 715–720. https://doi.org/10.1038/nsmb.2057

Becker, T., Franckenberg, S., Wickles, S., Shoemaker, C. J., Anger, A. M., Armache, J.-P., Sieber, H., Ungewickell, C., Berninghausen, O., Daberkow, I., Karcher, A., Thomm, M., Hopfner, K.-P., Green, R., & Beckmann, R. (2012). Structural basis of highly conserved ribosome recycling in eukaryotes and archaea. *Nature*, *482*(7386), 501–506. https://doi.org/10.1038/nature10829

Behrmann, E., Loerke, J., Budkevich, T. V., Yamamoto, K., Schmidt, A., Penczek, P. A., Vos, M. R., Bürger, J., Mielke, T., Scheerer, P., & Spahn,

C. M. T. (2015). Structural snapshots of actively translating human ribosomes. *Cell*, *161*(4), 845–857. https://doi.org/10.1016/j.cell.2015.03.052

Benard, L., Carroll, K., Valle, R. C. P., Masison, D. C., & Wickner, R. B. (1999). The Ski7 Antiviral Protein Is an EF1-α Homolog That Blocks Expression of Non-Poly(A) mRNA in Saccharomyces cerevisiae. *Journal of Virology*, *73*(4), 2893–2900. https://doi.org/10.1128/jvi.73.4.2893-2900.1999

Bertolotti, A, Wang, X., Novoa, I., Jungreis, R., Schlessinger, K., Cho, J. H., West, A. B., & Ron, D. (2001). Increased sensitivity to dextran sodium sulfate colitis in IRE1beta-deficient mice. *The Journal of Clinical Investigation*, *107*(5), 585–593. https://doi.org/10.1172/JCI11476

Bertolotti, Anne, Zhang, Y., Hendershot, L. M., Harding, H. P., & Ron, D. (2000). Dynamic interaction of BiP and ER stress transducers in the unfolded-protein response. *Nature Cell Biology*, *2*, 326–332. https://doi.org/10.1038/35014014

Bhushan, S., Hoffmann, T., Seidelt, B., Frauenfeld, J., Mielke, T., Berninghausen, O., Wilson, D. N., & Beckmann, R. (2011). SecM-stalled ribosomes adopt an altered geometry at the peptidyl transferase center. *PLoS Biology*, *9*(1). https://doi.org/10.1371/journal.pbio.1000581

Bhushan, S., Meyer, H., Starosta, A. L., Becker, T., Mielke, T., Berninghausen, O., Sattler, M., Wilson, D. N., & Beckmann, R. (2010). Structural basis for translational stalling by human cytomegalovirus and fungal arginine attenuator peptide. *Molecular Cell*, *40*(1), 138–146. https://doi.org/10.1016/j.molcel.2010.09.009

Brandman, O., Stewart-Ornstein, J., Wong, D., Larson, A., Williams, C. C., Li, G.-W., Zhou, S., King, D., Shen, P. S., Weibezahn, J., Dunn, J. G., Rouskin, S., Inada, T., Frost, A., & Weissman, J. S. (2012). A Ribosome-Bound Quality Control Complex Triggers Degradation of Nascent Peptides and Signals Translation Stress. *Cell*, *151*(5), 1042–1054. https://doi.org/https://doi.org/10.1016/j.cell.2012.10.044

Brar, G. A., Yassour, M., Friedman, N., Regev, A., Ingolia, N. T., & Weissman, J. S. (2012). *High-Resolution View of the Yeast Meiotic Program Revealed by Ribosome Profiling.* Science (New York, NY).

https://doi.org/10.1126/science.1215110

Brar, G. a, & Weissman, J. S. (2015). Ribosome profiling reveals the what, when, where and how of protein synthesis. *Nature Reviews. Molecular Cell Biology*, *16*(11), 651–664. https://doi.org/10.1038/nrm4069

Braunger, K., Pfeffer, S., Shrimal, S., Gilmore, R., Berninghausen, O., Mandon, E. C., Becker, T., Förster, F., & Beckmann, R. (2018). Structural basis for coupling protein transport and N-glycosylation at the mammalian endoplasmic reticulum. *Science*, *360*(6385), 215–219. https://doi.org/10.1126/science.aar7899

Brennan, C. M., & Steitz, J. A. (2001). HuR and mRNA stability. *Cellular and Molecular Life Sciences : CMLS*, *58*(2), 266–277. https://doi.org/10.1007/PL00000854

Brown, A., Shao, S., Murray, J., Hegde, R. S., & Ramakrishnan, V. (2015a). Structural basis for stop codon recognition in eukaryotes. *Nature*, *524*(7566), 493–496. https://doi.org/10.1038/nature14896

Brown, A., Shao, S., Murray, J., Hegde, R. S., & Ramakrishnan, V. (2015b). Structural basis for stop codon recognition in eukaryotes. *Nature*, *524*(7566), 493–496. https://doi.org/10.1038/nature14896

Brown, J. T., Bai, X., & Johnson, A. W. (2000). The yeast antiviral proteins Ski2p, Ski3p, and Ski8p exist as a complex in vivo. *RNA (New York, N.Y.)*, *6*(3), 449–457. https://doi.org/10.1017/S1355838200991787

Buschow, S. I., Lasonder, E., van Deutekom, H. W. M., Oud, M. M., Beltrame, L., Huynen, M. A., de Vries, I. J. M., Figdor, C. G., & Cavalieri, D. (2010). Dominant Processes during Human Dendritic Cell Maturation Revealed by Integration of Proteome and Transcriptome at the Pathway Level. *Journal of Proteome Research*, *9*(4), 1727–1737. https://doi.org/10.1021/pr9008546

Butkus, M. E., Prundeanu, L. B., & Oliver, D. B. (2003). Translocon “Pulling” of Nascent SecM Controls the Duration of Its Translational Pause and Secretion-Responsive secA Regulation. *Journal of Bacteriology*, *185*(22), 6719–6722. https://doi.org/10.1128/JB.185.22.6719-6722.2003

Calfon, M., Zeng, H., Urano, F., Till, J. H., Hubbard, S. R., Harding, H. P., Clark, S. G., & Ron, D. (2002). IRE1 couples endoplasmic reticulum load to secretory capacity by processing the XBP-1 mRNA. *Nature*, *415*(6867),

92–96. https://doi.org/10.1038/415092a

Ceppi, M., Clavarino, G., Gatti, E., Schmidt, E. K., De Gassart, A., Blankenship, D., Ogola, G., Banchereau, J., Chaussabel, D., & Pierre, P. (2009). Ribosomal protein mRNAs are translationally-regulated during human dendritic cells activation by LPS. *Immunome Research*, *5*(1), 1–12. https://doi.org/10.1186/1745-7580-5-5

Chartron, J. W., Hunt, K. C. L., & Frydman, J. (2016). Cotranslational signal-independent SRP preloading during membrane targeting. *Nature*, *536*(7615), 224–228. https://doi.org/10.1038/nature19309

Chen, C. Y., Gherzi, R., Ong, S. E., Chan, E. L., Raijmakers, R., Pruijn, G. J., Stoecklin, G., Moroni, C., Mann, M., & Karin, M. (2001). AU binding proteins recruit the exosome to degrade ARE-containing mRNAs. *Cell*, *107*(4), 451–464. https://doi.org/10.1016/s0092-8674(01)00578-5

Chen, V. B., Arendall, W. B., Headd, J. J., Keedy, D. A., Immormino, R. M., Kapral, G. J., Murray, L. W., Richardson, J. S., & Richardson, D. C. (2010). MolProbity: All-atom structure validation for macromolecular crystallography. *Acta Crystallographica Section D: Biological Crystallography*, *66*(1), 12–21. https://doi.org/10.1107/S0907444909042073

Chiba, S., & Ito, K. (2012). Multisite Ribosomal Stalling: A Unique Mode of Regulatory Nascent Chain Action Revealed for MifM. *Molecular Cell*, *47*(6), 863–872. https://doi.org/10.1016/j.molcel.2012.06.034

Chiba, S., Kanamori, T., Ueda, T., Akiyama, Y., Pogliano, K., & Ito, K. (2011). Recruitment of a species-specific translational arrest module to monitor different cellular processes. *Proceedings of the National Academy of Sciences*, *108*(15), 6073 LP – 6078. https://doi.org/10.1073/pnas.1018343108

Chiba, S., Lamsa, A., & Pogliano, K. (2009). A ribosome-nascent chain sensor of membrane protein biogenesis in Bacillus subtilis. *EMBO Journal*, *28*(22), 3461–3475. https://doi.org/10.1038/emboj.2009.280

Coller, J., & Parker, R. (2004). Eukaryotic mRNA decapping. *Annual Review of Biochemistry*, *73*, 861–890. https://doi.org/10.1146/annurev.biochem.73.011303.074032

Cruz-Vera, L. R., Sachs, M. S., Squires, C. L., & Yanofsky, C. (2011). Nascent

polypeptide sequences that influence ribosome function. *Current Opinion in Microbiology*, *14*(2), 160–166. https://doi.org/10.1016/j.mib.2011.01.011

Degnin, C. R., Schleiss, M. R., Cao, J., & Geballe, A. P. (1993). Translational inhibition mediated by a short upstream open reading frame in the human cytomegalovirus gpUL4 (gp48) transcript. *Journal of Virology*, *67*(9), 5514–5521. https://doi.org/10.1128/JVI.67.9.5514-5521.1993

Dever, T E, Feng, L., Wek, R. C., Cigan, A. M., Donahue, T. F., & Hinnebusch, A. G. (1992). Phosphorylation of initiation factor 2 alpha by protein kinase GCN2 mediates gene-specific translational control of GCN4 in yeast. *Cell*, *68*(3), 585–596. https://doi.org/10.1016/0092-8674(92)90193-g

Dever, Thomas E, & Green, R. (2012). Phases of Translation in Eukaryotes. *Cold Spring Harbor Perspectives in Biology Perspect Biology*, *4*, 1–16.

Dieu, M.-C., Vanbervliet, B., Vicari, A., Bridon, J.-M., Oldham, E., Aït-Yahia, S., Brière, F., Zlotnik, A., Lebecque, S., & Caux, C. (1998). Selective Recruitment of Immature and Mature Dendritic Cells by Distinct Chemokines Expressed in Different Anatomic Sites . *Journal of Experimental Medicine*, *188*(2), 373–386. https://doi.org/10.1084/jem.188.2.373

Dimitrova, L. N., Kuroha, K., Tatematsu, T., & Inada, T. (2009). Nascent Peptide-dependent Translation Arrest Leads to Not4p-mediated Protein Degradation by the Proteasome*. *Journal of Biological Chemistry*, *284*(16), 10343–10352. https://doi.org/https://doi.org/10.1074/jbc.M808840200

Doerfel, L. K., Wohlgemuth, I., Kubyshkin, V., Starosta, A. L., Wilson, D. N., Budisa, N., & Rodnina, M. V. (2015). Entropic Contribution of Elongation Factor P to Proline Positioning at the Catalytic Center of the Ribosome. *Journal of the American Chemical Society*, *137*(40), 12997–13006. https://doi.org/10.1021/jacs.5b07427

Doma, M. K., & Parker, R. (2006). Endonucleolytic cleavage of eukaryotic mRNAs with stalls in translation elongation. *Nature*, *440*(7083), 561–564. https://doi.org/10.1038/nature04530

Döring, K., Ahmed, N., Riemer, T., Suresh, H. G., Vainshtein, Y., Habich, M.,

Riemer, J., Mayer, M. P., O'Brien, E. P., Kramer, G., & Bukau, B. (2017). Profiling Ssb-Nascent Chain Interactions Reveals Principles of Hsp70-Assisted Folding. *Cell*, *170*(2), 298-311.e20. https://doi.org/10.1016/j.cell.2017.06.038

dos Reis, M., Savva, R., & Wernisch, L. (2004). Solving the riddle of codon usage preferences: a test for translational selection. *Nucleic Acids Research*, *32*(17), 5036–5044. https://doi.org/10.1093/nar/gkh834

Drummond, D. A., & Wilke, C. O. (2008). Mistranslation-induced protein misfolding as a dominant constraint on coding-sequence evolution. *Cell*, *134*(2), 341–352. https://doi.org/10.1016/j.cell.2008.05.042

Dziembowski, A., Lorentzen, E., Conti, E., & Séraphin, B. (2007). A single subunit, Dis3, is essentially responsible for yeast exosome core activity. *Nature Structural & Molecular Biology*, *14*(1), 15–22. https://doi.org/10.1038/nsmb1184

Eberle, A. B., Lykke-Andersen, S., Mühlemann, O., & Jensen, T. H. (2009). SMG6 promotes endonucleolytic cleavage of nonsense mRNA in human cells. *Nature Structural & Molecular Biology*, *16*(1), 49–55. https://doi.org/10.1038/nsmb.1530

Elgamal, S., Katz, A., Hersch, S. J., Newsom, D., White, P., Navarre, W. W., & Ibba, M. (2014). EF-P Dependent Pauses Integrate Proximal and Distal Signals during Translation. *PLoS Genetics*, *10*(8). https://doi.org/10.1371/journal.pgen.1004553

Emsley, P., & Cowtan, K. (2004). Coot: Model-building tools for molecular graphics. *Acta Crystallographica Section D: Biological Crystallography*, *60*(12 I), 2126–2132. https://doi.org/10.1107/S0907444904019158

Everts, B., Amiel, E., Huang, S. C.-C., Smith, A. M., Chang, C.-H., Lam, W. Y., Redmann, V., Freitas, T. C., Blagih, J., van der Windt, G. J. W., Artyomov, M. N., Jones, R. G., Pearce, E. L., & Pearce, E. J. (2014). TLR-driven early glycolytic reprogramming via the kinases TBK1-IKKε supports the anabolic demands of dendritic cell activation. *Nature Immunology*, *15*(4), 323–332. https://doi.org/10.1038/ni.2833

Fang, P., Spevak, C. C., Wu, C., & Sachs, M. S. (2004). A nascent polypeptide domain that can regulate translation elongation. *Proceedings of the National Academy of Sciences*, *101*(12), 4059 LP – 4064.

https://doi.org/10.1073/pnas.0400554101

Fang, P., Wang, Z., & Sachs, M. S. (2000). Evolutionarily conserved features of the arginine attenuator peptide provide the necessary requirements for its function in translational regulation. *Journal of Biological Chemistry*, *275*(35), 26710–26719. https://doi.org/10.1074/jbc.M003175200

Fields, A. P., Rodriguez, E. H., Jovanovic, M., Stern-Ginossar, N., Haas, B. J., Mertins, P., Raychowdhury, R., Hacohen, N., Carr, S. A., Ingolia, N. T., Regev, A., & Weissman, J. S. (2015). A Regression-Based Analysis of Ribosome-Profiling Data Reveals a Conserved Complexity to Mammalian Translation. *Molecular Cell*, *60*(5), 816–827. https://doi.org/10.1016/j.molcel.2015.11.013

Franckenberg, S., Becker, T., & Beckmann, R. (2012). Structural view on recycling of archaeal and eukaryotic ribosomes after canonical termination and ribosome rescue. *Current Opinion in Structural Biology*, *22*(6), 786–796. https://doi.org/https://doi.org/10.1016/j.sbi.2012.08.002

Frank, J., & Agrawal, R. K. (2000). A ratchet-like inter-subunit reorganization of the ribosome during translocation. *Nature*, *406*(6793), 318–322. https://doi.org/10.1038/35018597

Frischmeyer, P. A., Van Hoof, A., O'Donnell, K., Guerrerio, A. L., Parker, R., & Dietz, H. C. (2002). An mRNA surveillance mechanism that eliminates transcripts lacking termination codons. *Science*, *295*(5563), 2258–2261. https://doi.org/10.1126/science.1067338

Gaba, A., Jacobson, A., & Sachs, M. S. (2005). Ribosome occupancy of the yeast CPA1 upstream open reading frame termination codon modulates nonsense-mediated mRNA decay. *Molecular Cell*, *20*(3), 449–460. https://doi.org/10.1016/j.molcel.2005.09.019

Gandin, V., Masvidal, L., Hulea, L., Gravel, S. P., Cargnello, M., McLaughlan, S., Cai, Y., Balanathan, P., Morita, M., Rajakumar, A., Furic, L., Pollak, M., Porco, J. A., St-Pierre, J., Pelletier, J., Larsson, O., & Topisirovic, I. (2016). NanoCAGE reveals 5' UTR features that define specific modes of translation of functionally related MTOR-sensitive mRNAs. *Genome Research*, *26*(5), 636–648. https://doi.org/10.1101/gr.197566.115

Gatfield, D., & Izaurralde, E. (2004). Nonsense-mediated messenger RNA decay is initiated by endonucleolytic cleavage in Drosophila. *Nature*,

429(6991), 575–578. https://doi.org/10.1038/nature02559

Geballe, A. P., Leach, F. S., & Mocarski, E. S. (1986). Regulation of cytomegalovirus late gene expression: gamma genes are controlled by posttranscriptional events. *Journal of Virology*, *57*(3), 864–874. https://doi.org/10.1128/JVI.57.3.864-874.1986

Gebauer, F., & Hentze, M. W. (2004). Molecular mechanisms of translational control. *Nature Reviews Molecular Cell Biology*, *5*(10), 827–835. https://doi.org/10.1038/nrm1488

Geisberg, J. V., Moqtaderi, Z., Fan, X., Ozsolak, F., & Struhl, K. (2014). Global analysis of mRNA isoform half-lives reveals stabilizing and destabilizing elements in yeast. *Cell*, *156*(4), 812–824. https://doi.org/10.1016/j.cell.2013.12.026

Goddard, T. D., Huang, C. C., Meng, E. C., Pettersen, E. F., Couch, G. S., Morris, J. H., & Ferrin, T. E. (2018). UCSF ChimeraX: Meeting modern challenges in visualization and analysis. *Protein Science*, *27*(1), 14–25. https://doi.org/10.1002/pro.3235

Gogala, M., Becker, T., Beatrix, B., Armache, J.-P., Barrio-Garcia, C., Berninghausen, O., & Beckmann, R. (2014). Structures of the Sec61 complex engaged in nascent peptide translocation or membrane insertion. *Nature*, *506*(7486), 107–110. https://doi.org/10.1038/nature12950

Gong, F., Ito, K., Nakamura, Y., & Yanofsky, C. (2001). The mechanism of tryptophan induction of tryptophanase operon expression: Tryptophan inhibits release factor-mediated cleavage of TnaC-peptidyl-tRNAPro. *Proceedings of the National Academy of Sciences*, *98*(16), 8997–9001. https://doi.org/10.1073/pnas.171299298

Gong, F., & Yanofsky, C. (2002). Instruction of translating Ribosome. *Science*, *297*(September), 1864–1867.

Guo, H., Ingolia, N. T., Weissman, J. S., & Bartel, D. P. (2011). Mammalian microRNAs predominantly act to decrease target mRNA levels. *Nature*, *466*(7308), 835–840. https://doi.org/10.1038/nature09267.Mammalian

Gürel, G., Blaha, G., Moore, P. B., & Steitz, T. A. (2009). U2504 Determines the species specificity of the A-site cleft antibiotics. The structures of Tiamulin, Homoharringtonine and Bruceantin bound to the ribosome.

Journal of Molecular Biology, *389*(1), 146–156. https://doi.org/10.1038/mp.2011.182.doi

Gutierrez, E., Shin, B. S., Woolstenhulme, C. J., Kim, J. R., Saini, P., Buskirk, A. R., & Dever, T. E. (2013). eif5A promotes translation of polyproline motifs. *Molecular Cell*, *51*(1), 35–45. https://doi.org/10.1016/j.molcel.2013.04.021

Guydosh, N. R., & Green, R. (2014). Dom34 rescues ribosomes in 3′ untranslated regions. *Cell*, *156*(5), 950–962. https://doi.org/10.1016/j.cell.2014.02.006

Guydosh, N. R., & Green, R. (2017). Translation of poly (A) tails leads to precise mRNA cleavage and widespread ribosome rescue. *RNA (New York, N.Y.)*, *1*. https://doi.org/10.1261/rna.060418.116

Halbach, F., Reichelt, P., Rode, M., & Conti, E. (2013). The yeast ski complex: Crystal structure and rna channeling to the exosome complex. *Cell*, *154*(4), 814–826. https://doi.org/10.1016/j.cell.2013.07.017

Halbach, F., Rode, M., & Conti, E. (2012). The crystal structure of S. cerevisiae Ski2, a DExH helicase associated with the cytoplasmic functions of the exosome. *Rna*, *18*(1), 124–134. https://doi.org/10.1261/rna.029553.111

Halder, K., Wieland, M., & Hartig, J. S. (2009). Predictable suppression of gene expression by 5'-UTR-based RNA quadruplexes. *Nucleic Acids Research*, *37*(20), 6811–6817. https://doi.org/10.1093/nar/gkp696

Han, J., Back, S. H., Hur, J., Lin, Y.-H., Gildersleeve, R., Shan, J., Yuan, C. L., Krokowski, D., Wang, S., Hatzoglou, M., Kilberg, M. S., Sartor, M. A., & Kaufman, R. J. (2013). ER-stress-induced transcriptional regulation increases protein synthesis leading to cell death. *Nature Cell Biology*, *15*(5), 481–490. https://doi.org/10.1038/ncb2738

Han, P., Mito, M., Shichino, Y., Hashimoto, S., Udagawa, T., Kohno, K., Mishima, Y., Inada, T., & Iwasaki, S. (2019). Genome-wide survey of ribosome collision. *BioRxiv*.

Hansen, J. L., Ippolito, J. A., Ban, N., Nissen, P., Moore, P. B., & Steitz, T. A. (2002). The structures of four macrolide antibiotics bound to the large ribosomal subunit. *Molecular Cell*, *10*(1), 117–128. https://doi.org/10.1016/S1097-2765(02)00570-1

Harding, H P, Zhang, Y., & Ron, D. (1999). Protein translation and folding are coupled by an endoplasmic-reticulum-resident kinase. *Nature*, *397*(6716), 271–274. https://doi.org/10.1038/16729

Harding, Heather P, Zhang, Y., Zeng, H., Novoa, I., Lu, P. D., Calfon, M., Sadri, N., Yun, C., Popko, B., Paules, R., Stojdl, D. F., Bell, J. C., Hettmann, T., Leiden, J. M., & Ron, D. (2003). An integrated stress response regulates amino acid metabolism and resistance to oxidative stress. *Molecular Cell*, *11*(3), 619–633. https://doi.org/10.1016/s1097-2765(03)00105-9

Herb, M., Gluschko, A., Wiegmann, K., Farid, A., Wolf, A., Utermöhlen, O., Krut, O., Krönke, M., & Schramm, M. (2019). Mitochondrial reactive oxygen species enable proinflammatory signaling through disulfide linkage of NEMO. *Science Signaling*, *12*(568). https://doi.org/10.1126/scisignal.aar5926

Hershey, J. W. B., Sonenberg, N., & Mathews, M. B. (2012). Principles of translational control: an overview. *Cold Spring Harbor Perspectives in Biology*, *4*(12). https://doi.org/10.1101/cshperspect.a011528

Hetz, C., Zhang, K., & Kaufman, R. J. (2020). Mechanisms, regulation and functions of the unfolded protein response. *Nature Reviews Molecular Cell Biology*, *21*(8), 421–438. https://doi.org/10.1038/s41580-020-0250-z

HH, L., YS, K., KH, K., Heo, I., SK, K., Kim, O., HK, K., JY, Y., HS, K., DJ, K., SJ, L., HJ, Y., SJ, K., BG, L., HK, S., VN, K., CM, P., & SW, S. (2007). Structural and functional insights into Dom34, a key component of no-go mRNA decay. *Molecular Cell*, *27*(6), 938–950.

Hinnebusch, A. G., & Lorsch, J. R. (2012). The mechanism of eukaryotic translation initiation: New insights and challenges. *Cold Spring Harbor Perspectives in Biology*, *4*(10). https://doi.org/10.1101/cshperspect.a011544

Hogg, J. R., & Goff, S. P. (2010). Upf1 senses 3'UTR length to potentiate mRNA decay. *Cell*, *143*(3), 379–389. https://doi.org/10.1016/j.cell.2010.10.005

Hsu, C. L., & Stevens, A. (1993). Yeast cells lacking 5'-->3' exoribonuclease 1 contain mRNA species that are poly(A) deficient and partially lack the 5' cap structure. *Molecular and Cellular Biology*, *13*(8), 4826–4835.

https://doi.org/10.1128/mcb.13.8.4826-4835.1993

Hsu, F. J., Benike, C., Fagnoni, F., Liles, T. M., Czerwinski, D., Taidi, B., Engleman, E. G., & Levy, R. (1996). Vaccination of patients with B–cell lymphoma using autologous antigen–pulsed dendritic cells. *Nature Medicine*, *2*(1), 52–58. https://doi.org/10.1038/nm0196-52

Hu, W., Sweet, T. J., Chamnongpol, S., Baker, K. E., & Coller, J. (2009). Co-translational mRNA decay in Saccharomyces cerevisiae. *Nature*, *461*(7261), 225–229. https://doi.org/10.1038/nature08265

Hubo, M., Trinschek, B., Kryczanowsky, F., Tuettenberg, A., Steinbrink, K., & Jonuleit, H. (2013). Costimulatory molecules on immunogenic versus tolerogenic human dendritic cells. *Frontiers in Immunology*, *4*(APR). https://doi.org/10.3389/fimmu.2013.00082

Huch, S., & Nissan, T. (2014). Interrelations between translation and general mRNA degradation in yeast. *Wiley Interdisciplinary Reviews. RNA*, *5*. https://doi.org/10.1002/wrna.1244

Huter, P., Arenz, S., Bock, L. V., Graf, M., Frister, J. O., Heuer, A., Peil, L., Starosta, A. L., Wohlgemuth, I., Peske, F., Nováček, J., Berninghausen, O., Grubmüller, H., Tenson, T., Beckmann, R., Rodnina, M. V., Vaiana, A. C., & Wilson, D. N. (2017). Structural Basis for Polyproline-Mediated Ribosome Stalling and Rescue by the Translation Elongation Factor EF-P. *Molecular Cell*, *68*(3), 515-527.e6. https://doi.org/10.1016/j.molcel.2017.10.014

Ikeuchi, K., Tesina, P., Matsuo, Y., Sugiyama, T., Cheng, J., Saeki, Y., Tanaka, K., Becker, T., Beckmann, R., & Inada, T. (2019). Collided ribosomes form a unique structural interface to induce Hel2-driven quality control pathways. *The EMBO Journal*, *38*(5). https://doi.org/10.15252/embj.2018100276

Inada, T., & Aiba, H. (2005). Translation of aberrant mRNAs lacking a termination codon or with a shortened 3′-UTR is repressed after initiation in yeast. *EMBO Journal*, *24*(8), 1584–1595. https://doi.org/10.1038/sj.emboj.7600636

Ingolia, N. T., Brar, G. A., Rouskin, S., McGeachy, A. M., & Weissman, J. S. (2012). The ribosome profiling strategy for monitoring translation in vivo by deep sequencing of ribosome-protected mRNA fragments. *Nature*

Protocols, *7*(8), 1534–1550. https://doi.org/10.1038/nprot.2012.086

Ingolia, N. T., Brar, G. A., Stern-Ginossar, N., Harris, M. S., Talhouarne, G. J. S., Jackson, S. E., Wills, M. R., & Weissman, J. S. (2014). Ribosome Profiling Reveals Pervasive Translation Outside of Annotated Protein-Coding Genes. *Cell Reports*, *8*(5), 1365–1379. https://doi.org/10.1016/j.celrep.2014.07.045

Ingolia, N. T., Ghaemmaghami, S., Newman, J. R., & Weissman, J. S. (2009). Genome-wide analysis of in vivo of translation with nucleotide resolution using ribosome profiling. *Science*, *324*(5924), 218–223. https://doi.org/10.1126/science.1168978.Genome-Wide

Ingolia, N. T., Lareau, L., & Weissman, J. (2011). Ribosome Profiling of Mouse Embryonic Stem Cells Reveales Complexity of Mammalian Proteomes. *Cell*, *147*(4), 789–802. https://doi.org/10.1016/j.cell.2011.10.002.Ribosome

Irigoyen, N., Dinan, A. M., Brierley, I., & Firth, A. E. (2018). Ribosome profiling of the retrovirus murine leukemia virus. *Retrovirology*, *15*(1), 10. https://doi.org/10.1186/s12977-018-0394-5

Ishii, E., Chiba, S., Hashimoto, N., Kojima, S., Homma, M., Ito, K., Akiyama, Y., & Mori, H. (2015). Nascent chain-monitored remodeling of the Sec machinery for salinity adaptation of marine bacteria. *Proceedings of the National Academy of Sciences*, *112*(40), E5513–E5522. https://doi.org/10.1073/pnas.1513001112

Ismail, N., Hedman, R., Schiller, N., & von Heijne, G. (2012). A biphasic pulling force acts on transmembrane helices during translocon-mediated membrane integration. *Nature Structural & Molecular Biology*, *19*(10), 1018–1022. https://doi.org/10.1038/nsmb.2376

Ito-Harashima, S., Kuroha, K., Tatematsu, T., & Inada, T. (2007). Translation of the poly(A) tail plays crucial roles in nonstop mRNA surveillance via translation repression and protein destabilization by proteasome in yeast. *Genes and Development*, *21*(5), 519–524. https://doi.org/10.1101/gad.1490207

Ito, K., & Chiba, S. (2013). Arrest Peptides: Cis-Acting Modulators of Translation. *Annual Review of Biochemistry*, *82*(1), 171–202. https://doi.org/10.1146/annurev-biochem-080211-105026

Jackson, R. J. (2013). The current status of vertebrate cellular mRNA IRESs. *Cold Spring Harbor Perspectives in Biology*, *5*(2). https://doi.org/10.1101/cshperspect.a011569

Jackson, R. J., Hellen, C. U. T., & Pestova, T. V. (2010). The mechanism of eukaryotic translation initiation and principles of its regulation. *Nature Reviews Molecular Cell Biology*, *11*(2), 113–127. https://doi.org/10.1038/nrm2838

Jacquemyn, J., Cascalho, A., & Goodchild, R. E. (2017). The ins and outs of endoplasmic reticulum-controlled lipid biosynthesis. *EMBO Reports*, *18*(11), 1905–1921. https://doi.org/10.15252/embr.201643426

Janzen, D. M., Frolova, L., & Geballe, A. P. (2002). Inhibition of Translation Termination Mediated by an Interaction of Eukaryotic Release Factor 1 with a Nascent Peptidyl-tRNA. *Molecular and Cellular Biology*, *22*(24), 8562–8570. https://doi.org/10.1128/mcb.22.24.8562-8570.2002

Johansson, M., Ieong, K.-W., Trobro, S., Strazewski, P., Åqvist, J., Pavlov, M. Y., & Ehrenberg, M. (2011). pH-sensitivity of the ribosomal peptidyl transfer reaction dependent on the identity of the A-site aminoacyl-tRNA. *Proceedings of the National Academy of Sciences*, *108*(1), 79 LP – 84. https://doi.org/10.1073/pnas.1012612107

Jovanovic, M., Rooney, M. S., Mertins, P., Przybylski, D., Chevrier, N., Satija, R., Rodriguez, E. H., Fields, A. P., Schwartz, S., Raychowdhury, R., Mumbach, M. R., Eisenhaure, T., Rabani, M., Gennert, D., Lu, D., Delorey, T., Weissman, J. S., Carr, S. A., Hacohen, N., & Regev, A. (2015). Dynamic profiling of the protein life cycle in response to pathogens. *Science*, *6*(3476226), 1–16. https://doi.org/10.1126/science.1259038

K., D. L., Ingo, W., Christina, K., Frank, P., Henning, U., & V., R. M. (2013). EF-P Is Essential for Rapid Synthesis of Proteins Containing Consecutive Proline Residues. *Science*, *339*(6115), 85–88. https://doi.org/10.1126/science.1229017

Kanda, S., Yanagitani, K., Yokota, Y., Esaki, Y., & Kohno, K. (2016). Autonomous translational pausing is required for XBP1u mRNA recruitment to the ER via the SRP pathway. *Proceedings of the National Academy of Sciences of the United States of America*, *113*(40), E5886–

E5895. https://doi.org/10.1073/pnas.1604435113

Kasari, V., Margus, T., Atkinson, G. C., Johansson, M. J. O., & Hauryliuk, V. (2019). Ribosome profiling analysis of eEF3-depleted Saccharomyces cerevisiae. *Scientific Reports*, *9*(1), 3037. https://doi.org/10.1038/s41598-019-39403-y

Kashima, I., Yamashita, A., Izumi, N., Kataoka, N., Morishita, R., Hoshino, S., Ohno, M., Dreyfuss, G., & Ohno, S. (2006). Binding of a novel SMG-1-Upf1-eRF1-eRF3 complex (SURF) to the exon junction complex triggers Upf1 phosphorylation and nonsense-mediated mRNA decay. *Genes & Development*, *20*(3), 355–367. https://doi.org/10.1101/gad.1389006

Kaufman, R. J. (2002). Orchestrating the unfolded protein response in health and disease. *The Journal of Clinical Investigation*, *110*(10), 1389–1398. https://doi.org/10.1172/JCI16886

Kim, D., Pertea, G., Trapnell, C., Pimentel, H., Kelley, R., & Salzberg, S. L. (2013). TopHat2: accurate alignment of transcriptomes in the presence of insertions, deletions and gene fusions. *Genome Biology*, *14*(4), R36. https://doi.org/10.1186/gb-2013-14-4-r36

Kimanius, D., Forsberg, B. O., Scheres, S. H. W., & Lindahl, E. (2016). Accelerated cryo-EM structure determination with parallelisation using GPUs in RELION-2. *ELife*, *5*(NOVEMBER2016), 1–21. https://doi.org/10.7554/eLife.18722

Kontoyiannis, D., Pasparakis, M., Pizarro, T. T., Cominelli, F., & Kollias, G. (1999). Impaired on/off regulation of TNF biosynthesis in mice lacking TNF AU-rich elements: implications for joint and gut-associated immunopathologies. *Immunity*, *10*(3), 387–398. https://doi.org/10.1016/s1074-7613(00)80038-2

Koutmou, K. S., Schuller, A. P., Brunelle, J. L., Radhakrishnan, A., Djuranovic, S., & Green, R. (2015). Ribosomes slide on lysine-encoding homopolymeric A stretches. *ELife*, *2015*(4), 1–18. https://doi.org/10.7554/eLife.05534

Kozak, M. (1986). Point mutations define a sequence flanking the AUG initiator codon that modulates translation by eukaryotic ribosomes. *Cell*, *44*(2), 283–292. https://doi.org/10.1016/0092-8674(86)90762-2

Krawczyk, C. M., Holowka, T., Sun, J., Blagih, J., Amiel, E., DeBerardinis, R.

J., Cross, J. R., Jung, E., Thompson, C. B., Jones, R. G., & Pearce, E. J. (2010). Toll-like receptor-induced changes in glycolytic metabolism regulate dendritic cell activation. *Blood*, *115*(23), 4742–4749. https://doi.org/10.1182/blood-2009-10-249540

Kumari, S., Bugaut, A., & Balasubramanian, S. (2008). Position and stability are determining factors for translation repression by an RNA G-quadruplex-forming sequence within the 5' UTR of the NRAS proto-oncogene. *Biochemistry*, *47*(48), 12664–12669. https://doi.org/10.1021/bi8010797

Kuroha, K., Akamatsu, M., Dimitrova, L., Ito, T., Kato, Y., Shirahige, K., & Inada, T. (2010). Receptor for activated C kinase 1 stimulates nascent polypeptide-dependent translation arrest. *EMBO Reports*, *11*(12), 956–961.

Laplante, M., & Sabatini, D. M. (2012). mTOR Signaling in Growth Control and Disease. *Cell*, *149*(2), 274–293. https://doi.org/https://doi.org/10.1016/j.cell.2012.03.017

Law, G. L., Raney, A., Heusner, C., & Morris, D. R. (2001). Polyamine Regulation of Ribosome Pausing at the Upstream Open Reading Frame of S-Adenosylmethionine Decarboxylase. *Journal of Biological Chemistry*, *276*(41), 38036–38043. https://doi.org/10.1074/jbc.m105944200

Le Hir, H., Izaurralde, E., Maquat, L. E., & Moore, M. J. (2000). The spliceosome deposits multiple proteins 20-24 nucleotides upstream of mRNA exon-exon junctions. *The EMBO Journal*, *19*(24), 6860–6869. https://doi.org/10.1093/emboj/19.24.6860

Lebedeva, S., Jens, M., Theil, K., Schwanhäusser, B., Selbach, M., Landthaler, M., & Rajewsky, N. (2011). Transcriptome-wide analysis of regulatory interactions of the RNA-binding protein HuR. *Molecular Cell*, *43*(3), 340–352. https://doi.org/10.1016/j.molcel.2011.06.008

Lee, S. R., Pratt, G. A., Martinez, F. J., Yeo, G. W., & Lykke-Andersen, J. (2015). Target Discrimination in Nonsense-Mediated mRNA Decay Requires Upf1 ATPase Activity. *Molecular Cell*, *59*(3), 413–425. https://doi.org/10.1016/j.molcel.2015.06.036

Lelouard, H., Schmidt, E. K., Camosseto, V., Clavarino, G., Ceppi, M., Hsu, H. T., & Pierre, P. (2007). Regulation of translation is required for dendritic

cell function and survival during activation. *Journal of Cell Biology*, *179*(7), 1427–1439. https://doi.org/10.1083/jcb.200707166

Leppek, K., Das, R., & Barna, M. (2018). Functional 5′ UTR mRNA structures in eukaryotic translation regulation and how to find them. *Nature Reviews Molecular Cell Biology*, *19*(3), 158–174. https://doi.org/10.1038/nrm.2017.103

Li, G.-W., Oh, E., & Weissman, J. S. (2012). The anti-Shine–Dalgarno sequence drives translational pausing and codon choice in bacteria. *Nature*, *484*(7395), 538–541. https://doi.org/10.1038/nature10965

Lichtenegger, F. S., Mueller, K., Otte, B., Beck, B., Hiddemann, W., Schendel, D. J., & Subklewe, M. (2012). CD86 and IL-12p70 Are Key Players for T Helper 1 Polarization and Natural Killer Cell Activation by Toll-Like Receptor-Induced Dendritic Cells. *PLoS ONE*, *7*(9), 1–9. https://doi.org/10.1371/journal.pone.0044266

Liu, Q., Greimann, J. C., & Lima, C. D. (2006). Reconstitution, activities, and structure of the eukaryotic RNA exosome. *Cell*, *127*(6), 1223–1237. https://doi.org/10.1016/j.cell.2006.10.037

Loewith, R., Jacinto, E., Wullschleger, S., Lorberg, A., Crespo, J. L., Bonenfant, D., Oppliger, W., Jenoe, P., & Hall, M. N. (2002). Two TOR complexes, only one of which is rapamycin sensitive, have distinct roles in cell growth control. *Molecular Cell*, *10*(3), 457–468. https://doi.org/10.1016/s1097-2765(02)00636-6

Love, M. I., Huber, W., & Anders, S. (2014). Moderated estimation of fold change and dispersion for RNA-seq data with DESeq2. *Genome Biology*, *15*(12), 550. https://doi.org/10.1186/s13059-014-0550-8

Lu, J., & Deutsch, C. (2008). Electrostatics in the Ribosomal Tunnel Modulate Chain Elongation Rates. *Journal of Molecular Biology*, *384*(1), 73–86. https://doi.org/https://doi.org/10.1016/j.jmb.2008.08.089

Lu, P. D., Harding, H. P., & Ron, D. (2004). Translation reinitiation at alternative open reading frames regulates gene expression in an integrated stress response. *The Journal of Cell Biology*, *167*(1), 27–33. https://doi.org/10.1083/jcb.200408003

Lykke-Andersen, J., & Wagner, E. (2005). Recruitment and activation of mRNA decay enzymes by two ARE-mediated decay activation domains

in the proteins TTP and BRF-1. *Genes & Development*, *19*(3), 351–361. https://doi.org/10.1101/gad.1282305

Lynch, M., Scofield, D. G., & Hong, X. (2005). The Evolution of Transcription-Initiation Sites. *Molecular Biology and Evolution*, *22*(4), 1137–1146. https://doi.org/10.1093/molbev/msi100

Ma, X. M., & Blenis, J. (2009). Molecular mechanisms of mTOR-mediated translational control. *Nature Reviews Molecular Cell Biology*, *10*(5), 307–318. https://doi.org/10.1038/nrm2672

Makino, D. L., Baumgärtner, M., & Conti, E. (2013). Crystal structure of an RNA-bound 11-subunit eukaryotic exosome complex. *Nature*, *495*(7439), 70–75. https://doi.org/10.1038/nature11870

Maquat, L. E. (2002). Molecular biology. Skiing toward nonstop mRNA decay. *Science (New York, N.Y.)*, *295*(5563), 2221–2222. https://doi.org/10.1126/science.1071285

Maquat, L. E., Tarn, W.-Y., & Isken, O. (2010). The pioneer round of translation: features and functions. *Cell*, *142*(3), 368–374. https://doi.org/10.1016/j.cell.2010.07.022

Martin, M. (2011). Cutadapt removes adapter sequences from high-throughput sequencing reads. *EMBnet.Journal*, *17*, 10–12.

Martin Schmeing, T., Huang, K. S., Strobel, S. A., & Steitz, T. A. (2005). An induced-fit mechanism to promote peptide bond formation and exclude hydrolysis of peptidyl-tRNA. *Nature*, *438*(7067), 520–524. https://doi.org/10.1038/nature04152

Martínez, A. K., Gordon, E., Sengupta, A., Shirole, N., Klepacki, D., Martinez-Garriga, B., Brown, L. M., Benedik, M., Yanofsky, C., Mankin, A. S., Vazquez-Laslop, N., Sachs, M. S., & Cruz-Vera, L. R. (2014). Interactions of the TnaC nascent peptide with rRNA in the exit tunnel enable the ribosome to respond to free tryptophan. *Nucleic Acids Research*, *42*(2), 1245–1256. https://doi.org/10.1093/nar/gkt923

Matheisl, S., Berninghausen, O., Becker, T., & Beckmann, R. (2015). Structure of a human translation termination complex. *Nucleic Acids Research*, *43*(18), 8615–8626. https://doi.org/10.1093/nar/gkv909

Matsuo, Y., Ikeuchi, K., Saeki, Y., Iwasaki, S., Schmidt, C., Udagawa, T., Sato, F., Tsuchiya, H., Becker, T., Tanaka, K., Ingolia, N. T., Beckmann,

R., & Inada, T. (2017). Ubiquitination of stalled ribosome triggers ribosome-associated quality control. *Nature Communications*, *8*(1), 159. https://doi.org/10.1038/s41467-017-00188-1

Mayr, C. (2019). What are 3′ utrs doing? *Cold Spring Harbor Perspectives in Biology*, *11*(10). https://doi.org/10.1101/cshperspect.a034728

Mellman, I., & Steinman, R. M. (2001). Dendritic cells: specialized and regulated antigen processing machines. *Cell*, *106*(3), 255–258. https://doi.org/10.1016/s0092-8674(01)00449-4

Merchante, C., Brumos, J., Yun, J., Hu, Q., Spencer, K. R., Enríquez, P., Binder, B. M., Heber, S., Stepanova, A. N., & Alonso, J. M. (2015). Gene-specific translation regulation mediated by the hormone-signaling molecule EIN2. *Cell*, *163*(3), 684–697. https://doi.org/10.1016/j.cell.2015.09.036

Mignone, F., Gissi, C., Liuni, S., & Pesole, G. (2002). Untranslated regions of mRNAs. *Genome Biology*, *3*(3), reviews0004.1. https://doi.org/10.1186/gb-2002-3-3-reviews0004

Mills, E. W., Wangen, J., Green, R., & Ingolia, N. T. (2016). Dynamic Regulation of a Ribosome Rescue Pathway in Erythroid Cells and Platelets. *Cell Reports*, *17*(1), 1–10. https://doi.org/10.1016/j.celrep.2016.08.088

Mori, K. (2009). Signalling pathways in the unfolded protein response: Development from yeast to mammals. *Journal of Biochemistry*, *146*(6), 743–750. https://doi.org/10.1093/jb/mvp166

Muhlrad, D., & Parker, R. (1994). Premature translational termination triggers mRNA decapping. *Nature*, *370*(6490), 578–581. https://doi.org/10.1038/370578a0

Murshudov, G. N., Skubák, P., Lebedev, A. A., Pannu, N. S., Steiner, R. A., Nicholls, R. A., Winn, M. D., Long, F., & Vagin, A. A. (2011). REFMAC5 for the refinement of macromolecular crystal structures. *Acta Crystallographica Section D: Biological Crystallography*, *67*(4), 355–367. https://doi.org/10.1107/S0907444911001314

Muto, H., & Ito, K. (2008). Peptidyl-prolyl-tRNA at the ribosomal P-site reacts poorly with puromycin. *Biochemical and Biophysical Research Communications*, *366*(4), 1043–1047.

https://doi.org/https://doi.org/10.1016/j.bbrc.2007.12.072

Oh, E., Becker, A. H., Sandikci, A., Huber, D., Chaba, R., Gloge, F., Nichols, R. J., Typas, A., Gross, C. A., Kramer, G., Weissman, J. S., & Bukau, B. (2011). Selective ribosome profiling reveals the cotranslational chaperone action of trigger factor in vivo. *Cell*, *147*(6), 1295–1308. https://doi.org/10.1016/j.cell.2011.10.044

Okamura, K., Kimata, Y., Higashio, H., Tsuru, A., & Kohno, K. (2000). Dissociation of Kar2p/BiP from an ER Sensory Molecule, Ire1p, Triggers the Unfolded Protein Response in Yeast. *Biochemical and Biophysical Research Communications*, *279*(2), 445–450. https://doi.org/https://doi.org/10.1006/bbrc.2000.3987

Ozsolak, F., Kapranov, P., Foissac, S., Kim, S. W., Fishilevich, E., Monaghan, A. P., John, B., & Milos, P. M. (2010). Comprehensive polyadenylation site maps in yeast and human reveal pervasive alternative polyadenylation. *Cell*, *143*(6), 1018–1029. https://doi.org/10.1016/j.cell.2010.11.020

Parker, R. (2012). RNA degradation in Saccharomyces cerevisae. *Genetics*, *191*(3), 671–702. https://doi.org/10.1534/genetics.111.137265

Pavlov, M. Y., Watts, R. E., Tan, Z., Cornish, V. W., Ehrenberg, M., & Forster, A. C. (2009). Slow peptide bond formation by proline and other N-alkylamino acids in translation. *Proceedings of the National Academy of Sciences*, *106*(1), 50 LP – 54. https://doi.org/10.1073/pnas.0809211106

Pearce, E. J., & Everts, B. (2015). Dendritic cell metabolism. *Nature Reviews Immunology*, *15*(1), 18–29. https://doi.org/10.1038/nri3771

Pechmann, S., Chartron, J. W., & Frydman, J. (2014). Local slowdown of translation by nonoptimal codons promotes nascent-chain recognition by SRP in vivo. *Nature Structural & Molecular Biology*, *21*(12), 1100–1105. https://doi.org/10.1038/nsmb.2919

Pelechano, V., Wei, W., & Steinmetz, L. M. (2015). Widespread co-translational RNA decay reveals ribosome dynamics. *Cell*, *161*(6), 1400–1412. https://doi.org/10.1016/j.cell.2015.05.008

Pesole, G., Mignone, F., Gissi, C., Grillo, G., Licciulli, F., & Liuni, S. (2001). Structural and functional features of eukaryotic mRNA untranslated

regions. *Gene*, *276*(1), 73–81. https://doi.org/https://doi.org/10.1016/S0378-1119(01)00674-6

Pettersen, E. F., Goddard, T. D., Huang, C. C., Couch, G. S., Greenblatt, D. M., Meng, E. C., & Ferrin, T. E. (2004). UCSF Chimera - A visualization system for exploratory research and analysis. *Journal of Computational Chemistry*, *25*(13), 1605–1612. https://doi.org/10.1002/jcc.20084

Pisarev, A. V, Hellen, C. U. T., & Pestova, T. V. (2007). Recycling of eukaryotic posttermination ribosomal complexes. *Cell*, *131*(2), 286–299. https://doi.org/10.1016/j.cell.2007.08.041

Plumb, R., Zhang, Z. R., Appathurai, S., & Mariappan, M. (2015). A functional link between the co-translational protein translocation pathway and the UPR. *ELife*, *4*(MAY), 2–27. https://doi.org/10.7554/eLife.07426

Preis, A., Heuer, A., Barrio-Garcia, C., Hauser, A., Eyler, D. E., Berninghausen, O., Green, R., Becker, T., & Beckmann, R. (2014). Cryoelectron microscopic structures of eukaryotic translation termination complexes containing eRF1-eRF3 or eRF1-ABCE1. *Cell Reports*, *8*(1), 59–65. https://doi.org/10.1016/j.celrep.2014.04.058

Presnyak, V., Alhusaini, N., Chen, Y. H., Martin, S., Morris, N., Kline, N., Olson, S., Weinberg, D., Baker, K. E., Graveley, B. R., & Coller, J. (2015). Codon optimality is a major determinant of mRNA stability. *Cell*, *160*(6), 1111–1124. https://doi.org/10.1016/j.cell.2015.02.029

Radhakrishnan, A., Chen, Y. H., Martin, S., Alhusaini, N., Green, R., & Coller, J. (2016). The DEAD-Box Protein Dhh1p Couples mRNA Decay and Translation by Monitoring Codon Optimality. *Cell*, *167*(1), 122-132.e9. https://doi.org/10.1016/j.cell.2016.08.053

Raghavan, A., Ogilvie, R. L., Reilly, C., Abelson, M. L., Raghavan, S., Vasdewani, J., Krathwohl, M., & Bohjanen, P. R. (2002). Genome-wide analysis of mRNA decay in resting and activated primary human T lymphocytes. *Nucleic Acids Research*, *30*(24), 5529–5538. https://doi.org/10.1093/nar/gkf682

Raney, A., Law, G. L., Mize, G. J., & Morris, D. R. (2002). Regulated translation termination at the upstream open reading frame in s-adenosylmethionine decarboxylase mRNA. *The Journal of Biological Chemistry*, *277*(8), 5988–5994. https://doi.org/10.1074/jbc.M108375200

Raney, A., Lynn Law, G., Mize, G. J., & Morris, D. R. (2002). Regulated translation termination at the upstream open reading frame in S-adenosylmethionine decarboxylase mRNA. *Journal of Biological Chemistry*, *277*(8), 5988–5994. https://doi.org/10.1074/jbc.M108375200

Rolfe, D. F., & Brown, G. C. (1997). Cellular energy utilization and molecular origin of standard metabolic rate in mammals. *Physiological Reviews*, *77*(3), 731–758. https://doi.org/10.1152/physrev.1997.77.3.731

Ron, D., & Walter, P. (2007). Signal integration in the endoplasmic reticulum unfolded protein response. *Nature Reviews. Molecular Cell Biology*, *8*(7), 519–529. https://doi.org/10.1038/nrm2199

Roy, R. N., Lomakin, I. B., Gagnon, M. G., & Steitz, T. A. (2015). The mechanism of inhibition of protein synthesis by the proline-rich peptide oncocin. *Nature Structural & Molecular Biology*, *22*(6), 466–469. https://doi.org/10.1038/nsmb.3031

Saito, S., Hosoda, N., & Hoshino, S. (2013). The Hbs1-Dom34 Protein Complex Functions in Non-stop mRNA Decay in Mammalian Cells*. *Journal of Biological Chemistry*, *288*(24), 17832–17843. https://doi.org/https://doi.org/10.1074/jbc.M112.448977

Sallusto, F., & Lanzavecchia, A. (2000). Understanding dendritic cell and T-lymphocyte traffic through the analysis of chemokine receptor expression. *Immunological Reviews*, *177*, 134–140. https://doi.org/10.1034/j.1600-065x.2000.17717.x

Schaeuble, K., Hauser, M. A., Rippl, A. V, Bruderer, R., Otero, C., Groettrup, M., & Legler, D. F. (2012). Ubiquitylation of the chemokine receptor CCR7 enables efficient receptor recycling and cell migration. *Journal of Cell Science*, *125*(19), 4463–4474. https://doi.org/10.1242/jcs.097519

Schibich, D., Gloge, F., Pöhner, I., Björkholm, P., Wade, R. C., von Heijne, G., Bukau, B., & Kramer, G. (2016). Global profiling of SRP interaction with nascent polypeptides. *Nature*, *536*(7615), 219–223. https://doi.org/10.1038/nature19070

Schmidt, C., Becker, T., Heuer, A., Braunger, K., Shanmuganathan, V., Pech, M., Berninghausen, O., Wilson, D. N., & Beckmann, R. (2015). Structure of the hypusinylated eukaryotic translation factor eIF-5A bound to the ribosome. *Nucleic Acids Research*, *44*(4), 1944–1951.

https://doi.org/10.1093/nar/gkv1517

Schmidt, C., Kowalinski, E., Shanmuganathan, V., Defenouillère, Q., Braunger, K., Heuer, A., Pech, M., Namane, A., Berninghausen, O., Fromont-Racine, M., Jacquier, A., Conti, E., Becker, T., & Beckmann, R. (2016). The cryo-EM structure of a ribosome-Ski2-Ski3-Ski8 helicase complex. *Science*, *354*(6318), 1431–1433. https://doi.org/10.1126/science.aaf7520

Schuller, A. P., & Green, R. (2018). Roadblocks and resolutions in eukaryotic translation. *Nature Reviews Molecular Cell Biology*, *19*(8), 526–541. https://doi.org/10.1038/s41580-018-0011-4

Schwarz, D. S., & Blower, M. D. (2016). The endoplasmic reticulum: structure, function and response to cellular signaling. *Cellular and Molecular Life Sciences : CMLS*, *73*(1), 79–94. https://doi.org/10.1007/s00018-015-2052-6

Seefeldt, A. C., Nguyen, F., Antunes, S., Pérébaskine, N., Graf, M., Arenz, S., Inampudi, K. K., Douat, C., Guichard, G., Wilson, D. N., & Innis, C. A. (2015). The proline-rich antimicrobial peptide Onc112 inhibits translation by blocking and destabilizing the initiation complex. *Nature Structural & Molecular Biology*, *22*(6), 470–475. https://doi.org/10.1038/nsmb.3034

Segura, E., & Amigorena, S. (2013). Inflammatory dendritic cells in mice and humans. *Trends in Immunology*, *34*(9), 440–445. https://doi.org/https://doi.org/10.1016/j.it.2013.06.001

Sen, N. D., Zhou, F., Ingolia, N. T., & Hinnebusch, A. G. (2015). Genome-wide analysis of translational efficiency reveals distinct but overlapping functions of yeast DEAD-box RNA helicases Ded1 and eIF4A. *Genome Research*, *25*(8), 1196–1205. https://doi.org/10.1101/gr.191601.115

Shaffer, A. L., Shapiro-Shelef, M., Iwakoshi, N. N., Lee, A.-H., Qian, S.-B., Zhao, H., Yu, X., Yang, L., Tan, B. K., Rosenwald, A., Hurt, E. M., Petroulakis, E., Sonenberg, N., Yewdell, J. W., Calame, K., Glimcher, L. H., & Staudt, L. M. (2004). XBP1, Downstream of Blimp-1, Expands the Secretory Apparatus and Other Organelles, and Increases Protein Synthesis in Plasma Cell Differentiation. *Immunity*, *21*(1), 81–93. https://doi.org/10.1016/j.immuni.2004.06.010

Shanmuganathan, V., Schiller, N., Magoulopoulou, A., Cheng, J., Braunger,

K., Cymer, F., Berninghausen, O., Beatrix, B., Kohno, K., von Heijne, G., & Beckmann, R. (2019). Structural and mutational analysis of the ribosome-arresting human XBP1u. *ELife*, *8*, 1–22. https://doi.org/10.7554/ELIFE.46267

Shao, S., Murray, J., Brown, A., Taunton, J., Ramakrishnan, V., & Hegde, R. S. (2016). Decoding Mammalian Ribosome-mRNA States by Translational GTPase Complexes. *Cell*, *167*(5), 1229-1240.e15. https://doi.org/10.1016/j.cell.2016.10.046

Sheth, U., & Parker, R. (2003). Decapping and decay of messenger RNA occur in cytoplasmic processing bodies. *Science (New York, N.Y.)*, *300*(5620), 805–808. https://doi.org/10.1126/science.1082320

Shoemaker, C. J., & Green, R. (2012). Translation drives mRNA quality control " Nonsense-mediated decay (NMD) ." *Nature Structural & Molecular Biology*, *19*(6), 594–601. https://doi.org/10.1038/nsmb.2301.Translation

Sohmen, D., Chiba, S., Shimokawa-Chiba, N., Innis, C. A., Berninghausen, O., Beckmann, R., Ito, K., & Wilson, D. N. (2015). Structure of the Bacillus subtilis 70S ribosome reveals the basis for species-specific stalling. *Nature Communications*, *6*, 6941. https://doi.org/10.1038/ncomms7941

Song, H., Mugnier, P., Das, A. K., Webb, H. M., Evans, D. R., Tuite, M. F., Hemmings, B. A., & Barford, D. (2000). The crystal structure of human eukaryotic release factor eRF1--mechanism of stop codon recognition and peptidyl-tRNA hydrolysis. *Cell*, *100*(3), 311–321. https://doi.org/10.1016/s0092-8674(00)80667-4

Spevak, C. C., Ivanov, I. P., & Sachs, M. S. (2010). Sequence Requirements for Ribosome Stalling by the Arginine Attenuator Peptide*. *Journal of Biological Chemistry*, *285*(52), 40933–40942. https://doi.org/https://doi.org/10.1074/jbc.M110.164152

Sriburi, R., Jackowski, S., Mori, K., & Brewer, J. W. (2004). XBP1. *The Journal of Cell Biology*, *167*(1), 35–41. https://doi.org/10.1083/jcb.200406136

Steitz, J. A. (1969). Polypeptide chain initiation: nucleotide sequences of the three ribosomal binding sites in bacteriophage R17 RNA. *Nature*,

224(5223), 957–964. https://doi.org/10.1038/224957a0

Stern-Ginossar, N., Weisburd, B., Michalski, A., Le, V. T. K., Hein, M. Y., Huang, S. X., Ma, M., Shen, B., Qian, S. B., Hengel, H., Mann, M., Ingolia, N. T., & Weissman, J. S. (2012). Decoding human cytomegalovirus. *Science*, *338*(6110), 1088–1093. https://doi.org/10.1126/science.1227919

Su, T., Cheng, J., Sohmen, D., Hedman, R., Berninghausen, O., von Heijne, G., Wilson, D. N., & Beckmann, R. (2017). The force-sensing peptide VemP employs extreme compaction and secondary structure formation to induce ribosomal stalling. *ELife*, *6*, 1–17. https://doi.org/10.7554/eLife.25642

Susanne, U., Jürgen, L., L., S. A., Tobias, K., N., W. D., & Kirsten, J. (2013). Translation Elongation Factor EF-P Alleviates Ribosome Stalling at Polyproline Stretches. *Science*, *339*(6115), 82–85. https://doi.org/10.1126/science.1228985

Svidritskiy, E., Brilot, A. F., Koh, C. S., Grigorieff, N., & Korostelev, A. A. (2014). Structures of yeast 80S ribosome-tRNA complexes in the rotated and nonrotated conformations. *Structure*, *22*(8), 1210–1218. https://doi.org/10.1016/j.str.2014.06.003

Synowsky, S. A., & Heck, A. J. R. (2008). The yeast Ski complex is a hetero-tetramer. *Protein Science : A Publication of the Protein Society*, *17*(1), 119–125. https://doi.org/10.1110/ps.073155908

Tanner, D. R., Cariello, D. A., Woolstenhulme, C. J., Broadbent, M. A., & Buskirk, A. R. (2009). Genetic identification of nascent peptides that induce ribosome stalling. *Journal of Biological Chemistry*, *284*(50), 34809–34818. https://doi.org/10.1074/jbc.M109.039040

Tesina, P., Heckel, E., Cheng, J., Fromont-Racine, M., Buschauer, R., Kater, L., Beatrix, B., Berninghausen, O., Jacquier, A., Becker, T., & Beckmann, R. (2019). Structure of the 80S ribosome–Xrn1 nuclease complex. *Nature Structural and Molecular Biology*, *26*(4), 275–280. https://doi.org/10.1038/s41594-019-0202-5

Tesina, P., Lessen, L. N., Buschauer, R., Cheng, J., Wu, C. C.-C., Berninghausen, O., Buskirk, A. R., Becker, T., Beckmann, R., & Green, R. (2020). Molecular mechanism of translational stalling by inhibitory

codon combinations and poly(A) tracts. *The EMBO Journal*, *39*(3), e103365. https://doi.org/10.15252/embj.2019103365

Tharun, S., & Parker, R. (2001). Targeting an mRNA for decapping: displacement of translation factors and association of the Lsm1p-7p complex on deadenylated yeast mRNAs. *Molecular Cell*, *8*(5), 1075–1083. https://doi.org/10.1016/s1097-2765(01)00395-1

Thorvaldsdóttir, H., Robinson, J. T., & Mesirov, J. P. (2013). Integrative Genomics Viewer (IGV): High-performance genomics data visualization and exploration. *Briefings in Bioinformatics*, *14*(2), 178–192. https://doi.org/10.1093/bib/bbs017

Tsai, A., Kornberg, G., Johansson, M., Chen, J., & Puglisi, J. D. (2014). The dynamics of SecM-induced translational stalling. *Cell Reports*, *7*(5), 1521–1533. https://doi.org/10.1016/j.celrep.2014.04.033

Tucker, M., Valencia-Sanchez, M. A., Staples, R. R., Chen, J., Denis, C. L., & Parker, R. (2001). The transcription factor associated Ccr4 and Caf1 proteins are components of the major cytoplasmic mRNA deadenylase in Saccharomyces cerevisiae. *Cell*, *104*(3), 377–386. https://doi.org/10.1016/s0092-8674(01)00225-2

van Hoof, A., Frischmeyer, P. A., & Dietz, H. C. (2002). Exosome-Mediated Recognition and Degradation of mRNAs Lacking a Termination Codon. *Science*, *295*(5563), 2262–2264. https://doi.org/10.1126/science.1067272

Van Hoof, A., Frischmeyer, P. A., Dietz, H. C., & Parker, R. (2002). Exosome-mediated recognition and degradation of mRNAs lacking a termination codon. *Science*, *295*(5563), 2262–2264. https://doi.org/10.1126/science.1067272

van Hoof, A., Staples, R. R., Baker, R. R., & Parker, R. (2000). Function of the Ski4p (Csl4p) and Ski7p proteins in 3'-to-5' degradation of mRNA. *Molecular and Cellular Biology*, *20*(21), 8230–8243. https://doi.org/10.1128/MCB.20.21.8230-8243.2000

Vattem, K. M., & Wek, R. C. (2004). Reinitiation involving upstream ORFs regulates ATF4 mRNA translation in mammalian cells. *Proceedings of the National Academy of Sciences of the United States of America*, *101*(31), 11269–11274. https://doi.org/10.1073/pnas.0400541101

Voorhees, R. M., Fernández, I. S., Scheres, S. H. W., & Hegde, R. S. (2014).

Structure of the mammalian ribosome-Sec61 complex to 3.4 ?? resolution. *Cell*, *157*(7), 1632–1643. https://doi.org/10.1016/j.cell.2014.05.024

Voorhees, R. M., & Hegde, R. S. (2015). Structures of the scanning and engaged states of the mammalian SRP-ribosome complex. *ELife*, *4*(JULY 2015), 1–21. https://doi.org/10.7554/eLife.07975

W., H. M., Wright, C. S., A., R. T., G., B. J., Andrew, D., B., H. J., & D., K. R. (1987). Identification of the Iron-Responsive Element for the Translational Regulation of Human Ferritin mRNA. *Science*, *238*(4833), 1570–1573. https://doi.org/10.1126/science.3685996

Wallace, E. W. J., Maufrais, C., Sales-Lee, J., Tuck, L. R., de Oliveira, L., Feuerbach, F., Moyrand, F., Natarajan, P., Madhani, H. D., & Janbon, G. (2020). Quantitative global studies reveal differential translational control by start codon context across the fungal kingdom. *Nucleic Acids Research*, *48*(5), 2312–2331. https://doi.org/10.1093/nar/gkaa060

Walsh, K. P., & Mills, K. H. G. (2013). Dendritic cells and other innate determinants of T helper cell polarisation. *Trends in Immunology*, *34*(11), 521–530. https://doi.org/https://doi.org/10.1016/j.it.2013.07.006

Walter, P., & Blobel, G. (1983). Disassembly and reconstitution of signal recognition particle. *Cell*, *34*(2), 525–533. https://doi.org/10.1016/0092-8674(83)90385-9

Walter, P., & Ron, D. (2011). The Unfolded Protein Response: From Stress Pathway to Homeostatic Regulation. *Science*, *334*(6059), 1081–1086. https://doi.org/10.1126/science.1209038

Wang, J., Vasaikar, S., Shi, Z., Greer, M., & Zhang, B. (2017). WebGestalt 2017: a more comprehensive, powerful, flexible and interactive gene set enrichment analysis toolkit. *Nucleic Acids Research*, *45*(W1), W130–W137. https://doi.org/10.1093/nar/gkx356

Wang, Z., & Sachs, M. S. (1997). Arginine-specific regulation mediated by the Neurospora crassa arg-2 upstream open reading frame in a homologous, cell-free in vitro translation system. *Journal of Biological Chemistry*, *272*(1), 255–261. https://doi.org/10.1074/jbc.272.1.255

Wculek, S. K., Khouili, S. C., Priego, E., Heras-Murillo, I., & Sancho, D. (2019). Metabolic Control of Dendritic Cell Functions: Digesting

Information. *Frontiers in Immunology*, *10*, 775. https://doi.org/10.3389/fimmu.2019.00775

Weichhart, T., Hengstschläger, M., & Linke, M. (2015). Regulation of innate immune cell function by mTOR. *Nature Reviews Immunology*, *15*(10), 599–614. https://doi.org/10.1038/nri3901

Weinberg, D. E., Shah, P., Eichhorn, S. W., Hussmann, J. A., Plotkin, J. B., & Bartel, D. P. (2016). Improved Ribosome-Footprint and mRNA Measurements Provide Insights into Dynamics and Regulation of Yeast Translation. *Cell Reports*, *14*(7), 1787–1799. https://doi.org/10.1016/j.celrep.2016.01.043

Wek, R. C. (2018). Role of eIF2α Kinases in Translational Control and Adaptation to Cellular Stress. *Cold Spring Harbor Perspectives in Biology*, *10*(7). https://doi.org/10.1101/cshperspect.a032870

Wickham, H. (2009). *ggplot2: Elegant Graphics for Data Analysis.* Springer-Verlag New York. http://ggplot2.org

Wilson, D. N., Arenz, S., & Beckmann, R. (2016). Translation regulation via nascent polypeptide-mediated ribosome stalling. *Current Opinion in Structural Biology*, *37*, 123–133. https://doi.org/10.1016/j.sbi.2016.01.008

Wilson, D. N., & Beckmann, R. (2011). The ribosomal tunnel as a functional environment for nascent polypeptide folding and translational stalling. *Current Opinion in Structural Biology*, *21*(2), 274–282. https://doi.org/10.1016/j.sbi.2011.01.007

Wohlgemuth, I., Brenner, S., Beringer, M., & Rodnina, M. V. (2008). Modulation of the Rate of Peptidyl Transfer on the Ribosome by the Nature of Substrates*. *Journal of Biological Chemistry*, *283*(47), 32229–32235. https://doi.org/https://doi.org/10.1074/jbc.M805316200

Woolstenhulme, C. J., Guydosh, N. R., Green, R., & Buskirk, A. R. (2015). High-Precision analysis of translational pausing by ribosome profiling in bacteria lacking EFP. *Cell Reports*, *11*(1), 13–21. https://doi.org/10.1016/j.celrep.2015.03.014

Woolstenhulme, C. J., Parajuli, S., Healey, D. W., Valverde, D. P., Petersen, E. N., Starosta, A. L., Guydosh, N. R., Johnson, W. E., Wilson, D. N., & Buskirk, A. R. (2013). Nascent peptides that block protein synthesis in bacteria. *Proceedings of the National Academy of Sciences*, *110*(10),

E878 LP-E887. https://doi.org/10.1073/pnas.1219536110

Wu, T. D., & Nacu, S. (2010). Fast and SNP-tolerant detection of complex variants and splicing in short reads. *Bioinformatics (Oxford, England)*, *26*(7), 873–881. https://doi.org/10.1093/bioinformatics/btq057

Wu, T. D., Reeder, J., Lawrence, M., Becker, G., & Brauer, M. J. (2016). GMAP and GSNAP for Genomic Sequence Alignment: Enhancements to Speed, Accuracy, and Functionality. *Methods in Molecular Biology (Clifton, N.J.)*, *1418*, 283–334. https://doi.org/10.1007/978-1-4939-3578-9_15

Yaman, I., Fernandez, J., Liu, H., Caprara, M., Komar, A. A., Koromilas, A. E., Zhou, L., Snider, M. D., Scheuner, D., Kaufman, R. J., & Hatzoglou, M. (2003). The zipper model of translational control: a small upstream ORF is the switch that controls structural remodeling of an mRNA leader. *Cell*, *113*(4), 519–531. https://doi.org/10.1016/s0092-8674(03)00345-3

Yanagitani, K., Imagawa, Y., Iwawaki, T., Hosoda, A., Saito, M., Kimata, Y., & Kohno, K. (2009). Cotranslational Targeting of XBP1 Protein to the Membrane Promotes Cytoplasmic Splicing of Its Own mRNA. *Molecular Cell*, *34*(2), 191–200. https://doi.org/10.1016/j.molcel.2009.02.033

Yanagitani, K., Kimata, Y., Kadokura, H., & Kohno, K. (2011). Translational pausing ensures membrane targeting and cytoplasmic splicing of XBP1u mRNA. *Science*, *331*(6017), 586–589. https://doi.org/10.1126/science.1197142

Yang, D., Elner, S. G., Bian, Z.-M., Till, G. O., Petty, H. R., & Elner, V. M. (2007). Pro-inflammatory cytokines increase reactive oxygen species through mitochondria and NADPH oxidase in cultured RPE cells. *Experimental Eye Research*, *85*(4), 462–472. https://doi.org/10.1016/j.exer.2007.06.013

Yordanova, M. M., Loughran, G., Zhdanov, A. V, Mariotti, M., Kiniry, S. J., O'Connor, P. B. F., Andreev, D. E., Tzani, I., Saffert, P., Michel, A. M., Gladyshev, V. N., Papkovsky, D. B., Atkins, J. F., & Baranov, P. V. (2018). AMD1 mRNA employs ribosome stalling as a mechanism for molecular memory formation. *Nature*, *553*(7688), 356–360. https://doi.org/10.1038/nature25174

Yoshida, H., Matsui, T., Yamamoto, A., Okada, T., & Mori, K. (2001). XBP1

mRNA Is Induced by ATF6 and Spliced by IRE1 in Response to ER Stress to Produce a Highly Active Transcription Factor. *Cell*, *107*, 881–891. https://core.ac.uk/download/pdf/82191390.pdf

Young, D. J., Guydosh, N. R., Zhang, F., Hinnebusch, A. G., & Green, R. (2015). Rli1/ABCE1 Recycles Terminating Ribosomes and Controls Translation Reinitiation in 3'UTRs In Vivo. *Cell*, *162*(4), 872–884. https://doi.org/10.1016/j.cell.2015.07.041

Young, S. K., Willy, J. A., Wu, C., Sachs, M. S., & Wek, R. C. (2015). Ribosome Reinitiation Directs Gene-specific Translation and Regulates the Integrated Stress Response. *The Journal of Biological Chemistry*, *290*(47), 28257–28271. https://doi.org/10.1074/jbc.M115.693184

Youngman, E. M., Brunelle, J. L., Kochaniak, A. B., & Green, R. (2004). The active site of the ribosome is composed of two layers of conserved nucleotides with distinct roles in peptide bond formation and peptide release. *Cell*, *117*(5), 589–599. http://www.ncbi.nlm.nih.gov/pubmed/15163407

Zhang, E., Khanna, V., Dacheux, E., Namane, A., Doyen, A., Gomard, M., Turcotte, B., Jacquier, A., & Fromont-Racine, M. (2019). A specialised SKI complex assists the cytoplasmic RNA exosome in the absence of direct association with ribosomes. *The EMBO Journal*, e100640. https://doi.org/10.15252/embj.2018100640

Zhang, J., Pan, X., Yan, K., Sun, S., Gao, N., & Sui, S. F. (2015). Mechanisms of ribosome stalling by SecM at multiple elongation steps. *ELife*, *4*(DECEMBER2015), 1–25. https://doi.org/10.7554/eLife.09684.001

Zinoviev, A., Ayupov, R. K., Abaeva, I. S., Hellen, C. U. T., & Pestova, T. V. (2020). Extraction of mRNA from Stalled Ribosomes by the Ski Complex. *Molecular Cell*, *77*(6), 1340-1349.e6. https://doi.org/10.1016/j.molcel.2020.01.011

Zoschke, R., Watkins, K. P., & Barkan, A. (2013). A rapid ribosome profiling method elucidates chloroplast ribosome behavior in vivo. *The Plant Cell*, *25*(6), 2265–2275. https://doi.org/10.1105/tpc.113.111567

Acknowledgements

First of all, I would like to thank Prof. Roland Beckmann for giving me a wonderful opportunity to pursue PhD in his group. Next, for the range of projects I have been involved in, from establishing the technique of ribosome profiling, and applying it to study dendritic cells, contributing for the Ski project (with Chris and Thomas) and a cryo-EM project to visualize XBP1u within the exit tunnel. It has been one exciting and an exhilarating ride as well. This broad experience did provide me with solid training in bioinformatic analysis and also dealing with cryo-EM data. So, thanks to Roland again. Overall, the lab environment was very stimulating and intra-lab collaboration naturally progressed and was quite fruitful.

Next, I would like to thank my PhD defense committee members: Prof. Dr. Klaus Förstemann, Prof. Dr. Julian Stingele, Prof. Dr. Johannes Stigler, PD Dr. Gregor Witte and Prof. Dr. Marion Subklewe. Thanks for being in the committee.

Thanks to Dr. Thomas Becker for patiently reading the thesis draft atleast multiple times. Thanks Thomas!!!

One another person who needs to be mentioned here is Dr. Markus Pech. I learnt quite a lot from you, and the major role you played in establishing ribo-seq in the lab. Your knowledge in the field of ribosomes and biochemistry in general is pretty amazing. Hope to talk to you sometime soon!

Chris and Thomas, it was very nice to collaborate with you guys for the Ski project.

Eli, thanks for chaperoning me to the lab (to and fro) after I returned from nursing my broken leg (ankle). You were pretty kind to offer me these rides and I think it was for two - three weeks, until I could manage to walk normally again. Apart from these rides your tips regarding biochemistry were very very useful. It came in super-handy for cloning as well as for purifying the XBP1u-RNC complex. Thanks a lot Eli.

Alexej, your spontaneous cookie moments always kept the blood glucose levels high enough to pound through the day. Also, thanks for giving me your bike in return for a day’s lunch at the mensa.

Andre and Lukas, thanks for all the scripts and also for keeping the processing pipeline intact. Jingdong Cheng for building the initial model of the nascent chain and also for answering any question regarding data processing. Hanna and Tsai, nice to sit along with you guys and talk some random things. Katha, thanks for your help with the reconstitution experiments.

Ting, thanks for sharing your pymol scripts and tips for making amazing structure figures. We have had so many discussions about variety of topics. We should continue to keep in touch in the future as well.

One big thanks to the QBM grad school. First for inviting me to the interview week! Second, during the interview week, I missed my meeting with the interview panel. Thanks for finding a spot in another panel where Roland would also be there. Eventually it all worked out, and I got selected. Thanks for organizing the language courses, and as well as funding for scientific courses, and allowances to attend domestic and international conferences!! Introductory primers on statistics and programming with R were quite helpful.

I really need to thank my friends in Munich, you guys made me feel at home. I will cherish all the wonderful moments we had together. Finally, I would like to thank my family. They have been constant source of strength and support. Last but not the least, my wife Abhi without you this whole journey would not have been possible at all.